

DEPARTMENT OF MECHANICAL ENGINEERING
COLLEGE OF ENGINEERING AND TECHNOLOGY
OLD DOMINION UNIVERSITY
NORFOLK, VIRGINIA 23529

**NONLINEAR TRANSIENT THERMAL ANALYSIS BY THE
FORCE-DERIVATIVE METHOD**

By
Narayani V. Balakrishnan
and
Dr. Gene Hou, Principal Investigator

Final Report
For the period ending January 3, 1996

Prepared for
National Aeronautics and Space Administration
Langley Research Center
Attn.: Joseph Murray, Grants Officer
Mail Stop 126
Hampton, VA 23681-0001

Under
Research Grant NAG-1-1567
Dr. Charles J. Camarda, Technical Monitor
ODURF #140452

Submitted by
Old Dominion University Research Foundation
Norfolk, VA 23508

November 1997



NONLINEAR TRANSIENT THERMAL ANALYSIS
BY THE FORCE-DERIVATIVE METHOD

by

Narayani V. Balakrishnan
B.E., May 1982, Madras University, India
M. Tech., May 1984, Indian Institute of Technology, Madras, India

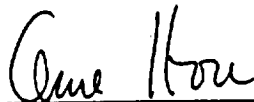
A Dissertation Submitted to the Faculty of
Department of Mechanical Engineering in Partial Fulfillment of the
Requirements for the Degree of

DOCTOR OF PHILOSOPHY

in

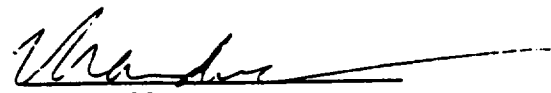
ENGINEERING MECHANICS

OLD DOMINION UNIVERSITY
August 1995


Dr. Jean W. Hou (Director)


Dr. Charles Camarda


Dr. Chuh Mei


Dr. Duc Nguyen

DEDICATION

Dedicated to my beloved father, Mahadeva Iyer Venkatraman, and my dear brother, Venkatraman Raghavan.

ACKNOWLEDGMENTS

My sincere thanks are due to Professor Jean W. Hou, chairman of my dissertation committee, for providing excellent technical guidance during the course of this research. I extend my gratitude to the members of the committee, Drs. Charles Camarda, Chuh Mei and Duc Nguyen for their valuable suggestions. This work was supported by the Thermal Structures Branch of NASA Langley Research Center under grant no. NAG-1-1567. Dr. Charles Camarda, who originally suggested this research topic, was the technical monitor. I also thank Dr. Kim S. Bey for her enlightening discussions. The wonderful typing job of Ms. Michelle Dail is highly appreciated.

I wish to express my heartfelt gratitude to my husband for his extreme patience and effective encouragement throughout this endeavor. To my adorable mother, and to my dear brothers, sisters, and their families I am deeply indebted for their invaluable help and their strong faith in me. The appropriate words of comfort and encouragement from my friends and the support of my in-laws are sincerely appreciated. Last, but most important, this dissertation would have never been completed but for the unbelievable understanding of and the sacrifices made by my precious little daughters Vidya and Divya, and to them I am grateful beyond measure.

TABLE OF CONTENTS

	Page
DEDICATION	ii
ACKNOWLEDGMENTS	iii
LIST OF TABLES	vi
LIST OF FIGURES	vii
LIST OF SYMBOLS	xi
 Chapter	
1. INTRODUCTION	1
1.1 Motivation of Current Research.....	1
1.2 Literature Survey.....	2
1.2.1 Approximate Numerical Methods.....	2
1.2.2 Time-Integration Algorithms	5
1.2.3 Adaptive Mesh Generation Techniques	8
1.2.4 Reduced-Basis Methods.....	10
1.3 Objective of Study	16
1.4 Scope of Study	17
2. GOVERNING EQUATION FOR TRANSIENT HEAT CONDUCTION	19
2.1 Problem Statement	20
2.2 Finite Element Formulation	22
3. THE FORCE-DERIVATIVE METHOD FOR LINEAR TRANSIENT THERMAL PROBLEMS	24
3.1 Unified Derivation of the Modal Methods.....	24
3.1.1 The Mode-Displacement Method	24
3.1.2 The Mode-Acceleration Method.....	26
3.1.3 The Force-Derivative Method.....	28
3.2 Modal Coordinates for a Linearly Time-Varying Load.....	30
3.3 A Priori Estimate of the Required Number of Modes	32

4. METHOD OF SOLUTION FOR NONLINEAR TRANSIENT THERMAL PROBLEMS	37
4.1 Linearization of the System of Equations	37
4.1.1 Derivation of the Newton-Raphson Method	37
4.1.2 Application of the Newton-Raphson Method with Simplifications	39
4.2 The Force-Derivative Method for the Transient Response	41
4.2.1 One-Step Approach	41
4.2.2 Multi-Step Approach	43
4.3 Modal Coordinates for a Piecewise Linear Time-Varying Load	46
4.4 Convergence Criterion and Distribution Error Norm	47
4.5 A Note on the Required Number of Modes	47
4.6 A Note on the Computational Effort Involved	48
5. LINEAR TRANSIENT EXAMPLE PROBLEMS	51
5.1 Rod Subject to Convection at One End	51
5.2 Plate Subject to Uniform Surface Heating	57
6. NONLINEAR TRANSIENT EXAMPLE PROBLEMS	73
6.1 Rod Subject to Convection at One End with Temperature-Dependent Thermal Conductivity	73
6.1.1 Case 1: $k(T) = 0.0001 + 0.5 E - 06 T$	73
6.1.2 Case 2: $k(T) = 0.0001 + 0.1 E - 04 T$	82
6.2 Lower Surface of Bay 3 of Shuttle Wing Segment	95
6.2.1 Simplified One-Dimensional Model	100
6.2.2 Two-Dimensional Model	125
7. CONCLUSIONS AND RECOMMENDATIONS	138
REFERENCES	141
APPENDIX: COMPUTATIONAL PROCEDURES USED IN THE IMPLEMENTATION OF THE MDM, MAM, AND THE FDM	146

LIST OF TABLES

TABLE		PAGE
5.1	A priori estimate of the number of modes required at time $t = 2$ sec (Linear example problem 2).	61
6.1	Effect of time step on the solution accuracy of the FDM (Case 1 of nonlinear example problem 1)	82
6.2	Effect of time-marching parameters on the number of modes required at time $t = 0.1$ sec (Case 1 of nonlinear example problem 1).	87
6.3	Effect of time-marching parameters on the number of modes required at time $t = 0.05$ sec (Case 2 of nonlinear example problem 1).	95
6.4	Comparison of reduction achieved by the MDM and the MAM for Shuttle one-dimensional thermal model.	111

LIST OF FIGURES

FIGURE	PAGE
2.1 Three-dimensional solution domain for general heat conduction.....	21
3.1 Forcing function that varies linearly with time.....	31
5.1 Thermal finite element model of a rod subject to transient convective heating at one end (Linear example problem 1).	52
5.2 Temperature distribution along a rod subject to transient convection at one end at time $t = 0.02$ sec (Linear example problem 1): a) Mode-displacement method (MDM); b) Mode-acceleration method (MAM); c) Force-derivative method (FDM).	54
5.3 Convergence of the modal methods at time $t = 0.02$ sec (Linear example problem 1).	58
5.4 Thermal finite element model (165 DOF) of a plate subject to uniform, transient heating over the surface and convection along the entire boundary (Linear example problem 2).....	59
5.5 Convergence of the error, e_1 , in the load vector used to predict the number of modes required by the MDM at times $t = 2.0$ sec and 9.0 sec (Linear example problem 2).	60
5.6 Convergence of the error, e_2 , in the pseudo steady-state response used to predict the number of modes required by the MAM at times $t = 2.0$ sec and 9.0 sec (Linear example problem 2).....	62
5.7 Convergence of the error, e_3 , in the derivative form of the pseudo steady-state response used to predict the number of modes required by the FDM at times $t = 2.0$ sec and 9.0 sec (Linear example problem 2).	63
5.8 Temperature distribution at time $t = 2.0$ sec along $y = 0.0$ in. (Linear example problem 2): a) Mode-displacement method (MDM); b) Mode-acceleration method (MAM); c) Force-derivative method (FDM).	65
5.9 Convergence of the correction offered by the MAM, CMAM, at times $t = 2.0$ sec and 9.0 sec (Linear example problem 2).	68
5.10 Convergence of the correction offered by the FDM, CFDM, at times $t = 2.0$ sec and 9.0 sec (Linear example problem 2).	69
5.11 Temperature distribution at time $t = 9.0$ sec along $y = 0.0$ in. (Linear example problem 2).	71

5.12	Convergence of the modal methods at times $t = 2.0$ sec and 9.0 sec (Linear example problem 2).	72
6.1	Thermal finite element model of a rod subject to transient convective heating at one end with temperature-dependent thermal conductivity (Nonlinear example problem 1).	74
6.2	History of iterations required by the FDM to determine the time for an EVP update (Case 1 of nonlinear example problem 1).	76
6.3	Temperature distribution obtained by the MDM, MAM, and the FDM using two modes at time $t = 0.1$ sec (Case 1 of nonlinear example problem 1).	78
6.4	Convergence of the modal methods at time $t = 0.1$ sec (Case 1 of nonlinear example problem 1).	79
6.5	Effect of time step on the response of the FDM at time $t = 0.1$ sec with initial condition at time $t = 0.0$ sec and one EVP update at time $t = 0.05$ sec (Case 1 of nonlinear example problem 1).	80
6.6	Effect of time step on the response of the FDM at time $t = 0.2$ sec with initial condition at time $t = 0.1$ sec and no EVP update (Case 1 of nonlinear example problem 1).	81
6.7	Effect of time-marching parameters on the number of modes required by the MDM, MAM, and the FDM at time $t = 0.1$ sec (Case 1 of nonlinear example problem 1): a) Mode-displacement method (MDM); b) Mode-acceleration method (MAM); c) Force-derivative method (FDM).	83
6.8	Comparison of temperature distributions at time $t = 0.05$ sec for the two cases of nonlinear example problem 1.	86
6.9	Error history of the FDM to determine the time for an EVP update (Case 2 of nonlinear example problem 1).	88
6.10	Convergence of the modal methods at time $t = 0.05$ sec (Case 2 of nonlinear example problem 1).	90
6.11	Effect of time step on the response of the FDM at time $t = 0.05$ sec with initial condition at time $t = 0.0$ and one EVP update at time $t = 0.025$ sec (Case 2 of nonlinear example problem 1).	91
6.12	Effect of time-marching parameters on the number of modes required by the MDM, MAM, and the FDM at time $t = 0.05$ sec (Case 2 of nonlinear example problem 1): a) Mode-displacement method (MDM); b) Mode-acceleration method (MAM); c) Force-derivative method (FDM).	92
6.13	History of the corrections made by the MAM and the FDM: a) Case 1 of nonlinear example problem 1; b) Case 2 of nonlinear example problem 1.	96
6.14	Geometry of Shuttle wing segment at Wing Station 240.	98
6.15	Thermal model of the lower surface of bay 3 of Shuttle wing segment.	99

6.16	Heating history for the lower surface of bay 3 of Shuttle wing segment.....	101
6.17	Spatial distribution of discontinuous heat load on the lower surface of bay 3 at selected times	102
6.18	Temperature-dependent quantities: a) Convection coefficient; b) HRSI thermal properties.	103
6.19	Finite element mesh (16 DOF, uniform) for Shuttle one-dimensional thermal model.	105
6.20	Temperature histories at different locations through a Shuttle tile and substructure obtained from a one-dimensional thermal model.	107
6.21	Comparison of full-system solutions of different meshes for Shuttle one-dimensional thermal model.	108
6.22	Effect of finite element mesh on efficiency of the MAM for Shuttle one-dimensional thermal model.	110
6.23	Comparison of eigenvalues at time $t = 350$ sec of the different meshes for Shuttle one-dimensional thermal model.	112
6.24	Mode shapes at time $t = 350$ sec of the 16 DOF meshes for Shuttle one-dimensional thermal model: a) Uniform mesh; b) Graded mesh.	113
6.25	Convergence of the corrections offered by the MAM and the FDM, CMAM and CFDM respectively, at time $t = 50$ sec using the Shuttle one-dimensional thermal model with 166 DOF.	116
6.26	Temperature distributions obtained by the MAM and the FDM at time $t = 50$ sec using the Shuttle one-dimensional thermal model with 166 DOF. .	117
6.27	Convergence of the corrections offered by the MAM and the FDM, CMAM and CFDM respectively, at different times for Shuttle one-dimensional thermal model: a) 166 DOF uniform mesh; b) 16 DOF graded mesh.	118
6.28	Comparison of the histories of the first derivative of the specified and convective heat loads for the Shuttle one-dimensional thermal model.	121
6.29	Comparison of the histories of the specified and convective heat loads for the Shuttle one-dimensional thermal model.	122
6.30	Comparison of the histories of the eigenvalues of the 16 DOF graded mesh for Shuttle one-dimensional thermal model.	123
6.31	Variation of the normalized mode-participation factors with time for different meshes of Shuttle one-dimensional thermal model.	124
6.32	Comparison of temperature histories of the different modal solutions for the 16 DOF graded mesh using a time step $dt = 2$ sec with the eigensolution updated every 50 sec for Shuttle one-dimensional thermal model.	126

6.33	Spatial distribution of heating on the lower surface of bay 3 at selected times (Smoothly-varying load).	127
6.34	Temperature contours at time $t = 1000$ sec of Shuttle two-dimensional thermal model with 187 DOF and discontinuous load.	129
6.35	Finite element mesh (578 DOF) for Shuttle two-dimensional thermal model with discontinuous load.	130
6.36	Temperature contours at time $t = 1000$ sec of Shuttle two-dimensional thermal model with 578 DOF and discontinuous load.	131
6.37	Convergence of the correction offered by the MAM, CMAM, at time $t = 350$ sec using the Shuttle two-dimensional thermal model with 578 DOF and discontinuous load.	133
6.38	Comparison of the error histories of the different modal solutions of the Shuttle two-dimensional thermal model with discontinuous load and 578 DOF.	134
6.39	Convergence of the MDM and the MAM at time $t = 1000$ sec using the Shuttle two-dimensional thermal model with 578 DOF and discontinuous load.	135
6.40	Finite element mesh (986 DOF) for Shuttle two-dimensional thermal model with smoothly-varying load.	136
6.41	Temperature contours at time $t = 1000$ sec of Shuttle two-dimensional thermal model with 986 DOF and smoothly-varying load.	137

LIST OF SYMBOLS

A	cross-sectional area
B	temperature-gradient interpolation matrix
C	capacitance matrix
c	specific heat
dt	time step
e	distribution error norm
e ₁	error in the representation of the load vector, $R(t)$
e ₂	error in the representation of the pseudo steady-state response, $K^{-1}R(t)$
e ₃	error in the representation of the vector, $K^{-1}CK^{-1}\dot{R}(t)$
F	unbalanced load vector
h	convection coefficient
I	identity matrix
J ₁ , J ₂	Jacobian matrices with respect to temperature and its time derivative, respectively
j	order of differentiability of the forcing function
K	conductance matrix
K _c	conduction matrix
K _h	convection matrix
K _r	radiation matrix
k	thermal conductivity
k _{ij}	components of the thermal conductivity tensor
L	length
m	number of time steps between eigensolution updates

N	row vector of temperature interpolation functions
n	total number of degrees of freedom
n_x, n_y, n_z	cartesian components of a unit normal vector
p	reduced number of degrees of freedom, or, reduced number of modes used in the solution
Q	generalized heat load vector
Q_{int}	rate of internal volumetric heat generation
Q_{NL}	nonlinear corrective load vector
q_i	components of the heat flux vector
q_r	rate of incident surface radiation
q_s	specified surface heating rate
R	applied heat load vector
R_L, R_{NL}	linear and nonlinear components of the applied load vector
R_Q	load vector due to internal volumetric heat generation
R_q	load vector due to specified surface heating
R_h	load vector due to surface convection
R_r	load vector due to incident surface radiation
r	number of nodes per element
S	boundary surface of integration
S_1, S_2, S_3, S_4	parts of the boundary surface
T	temperature vector
(T)	function of temperature
T_e	environment temperature
T_s	surface temperature
\bar{T}	exact solution vector of a nonlinear system of equations
t	time
(t)	function of time
u	unit internal energy

V	volume of integration
x,y,z	rectangular Cartesian coordinates
x_i	coordinate ($i = 1, 2, 3$)
Z	vector of modal coordinates
z	modal coordinate
<u>Greek</u>	
α	surface absorptivity
Δ	incremental quantity
δ	Kronecker delta
ϵ	surface emissivity; specified tolerance for iteration convergence
ϵ_{ij}	components of the strain tensor
Φ	matrix of thermal eigenvectors
ϕ	thermal eigenvector
η	mode participation factor
κ	thermal conductivity tensor
Λ	diagonal matrix of thermal eigenvalues
λ	thermal eigenvalue
ρ	density
σ	Stefan-Boltzmann constant
σ_{ij}	components of the stress tensor
τ	dummy variable of time integration
χ, φ	variables used to define the Leibnitz's rule for differentiation of an integral
ψ, μ	functions used to define the Leibnitz's rule for differentiation of an integral

Subscripts

0	evaluated based on initial condition
n, n-1, n-k	evaluated at current time, previous time, or k time steps earlier
p, q	free indices
r	modal index
i, j, s, m	dummy summation indices
x, y, z	directional components in the cartesian coordinate system

Superscripts

., ..	first and second derivatives with respect to time
', "	first and second derivatives with respect to temperature
^	matrix of reduced number of eigenvectors; vector of reduced number of eigenvalues or modal coordinates; heat load vector represented by a reduced number of eigenvectors
a	approximate
e	finite element
i	iteration index
m	raised to m th power
(m-1)	(m-1)th derivative with respect to time
T	transpose

Abbreviations

BIEM	boundary integral equation method
CFDM	corrective vector added by the FDM to the response from the MAM
CMAM	corrective vector added by the MAM to the response from the MDM
COMET	computational mechanics testbed
CPU	central processor unit
DOF	degrees of freedom
EVP	eigenvalue problem

FDM	force-derivative method
FEM	finite element method
HRSI	high-temperature reusable surface insulation
MAM	mode-acceleration method
MDM	mode-displacement method
MITAS	Martin interactive thermal analyses system
RTV	room temperature vulcanized
SIP	strain-isolator pad
TPS	thermal protection system

Chapter 1

INTRODUCTION

1.1 Motivation of Current Research

High-speed vehicles such as the Space Shuttle Orbiter must withstand severe aerodynamic heating during reentry through the atmosphere. The Shuttle skin and substructure are constructed primarily of aluminum, which must be protected during reentry with a thermal protection system (TPS) from being overheated beyond the allowable temperature limit, so that the structural integrity is maintained for subsequent flights. High-temperature reusable surface insulation (HRSI), a popular choice of passive insulation system, typically absorbs the incoming radiative or convective heat at its surface and then re-radiates most of it to the atmosphere while conducting the smallest amount possible to the structure by virtue of its low diffusivity.

In order to ensure a successful thermal performance of the Shuttle under a prescribed reentry flight profile, a preflight reentry heating thermal analysis of the Shuttle must be done. The surface temperature profile, the transient response of the HRSI interior, and the structural temperatures are all required to evaluate the functioning of the HRSI. Transient temperature distributions which identify the regions of high temperature gradients, are also required to compute the thermal loads for a structural thermal stress analysis. Furthermore, a nonlinear analysis is necessary to account for the temperature-dependent thermal properties of the HRSI as well as to model radiation losses.

Based on the capability to handle time-dependent as well as nonlinear boundary conditions and thermal properties, and programmability in general purpose codes, the finite element method is used to discretize the governing energy equation. When the

structure is subjected to severe thermal loads, the discretization level must often be increased by adding degrees of freedom to predict accurately the temperature gradients and the subsequent stress response. The addition of degrees of freedom significantly increases the computational cost of transient nonlinear thermal analysis. Hence, it is desirable to employ a method which can effectively reduce the computational problem size while maintaining accuracy, thus enabling an efficient solution of large or complex thermal problems.

The force-derivative method has shown tremendous success, in terms of the reduction achieved, in a variety of structural problems and also when applied to a simple linear transient thermal problem. This observation has motivated the present study on the feasibility of using the force-derivative method as a reduction technique for solving nonlinear transient thermal problems.

1.2 Literature Survey

This section summarizes the research done in the past to predict the thermal response with greater efficiency and accuracy in a wide range of problems. After an introduction to the different approximation methods available, the commonly used finite element time integration algorithms are discussed along with measures proposed in the earlier studies to overcome the demerits associated with such algorithms. Then, studies on the concept and usefulness of adaptive mesh generation techniques are presented. Finally, the evolution of the reduction methods to improve the computational efficiency of large-scale structural problems is outlined, followed by a review of the status of the reduction methods as applied to thermal problems.

1.2.1 Approximate Numerical Methods

Analytical or exact methods to obtain the temperature response are often impossible or impractical, due to the arbitrariness or irregularity of the geometry, or other features of the problem. Therefore, approximate numerical methods are often employed

for this purpose. The thermal analysis of convectively-cooled structures by Wieting and Guy [1]* was based on the finite difference lumped-parameter technique such as used in the Martin Interactive Thermal Analyses System (MITAS) [2]. The finite difference model of a problem gives a pointwise approximation to the governing equation of heat transfer. The model is formed by writing difference equations for an array of grid points, and hence is improved as more points are used. Bhattacharya [3] and Lick [4] used an improved finite difference method for time-dependent heat conduction problems. However, the method performed poorly when faced with irregular geometries or complicated boundary conditions.

Another numerical approach is the boundary integral equation method (BIEM) where an exact integral formula is derived relating boundary heat flux and boundary temperature from a fundamental singular solution to the governing equation. The part of the boundary data not already prescribed in the problem statement is obtained numerically from the formula. The temperature throughout the body is then generated by means of a Green's type integral identity directly in terms of the boundary data. A hybrid method which combined the BIEM with the Laplace transform technique to solve transient heat conduction problems was developed by Rizzo and Shippy [5] in 1970. Rources and Alarcon [6] presented the formulation for a two-dimensional isotropic continuous solid using the BIEM with a finite difference approach in time.

The finite element method (FEM) represented a major breakthrough in solid mechanics. Although the concepts of the FEM were well in use already, the method gained momentum in 1965 when Zienkiewicz and Cheung [7] introduced it as a method applicable to all field problems that can be stated in a variational form. This method gives a piecewise approximation to the governing equation. The finite element model replaces the solution region by an assemblage of discrete elements, and thereby reduces

*Numbers in brackets indicate References.

the continuum problem to one of a finite number of unknowns at points called nodes along element boundaries (and sometimes within the elements too). The variation of the field variable within the elements is expressed in terms of the nodal values of the variable and the assumed approximating functions called interpolating functions within each element.

The finite element method was first extended to linear thermal analysis by Wilson and Nickell [8] and by Becker and Parr [9] to solve steady and transient heat conduction problems. With this introduction, the potential of the method to perform thermal analysis was realized as it could not only represent irregular geometry but could improve accuracy and sometimes could perform more efficiently for a given accuracy than finite difference methods. It has the added advantage that it can model both thermal and structural problems. The various parameters in the method that can affect the nature of the solution, in terms of efficiency and accuracy, have been studied extensively since the method evolved. The ease in modeling complex geometry, the capability to handle time-dependent as well as nonlinear boundary conditions and thermal properties, programmability in general purpose codes, and compatibility with a subsequent structural analysis have made the FEM a very useful and effective method in engineering applications in general.

One of the early works in nonlinear heat transfer using finite elements was by Richardson and Shum [10], who included nonlinear radiation-convection heat flux boundary conditions in an explicit formulation. The convergence characteristics were improved by an alternative implicit-direct iteration scheme by Beckett and Chu [11]. Aguirre-Ramirez and Oden [12] applied the FEM to solve nonlinear heat conduction problems with temperature-dependent conductivity by the Runge-Kutta numerical integration scheme, while Thornton and Wieting [13] developed a procedure to handle several temperature-dependent parameters for simple elements based on the generalized

Newton-Raphson iteration technique [14]. The procedure which relies on the assumptions that thermal parameters are constant within an element and depend only on the average element temperature, was applied to convectively cooled structures [15]. While the early studies employed the variational principles introduced by Gurtin [16] (traditionally used in structural analysis) to derive the finite element equations, subsequent researchers used the Galerkin method of weighted residuals with interpolation functions as the weighting functions, commonly referred to as the conventional formulation.

1.2.2 Time-Integration Algorithms

Transient problems require the numerical solution of a set of first-order simultaneous ordinary differential equations. This was done by solving the incremental form of the governing equation [17], using an implicit time integration and modified Newton-Raphson iteration to establish equilibrium at every time increment. The direct integration techniques start from a known initial condition and then solve recursively for the solution at successive intervals of time based on a finite difference approximation of the time derivative of the temperature at an intermediate time within each time interval. This approximation has a significant effect on the behavior of the transient response. The study of the oscillation and stability characteristics of direct integration algorithms has received considerable attention over the years.

In the explicit forward-difference scheme, the set of temperatures at a given time is expressed as an explicit function of the set of previous temperatures in the structure. It requires minimal computation per time step to solve uncoupled algebraic equations. Capacitance has to be lumped, which may have its own inaccuracies as discussed in reference [18]. It is only conditionally stable with severe restrictions on the time step for short or thin elements having high diffusivity. This makes computation costs very prohibitive when the response is calculated over a long duration. Implicit schemes are

unconditionally stable even for nonlinear problems [19] thus permitting larger step sizes. However, they require considerable computational effort to solve coupled equations and significant additional computational effort for nonlinear problems because of the need for iterations at each time step and the need to factor the effective coefficient matrix every time step. Nevertheless, implicit algorithms are more efficient for solving stiff equations with widely-separated eigenvalues. In the popular Crank-Nicholson implicit algorithm the step size is often dictated by solution accuracy, for too large a step especially in nonlinear applications, can introduce errors in the spatial temperature distributions. Myers [20] has presented a method for estimating time steps required in heat conduction problems.

Adelman and Haftka [21] have identified some essential features of most transient heat conduction problems with respect to integration techniques,

1. The thermal response may be divided into regions of slowly and rapidly varying temperatures. Steep transients accompany initial conditions or sudden changes in the heat load.
2. The rapidity of variation of the transient portion of the temperature history is proportional to the quantity equal to the square of the length of the element divided by the diffusivity of the material. During such a transient, time steps much smaller than this quantity must be taken no matter what type of integration technique is used.
3. During a period of slowly-varying temperatures, large time steps may be taken by implicit integration techniques but explicit algorithms still have the above-mentioned restriction on the time step size.

Extensive research has been performed to improve the efficiency and accuracy of these algorithms. Subcycling and mixed time integration algorithms are some techniques

that have been investigated. Subcycling uses different time steps in different subdomains of a problem whereas mixed time integration uses different integrators and a single time step. However, application to nonlinear problems faces difficulties as the critical time step varies and stability characteristics are not well defined for implicit integrators. Orivuori [22] improved the efficiency of the Crank-Nicholson method to solve a nonlinear problem (nonlinearity being due to temperature-dependent material properties and boundary conditions), by using constant reference values for the effective coefficient matrices and load vector but periodically multiplying them by time-dependent functions to account for the nonlinearities, thus avoiding repeated factorizations. Efforts to couple the development of a set of various-order implicit algorithms and a strategy to automatically select both the largest possible time step as well as the appropriate algorithm throughout the solution process have resulted in the GEAR algorithms [23]. Reference [21] compares the GEAR algorithms against those used in SPAR [24] and MITAS [2].

The Taylor-Galerkin approach first introduced in convective transport problems was extended to transient nonlinear thermal-structural problems by Thornton and Dechaumphai [25] and applied to aerodynamically heated leading edges [26]. This algorithm utilizes first-order Taylor series in time and Galerkin method for spatial discretization. Unlike conventional algorithms, this approach treats the conservation variable and not temperature as the unknown. The nonlinearities are conveniently handled through the flux components thus avoiding the need to regenerate element matrices for nonlinear problems. The fluxes are interpolated from nodal values, in the same form as the conservation variable. The resulting element matrices could be evaluated in closed form thus avoiding the numerical integration for complex finite element shapes. The merits of this linear flux approach were seen again in steady-state thermal-structural analysis by Pandey et al., [27]. A second-order accurate explicit scheme was proposed by Tamma and Namburu [28] by including higher-order time

derivatives in the Taylor series which are evaluated from the governing equation. An alternate implicit, second-order accurate approach was presented by Thornton and Balakrishnan [29] which uses enthalpy as the dependent variable, thereby handling temperature-dependent specific heat outside the element integral as well and also permitting larger time steps than the explicit form.

High conductivity or very small element sizes, as may result from adaptive techniques, could severely restrict time step sizes from accuracy and stability considerations. As a means of replacing time-integration techniques and their associated complexities, hybrid methods have been developed which employ the Laplace transform technique to remove the time derivative from the governing equation and then solve the equation in the transform domain by the BIEM [5], finite difference [30] or FEM [31-33]. The temperature response is then obtained directly at the selected time of interest by applying an inverse transform to the solution in the transform domain. Although this technique was used very efficiently for linear problems in Ref. [33], its accuracy as a general nonlinear solution technique is questionable. Cerro and Scotti [34] have shown that the linearization involved before the Laplace transform is applied, neglects the time-dependent behavior of the terms which define the nonlinear problem, and hence produces significant inaccuracies as the nonlinearity increases.

1.2.3 Adaptive Mesh Generation Techniques

Severe aerodynamic heating produces non-uniform temperatures and stress gradients over the structure and the distributions are also time-dependent. Adaptive mesh generation techniques are employed to capture such localized effects and thus improve solution accuracy for a given computational effort. The two basic approaches are :

1. adaptive refinement/derefinement which includes
 - (a) the h-method,
 - (b) the p-method,
 - (c) the r-method, and

2. remeshing.

The h-method increases/decreases the number of degrees of freedom (DOF) by adding/removing elements in the original mesh in regions of interest. It is commonly used in production-type codes but orientation of elements cannot change to accommodate the varying field. The p-method maintains the geometry of the elements of the initial mesh but increases/decreases the DOF by increasing/decreasing the order of the interpolating polynomial by the use of nodeless variables. The hierarchical temperature interpolating functions need not be of the same order as displacement interpolating functions; therefore independent refinement is possible which is useful in integrated thermal-structural analysis [35] but has its complexities during implementation in computer programs. The r-method keeps the number of elements and their connectivities the same but relocates the nodes. This could sometimes result in distorted elements. The inherent drawbacks in the refinement approaches led to the use of the remeshing technique [36-37], wherein a new mesh is generated based on the solution obtained from the previous mesh. The new mesh consists of small elements in the regions with large changes in solution gradients and large elements in the regions where the gradient changes are small. For thermal problems, especially where the thermal loads move along the body of the structure and the magnitudes also vary with time, the mesh employed must adapt itself both in time and space (mesh movement) to accurately capture the transient temperature response. Remeshing has proved to be beneficial where steep gradients are involved because of high convergence rates. Mesh adaptivity based on relative error indicators estimated from the previous finite element solutions, avoids the need to know the behavior a priori. For a plate subject to nonuniform surface heating, when compared with a uniformly refined structured mesh, an adaptive unstructured mesh required much fewer nodes for a given acceptable error or produced a much smaller error for a given number of degrees of freedom (nodes).

1.2.4 Reduced-Basis Methods

A class of methods known as the reduced-basis methods retain the modeling versatility of the FEM while simultaneously reducing the number of DOF. The central idea is to solve the problem in a reduced subspace of the original space of discretization. This is done by replacing the governing equations of the structure by a reduced system of equations with considerably fewer unknowns. Thus, the actual solution vector is approximated by the Rayleigh-Ritz technique as a linear combination of a reduced set of linearly independent basis vectors. The approximate solution vector is then given by the product of a transformation matrix whose columns are the basis vectors, and a vector of undetermined coefficients which is obtained by solving the reduced system of equations.

The key to an effective reduction technique is the proper choice of the basis vectors which may include eigenmodes, Ritz vectors, Lanczos vectors or any suitable combination of the above. The following guidelines aid in the choice of appropriate basis vectors:

1. The vectors must be linearly independent and span the space of solutions in the neighborhood of the point considered on the solution path, and therefore fully characterize the nonlinear response in that neighborhood.
2. Their generation should be both simple and computationally inexpensive, and their number can be automatically selected for any given problem.
3. The vectors must have good approximation properties so that they provide highly accurate solutions on a large interval of the solution path.

While the first property guarantees convergence of the Bubnov-Galerkin approximation, the other two decide the efficiency and effectiveness of the method in solving large-scale nonlinear thermal problems. The review of the literature available for reduced-basis methods is presented in separate sections for structural and thermal problems.

Structural Problems

The use of modal methods as a reduction technique has increased by leaps and bounds since its introduction in 1944 by Biot and Bisplinghoff [38] to solve dynamic structural problems. The eigenmodes of a structure were then recognized, for the first time, to form a complete set of orthogonal and linearly independent vectors whose superposition could therefore represent the transient, linear structural response. This method henceforth came to be known as the mode-displacement method (MDM). Its attractive feature was that the reduced system of equations that resulted from this transformation were uncoupled, and hence could be solved individually as single degree of freedom systems.

The use of modal techniques for nonlinear problems is based on the principle of local mode superposition. For mildly nonlinear problems, Bathe and Gracewski [39] successfully employed the MDM coupled with the residual force technique. Herein, a single set of modes (based on linear analysis) and a constant effective stiffness matrix is used throughout the analysis, while the nonlinearities are fully taken into account in the evaluation of the residual force vector. However, for highly nonlinear problems this could yield erroneous results as the system characteristics are continually changing, while an accurate solution might require too frequent basis updates which could prove to be expensive. Noor [40] observed that the use of the linear solution as a basis vector necessitates frequent additions of corrective basis vectors, where each additional vector is obtained by solving the full system of nonlinear equations. To avoid this, Noor suggested the use of a nonlinear solution and its various order path derivatives as basis vectors in nonlinear structural problems. To accomplish the same task, Idelsohn and Cardona [41-42] suggested the inclusion of derivatives of the basis eigenmodes and Ritz vectors. The Ritz vectors have the advantage of accounting for the spatial distribution of the load at the basis generation itself.

The efficiency of a reduction method is measured by its ability to accurately predict the transient response by using as few basis vectors as possible. This ability is all the more crucial for a modal method where the complete solution of a large eigenvalue problem is rather expensive and also entails huge computer storage requirements. Although the MDM proved to be accurate and cost effective for solving many dynamic structural problems, the method experienced convergence difficulties when dealing with problems that exhibited discontinuities in time or space, or problems with closely-spaced natural frequencies [50-51]. The MDM often required a large number of modes to predict even the displacement response accurately and was ineffective in predicting the stresses (which is expected since the stresses are functions of the spatial derivatives of the displacements and the process of differentiation tends to magnify errors already existing in the displacement calculations). Kline [43] attempted to improve the MDM by adding a suitable choice of Ritz vectors to the system eigenmodes for linear dynamic problems. Several researchers [44-47] have worked on developing improved higher-order or faster-convergent modal solutions. The improved convergence of the mode-acceleration method (MAM) over the MDM is due to the additional term which represents the pseudo-static response thus including to some extent, the flexibility of the higher modes which are totally neglected in the MDM.

Camarda [48-50] identified a unified approach for deriving successively higher-order modal methods, which are collectively called the force-derivative method (FDM) and offer an increasingly improved approximation of the higher modes neglected in the basic MDM. As the name indicates, the additional terms in the FDM involve an increasing order of the time derivatives of the forcing function, which are obtained by repeated integration by parts with respect to time, of the convolution integral form of the modal response. Thus the MAM, which supplements the MDM with one correction term that depends on the forcing function itself, is the first-order FDM.

The FDM has established its superiority over lower-order modal methods by the consistently faster convergence and greater accuracy in a wide variety of linear structural problems [48-50]. It must be noted that if the forcing function or its time derivatives are discontinuous in time, the higher-order modal methods should include appropriate jump conditions to avoid errors in the solution close to the time of discontinuity. This is because the development of higher-order methods is based on the assumption that the forcing function and its time derivatives are continuous. McGowan and Bostic [51] have demonstrated that for a multi-span beam (which has closely-spaced frequencies) subject to a uniformly distributed load which varies as a quintic function of time, the FDM (order 4 and 6) not only significantly reduced the number of modes necessary to represent an accurate response, but also required considerably less computational time as compared to the lower-order modal methods and the Lanczos method. The highly desirable rapid convergence property of the FDM was further exhibited in the analysis of an unconstrained high-speed civil transport structure [52], which used an elastic flexibility matrix to replace the inverse of the stiffness matrix which was singular. However, a comparative study of the central processor unit (CPU) times in this case showed an increased CPU time required by the higher-order FDM as it performed more calculations involving the elastic flexibility matrix.

Thermal Problems

Transient thermal problems exhibit a wide spectrum response and the higher thermal modes excited by the heat supply intensities generally dominate the response. Bushard [53] employed the Guyan reduction technique (commonly used in structural dynamics) to solve transient thermal problems. The mode-superposition technique was introduced in thermal analysis as well by Biot [54] in 1957. However, too many DOF had to be retained in the reduced system for the MDM to predict an accurate temperature

response even for linear thermal problems. The slow convergence of the MDM can be traced to the omission of the important higher modes.

Nour-Omid et al., [55] recognized that the Lanczos algorithm, which originated to solve the symmetric eigenvalue problem, was an efficient tool to extract eigenvalues/eigenmodes at both ends of the spectrum. This capability enabled the algorithm to generate a sequence of orthogonal vectors which served as an effective basis in the transient thermal analyses by Nour-Omid [56] and Coutinho et al., [57]. By reducing the system of equations to the tridiagonal form, the solution required little numerical effort. The vectors were themselves inexpensive to generate. Assuming the spatial distribution of load does not vary with time, the steady-state solution was used as the starting vector for linear problems, and with few vectors generated, the coordinate transformation matrix contained vectors which were also global approximations of the higher modes [57]. Thus, Lanczos vectors served as an effective reduced-basis for thermal analysis. Subsequently, in an attempt to capture steep gradients in the solution, Cardona and Idelsohn [58] employed the increment of the nodal temperatures for the first time step as the starting vector to generate the orthogonal Lanczos vectors, and then supplemented with a constant vector for successive time steps.

Nonlinear thermal problems were handled by Cardona and Idelsohn [58] in a manner similar to nonlinear structural problems by augmenting the set of basis vectors with derivatives of the same with respect to their own amplitude parameters, thus accounting for the variation of the system properties caused by changes in temperature. Noor et al., [59] extended the path-parameter approach to solve nonlinear steady-state thermal problems. The governing equation is embedded in a single or multiple-parameter family of equations. The path derivatives obtained by successive differentiation of the finite element equations of the initial discretization, are computed at zero values of the path parameters so that only one matrix factorization is needed. Often an augmented set

is used which includes a constant vector to represent a uniform temperature mode and reciprocal vectors along with the first few path derivatives. The cost of evaluating the basis vectors and generating the reduced equations can be rather high relative to the cost of solving the reduced nonlinear algebraic equations. This is because the expressions for the basis vectors grow in complexity for higher-order derivatives and their computation involves contractions of multidimensional arrays with the basis vectors. Besides, all the lower-order derivatives must be obtained before any subsequent order derivatives can be computed.

On the other hand, a modified modal method reviewed in reference [40] yielded reasonably accurate solutions for step loaded dynamic problems by employing two sets of vibration modes as basis vectors, namely

1. Few modes of a linear eigenvalue problem based on initial conditions;
2. Few modes of the nonlinear steady-state of the structure.

This success prompted the application of the modified method by Shore [60-62] to obtain the temperature history of a model of the Space Shuttle Orbiter wing subject to reentry heating. The nonlinearities arose from temperature-dependent properties and radiation from the surface. For temporally varying heat loads, provided the uniform or nonuniform spatial distribution of the heat loads remained constant in time, excellent results were achieved. This was made possible by a careful construction of the basis which included an adaptively generated vector based on the temperature distribution from the previous time interval among others. When spatially varying heat loads were considered, further enrichment of the basis via an analytically generated vector based on the changing heating distribution became necessary.

The unified approach to develop the higher-order FDM for structural problems has been extended to linear thermal analysis [50]. When applied to a simple

one-dimensional thermal problem of a rod heated at one end, the first- and the second-order FDM converged faster than the MDM as they did in structural applications.

1.3 Objective of Study

In spite of the versatility of the FEM, an unwieldy number of degrees of freedom are often required to model complex geometries or to capture the temperature gradients arising from severe thermal loads and hence to accurately predict the stress response subsequently. The important step in nonlinear analyses, the solution of the system of algebraic equations associated with the finite element model, therefore remains very expensive even with improved numerical and programming techniques. This is especially true when analyzing large, complex structures under severe thermal effects since the analyses need to be carried out for long durations and involve full-size system matrices which result in prohibitive computer storage and analysis costs.

Literature review indicates that reduced-basis methods have been used extensively to provide very efficient solutions to large-scale structural problems, and to some extent even for thermal problems. The modal methods use a reduced set of the lower eigenmodes directly as the basis vectors. The effectiveness of the FDM, measured by the reduction achieved in a multitude of structural problems as well as in a linear thermal problem, is very impressive. Nevertheless, the method has heretofore never been applied to nonlinear thermal analysis. The FDM has therefore been chosen as the reduction technique in this research effort.

The primary objective of this study is to develop and validate a solution procedure that employs the FDM to obtain the transient response for nonlinear thermal problems. The specific objective of this study is to compare numerically the efficiency (in terms of the reduction in the number of equations to be solved only) of the FDM with that of the fundamental modal method, the MDM, in obtaining the nonlinear transient thermal

response (within the desired accuracy) of a realistic structure such as the lower surface of a segment of the Shuttle wing.

1.4 Scope of Study

To achieve the aforementioned objectives, first of all a new finite element algorithm has been developed for solving nonlinear transient thermal problems, which incorporates the modal methods (ranging from the MDM to the second-order FDM) and a fixed-point iteration scheme. The modal methods have been derived in a form that can be easily implemented in existing computer programs. This fact coupled with the desire to take advantage of existing advanced finite element software, has led to the implementation of the new algorithm in the COmputational MEchanics Testbed (COMET) system [63].

The analytical solution has been used to solve the reduced system of uncoupled modal equations, thus eliminating the need to employ a finite difference approximation in time to solve the full-system of finite element equations. The solution, which is in the form of a convolution integral, is obtained by stepping in time though, in order to facilitate a piecewise linear approximation to all nonlinear quantities involved, thus minimizing the error that could result from a totally linearized approach. In this approach, the obvious restriction on the time step size is imposed by the degree of nonlinearity of the problem; unlike in conventional time-integration algorithms, where the time step size is directly dictated by the stability criteria. A study of the effect of time step size and frequency of eigensolution updates on the solution accuracy has been performed, to a limited extent, for a one-dimensional nonlinear problem.

A basic understanding of the role played by the correction terms of the higher-order modal methods in predicting the response accurately with fewer modes has been provided. Guidelines are presented to show how the relative rate of convergence of the correction terms as more modes are included in the solution, can be used to make a priori

estimate of the number of modes required. Attempts have also been made to examine the effect of the finite element mesh on the efficiency of the reduction process. Finally, to assess the applicability and the effectiveness of the FDM as a reduction technique, the method has been applied to perform the thermal analysis of the lower surface of a segment of the Shuttle wing.

A statement of the general transient heat conduction problem and the finite element formulation, both linear and nonlinear, are presented in chapter 2. For linear problems, the modal methods up to the second-order FDM, the modal coordinates for the specific case of a linearly time-varying load, and guidelines for a priori estimate of the required number of modes are all derived in chapter 3. A simplified Newton-Raphson iteration scheme, and the modified modal methods to obtain the transient response for nonlinear problems are described in detail in chapter 4. The results of linear example problems are discussed in chapter 5. Nonlinear thermal problems in one and two dimensions have been solved, and the results are discussed in chapter 6. A summary of the conclusions and suggestions for future research appear in chapter 7.

Chapter 2

GOVERNING EQUATION FOR TRANSIENT HEAT CONDUCTION

In this chapter, a finite element formulation is presented for the computation of transient temperature distribution in solids with general surface heat transfer. It begins with a statement of the law of conservation of energy which considers the work done by the stresses, thermal energy transported across surfaces by conduction, thermal and mechanical energies stored within the material, and kinetic energy due to deformation.

The energy equation for a continuum in solid mechanics is

$$\frac{\partial q_i}{\partial x_i} - \sigma_{ij} \frac{\partial \epsilon_{ij}}{\partial t} + \rho \frac{\partial u}{\partial t} = Q_{int} \quad (2.1)$$

where the subscripts i and j are dummy summation indices ranging from 1 to 3, q_i are the heat flux components in the coordinate directions x_i , σ_{ij} are the stress components, ϵ_{ij} are the strain components, u is the unit internal energy, ρ is the density, and Q_{int} is the volumetric rate of internal heat generation. The equation indicates a thermomechanical coupling which is the conversion of mechanical to thermal energy. Extensive studies on coupled thermoelasticity have shown that this coupling effect can often be neglected in the analyses of flight structures, because the thermal energy converted from mechanical energy is insignificant compared to the external energy resulting from intensive aerodynamic heating [64]. Based on this assumption, the solid is considered undeformable and the internal energy becomes a function of temperature alone. To be specific, the term $\sigma_{ij} \frac{\partial \epsilon_{ij}}{\partial t}$ may be dropped from Eq. (2.1) and $\rho \frac{\partial u}{\partial t}$ can be expressed as $\rho \frac{\partial (cT)}{\partial t}$.

2.1 Problem Statement

With the above-mentioned simplification, the energy equation in Cartesian coordinates for a general three-dimensional anisotropic solid of volume V bounded by a surface S , Fig. 2.1, is

$$-\frac{\partial q_i}{\partial x_i} + Q_{\text{int}} = \rho \frac{\partial (cT)}{\partial t} \quad (2.2)$$

where ρ is the density, c is the specific heat, and the heat flux components are given by Fourier's law as

$$q_i = -k_{ij} \frac{\partial T}{\partial x_j} \quad (2.3)$$

The material properties ρ , c and k_{ij} may be temperature-dependent, where k_{ij} are the components of the symmetric conductivity tensor, κ . Substituting Eq. (2.3) in Eq. (2.2) we obtain the governing heat conduction equation which is solved subject to an initial condition

$$T(x_1, x_2, x_3, 0) = T_0(x_1, x_2, x_3) \quad (2.4)$$

and general boundary conditions which include prescribed boundary temperatures T_s on surface S_1 , specified surface heating on S_2 , convective heat exchange on S_3 , and incident and/or emitted radiation on S_4

$$T_s = T_1(x_1, x_2, x_3, t) \quad \text{on } S_1 \quad (2.5a)$$

$$q_i n_i = -q_s \quad \text{on } S_2 \quad (2.5b)$$

$$q_i n_i = h(T_s - T_e) \quad \text{on } S_3 \quad (2.5c)$$

$$q_i n_i = \sigma \epsilon T_s^4 - \alpha q_r \quad \text{on } S_4 \quad (2.5d)$$

The prescribed temperature, T_1 , may be a function of position and time, the specified heating rate, q_s , could be time-dependent, the convective heat transfer coefficient, h , may depend on the environment temperature, T_e , and/or time, T_s is the unknown surface temperature, σ is the Stefan-Boltzmann constant, ϵ is the surface emissivity that may be a

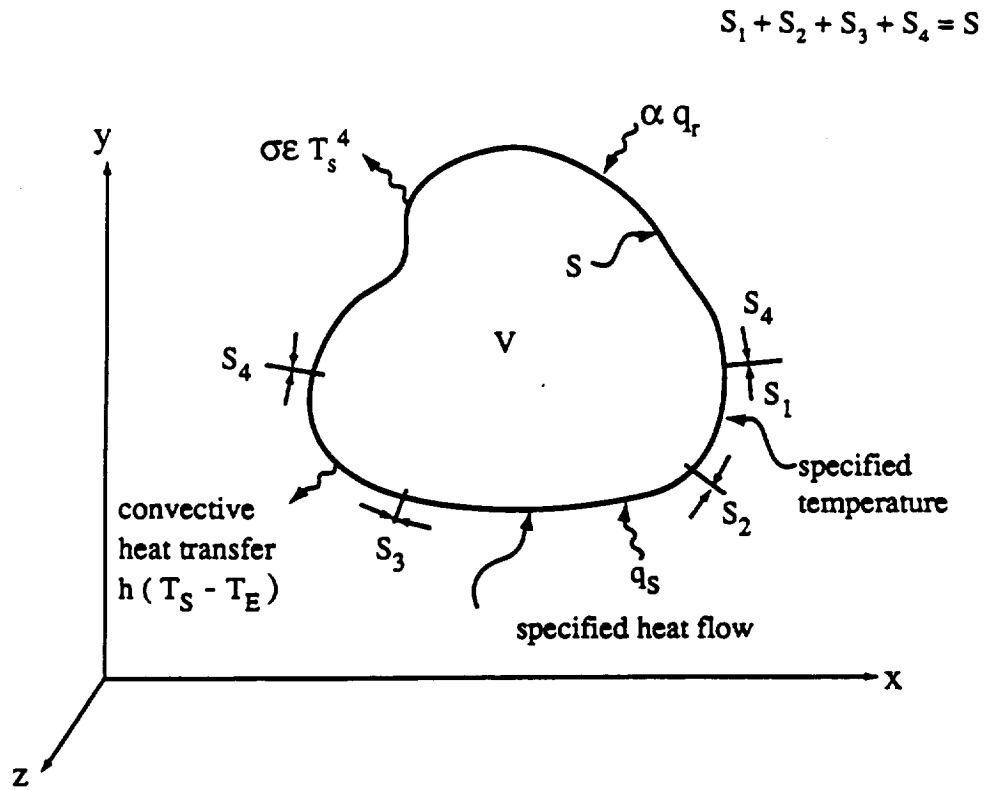


Fig. 2.1 Three-dimensional solution domain for general heat conduction.

function of T_s , α is the surface absorptivity, q_r is the rate of incident radiation per unit area, and n_j are the components of an outward unit normal vector.

2.2 Finite Element Formulation

The solution domain is discretized into elements with r nodes each. The conventional approach is to express the temperature and temperature gradients within an element in terms of the interpolation functions and their gradients. The element temperature is defined as

$$T^e(x_1, x_2, x_3, t) = N(x_1, x_2, x_3) T(t) \quad (2.6)$$

where N is the row vector of temperature interpolation functions and $T(t)$ is the column vector of nodal temperatures. The components of the temperature-gradient interpolation matrix are given by

$$B_{ij}(x_1, x_2, x_3) = \frac{\partial N_j}{\partial x_i}; \quad i = 1, 2, 3; \quad j = 1, 2, \dots, r \quad (2.7)$$

Starting with the energy equation, applying the method of weighted residuals, integrating using Gauss Divergence Theorem, and finally introducing the boundary conditions results in a set of nonlinear finite element equations given in matrix form as

$$\begin{aligned} C(T) \dot{T} + (K_c(T) + K_h(T, t) + K_r(T)) T(t) \\ = R_Q(T, t) + R_q(T, t) + R_h(T, t) + R_r(T, t) \end{aligned} \quad (2.8)$$

The details of the manipulation required to obtain Eq. (2.8) can be found in Ref. [18]. The element capacitance matrix C , and the coefficient matrices K_c and K_h related to conduction and convection respectively, are defined in Eqs. 2.9a–2.9c below, while the radiation matrix, K_r , implicitly given by Eq. (2.9d) is explicitly given in Eq. (2.9e):

$$C = \int_{V^e} \rho c N^T N dV \quad (2.9a)$$

$$K_c = \int_{V^e} B^T \kappa B dV \quad (2.9b)$$

$$\mathbf{K}_h = \int_{S_3} h \mathbf{N}^T \mathbf{N} dS \quad (2.9c)$$

$$\mathbf{K}_r T = \int_{S_4} \sigma \epsilon T^4 \mathbf{N}^T dS \quad (2.9d)$$

$$\mathbf{K}_r = \int_{S_4} \sigma \epsilon T^3 \mathbf{N}^T \mathbf{N} dS \quad (2.9e)$$

The heat load vectors due to internal heat generation, specified surface heating, surface convection and incident surface radiation, R_Q , R_q , R_h , and R_r respectively, are defined as:

$$R_Q = \int_V Q_{int} \mathbf{N}^T dV \quad (2.10a)$$

$$R_q = \int_{S_2} q_s \mathbf{N}^T dS \quad (2.10b)$$

$$R_h = \int_{S_3} h T_e \mathbf{N}^T dS \quad (2.10c)$$

$$R_r = \int_{S_4} \alpha q_r \mathbf{N}^T dS \quad (2.10d)$$

For the sake of brevity, Eq. (2.8) is hereafter written as

$$\mathbf{C}(\mathbf{T}) \dot{\mathbf{T}} + \mathbf{K}(\mathbf{T}, t) \mathbf{T}(t) = \mathbf{R}(\mathbf{T}, t) \quad (2.11)$$

where $\mathbf{K}(\mathbf{T}, t)$ is the system conductance matrix which contains the contributions from Eqs. (2.9b) - (2.9d) and $\mathbf{R}(\mathbf{T}, t)$ is the system combined load vector made up of the vectors defined in Eqs. (2.10a) - (2.10d). Equation (2.11) is a general nonlinear formulation of finite element equations for transient heat conduction in an anisotropic medium, and the solution requires an iterative scheme combined with a suitable time-integration scheme. For linear thermal problems \mathbf{K} is independent of temperature. If \mathbf{K} is further simplified to be time-independent, Eq. (2.11) becomes

$$\mathbf{C} \dot{\mathbf{T}} + \mathbf{K} \mathbf{T}(t) = \mathbf{R}(t) \quad (2.12)$$

The solution of Eq. (2.12) requires a time-integration scheme alone.

Chapter 3

THE FORCE-DERIVATIVE METHOD FOR LINEAR TRANSIENT THERMAL PROBLEMS

3.1 Unified Derivation of the Modal Methods

For the purpose of completeness, the mode-displacement method used to obtain the transient response for linear thermal problems is first presented, followed by the unified derivation of the higher-order force-derivative method assuming the forcing function possesses continuous derivatives.

3.1.1 The Mode-Displacement Method (MDM)

The governing finite element equation for a linear transient thermal problem, Eq. (2.12), is reproduced below

$$C \dot{T} + K T(t) = R(t) \quad (3.1)$$

with initial condition

$$T(0) = T_0 \quad (3.2)$$

where in general, the applied load vector R , may be time-dependent. As mentioned at the end of chapter 2, although the system matrix K can be time-dependent for linear problems, it is assumed constant in this study. The solution to the homogeneous form of the linear conduction equation Eq. (3.1) is given as

$$T(t) = e^{-\lambda_r t} \phi_r; \quad r = 1, 2, \dots, n \quad (3.3)$$

where ϕ_r is a modal vector of unknown amplitude, λ_r is the associated decay constant (analogous to the natural frequency in structural dynamics), r is a summation index and n

is the number of unconstrained degrees of freedom. Use of Eq. (3.3) in Eq. (3.1) results in the following constant eigenvalue problem (EVP):

$$\mathbf{K} \phi_r - \lambda_r \mathbf{C} \phi_r = 0; \quad r = 1, 2, \dots, n \quad (3.4)$$

where n is the total number of degrees of freedom. The eigenvectors are normalized such that

$$\phi_p^T \mathbf{C} \phi_q = \delta_{pq}; \quad p, q = 1, 2, \dots, n \quad (3.5)$$

and

$$\phi_p^T \mathbf{K} \phi_q = \delta_{pq} \lambda_{pq}; \quad p, q = 1, 2, \dots, n \quad (3.6)$$

where δ_{pq} is the Kronecker delta. In matrix form (Eqs. (3.5) and (3.6) become,

$$\Phi^T \mathbf{C} \Phi = \mathbf{I} \quad (3.7)$$

and

$$\Phi^T \mathbf{K} \Phi = \Lambda \quad (3.8)$$

where \mathbf{I} is the identity matrix and Λ is a diagonal matrix with entries that are the eigenvalues. The homogeneous solution to Eq. (3.1) in the form of a modal summation is given by

$$\mathbf{T}(t) = \sum_{r=1}^n \phi_r z_r(t) \quad (3.9)$$

where the solution is expressed as a linear combination of all the eigenvectors of the system weighted by the unknown modal coordinates.

Substitution of Eq. (3.9) in Eq. (3.1), premultiplication by ϕ_r^T , and the use of the orthogonality of the modes, Eqs. (3.5) and (3.6), result in the following uncoupled modal equations:

$$\dot{z}_r(t) + \lambda_r z_r(t) = \phi_r^T \mathbf{R}(t); \quad r = 1, 2, \dots, n \quad (3.10)$$

Pre-multiplying Eq. (3.9) by $\phi_r^T C$ and setting $t = 0$, the initial condition becomes

$$z_{r0} = \phi_r^T C T_0 \quad (3.11)$$

The analytical solution to the nonhomogeneous problem represented by Eqs. (3.10) and (3.11) is given as follows:

$$z_r(t) = z_{r0} e^{-\lambda_r t} + \int_0^t e^{-\lambda_r(t-\tau)} \phi_r^T R(\tau) d\tau \quad (3.12)$$

where the integral is called the convolution of the functions $e^{-\lambda_r(t)}$ and $\phi_r^T R(t)$. Approximating the solution to Eq. (3.1) by using a truncated set of modes, one has:

$$T(t) \cong \sum_{r=1}^p \phi_r z_r(t); \quad p \leq n \quad (3.13)$$

where $z_r(t)$ is given by Eq. (3.12) and ϕ_r , and λ_r are obtained from the solution of Eq. (3.4). Rewriting Eq. (3.13) in matrix form results in

$$T(t) \cong \hat{\Phi} \hat{Z}(t) \quad (3.14)$$

where $\hat{}$ denotes a reduced set of modes. The approximate solution given by Eq. (3.13) or (3.14) is commonly referred to as the mode-displacement method (MDM) in structural dynamics.

3.1.2 The Mode-Acceleration Method (MAM)

Equation (3.10) may be rearranged as follows:

$$z_r(t) = \frac{1}{\lambda_r} \phi_r^T R(t) - \frac{1}{\lambda_r} \dot{z}_r(t) \quad (3.15)$$

So Eq. (3.9) becomes

$$T(t) = \sum_{r=1}^n \phi_r \frac{1}{\lambda_r} \phi_r^T R(t) - \sum_{r=1}^n \phi_r \frac{1}{\lambda_r} \dot{z}_r(t) \quad (3.16)$$

Using the orthogonality of the modes and taking the inverse of the square matrix on either side of Eq. (3.8) yields

$$\Phi^{-1} \mathbf{K}^{-1} \Phi^{-T} = \frac{1}{\Lambda} \quad (3.17)$$

Pre- and post-multiplying both sides of the above equation by Φ and Φ^T , and noting that $\Phi \Phi^{-1} = \Phi^{-1} \Phi = \mathbf{I}$, leads to the following identity:

$$\mathbf{K}^{-1} = \Phi \frac{1}{\Lambda} \Phi^T \quad (3.18)$$

or

$$\mathbf{K}^{-1} = \sum_{r=1}^n \phi_r \frac{1}{\lambda_r} \phi_r^T \quad (3.19)$$

Now Eq. (3.16) may be written as follows:

$$\mathbf{T}(t) = \mathbf{K}^{-1} \mathbf{R}(t) - \sum_{r=1}^n \phi_r \frac{1}{\lambda_r} \dot{z}_r(t) \quad (3.20)$$

The Leibnitz's rule for differentiation of an integral states that if $f(\chi, \varphi)$ and $\frac{\partial f(\chi, \varphi)}{\partial \varphi}$ are continuous functions of χ and φ , then

$$\frac{d}{d\varphi} \left[\int_{\mu(\varphi)}^{\psi(\varphi)} f(\chi, \varphi) d\chi \right] = \int_{\mu(\varphi)}^{\psi(\varphi)} \frac{\partial f(\chi, \varphi)}{\partial \varphi} d\chi - \frac{d\mu}{d\varphi} f[\mu(\varphi), \varphi] + \frac{d\psi}{d\varphi} f[\psi(\varphi), \varphi] \quad (3.21)$$

provided μ and ψ have a continuous first-order derivative with respect to φ . If the forcing function is C^0 continuous, then the Leibnitz's rule can be applied to Eq. (3.12) to replace the term $\dot{z}_r(t)$ in Eq. (3.20) as follows:

$$\dot{z}_r(t) = \phi_r^T \mathbf{R}(t) - \lambda_r z_{r0} e^{-\lambda_r t} - \lambda_r \int_0^t e^{-\lambda_r(t-\tau)} \phi_r^T \mathbf{R}(\tau) d\tau \quad (3.22)$$

Substituting Eq. (3.22) in Eq. (3.20) and rearranging gives:

$$\mathbf{T}(t) = \sum_{r=1}^n \phi_r z_r(t) + \left(\mathbf{K}^{-1} - \sum_{r=1}^n \phi_r \frac{1}{\lambda_r} \phi_r^T \right) \mathbf{R}(t) \quad (3.23)$$

Now introduce an approximation to the solution by using only a subset of the modes, so that

$$T(t) \equiv \sum_{r=1}^p \phi_r z_r(t) + \left(K^{-1} - \sum_{r=1}^p \phi_r \frac{1}{\lambda_r} \phi_r^T \right) R(t); \quad p \leq n \quad (3.24)$$

or, in matrix notation

$$T(t) \equiv \hat{\Phi} \hat{Z}(t) + \left(K^{-1} - \frac{\hat{\Phi} \frac{1}{\hat{\Lambda}} \hat{\Phi}^T}{\hat{\Lambda}} \right) R(t) \quad (3.25)$$

Equations (3.24) and (3.25) are alternate forms of the MAM, where the second term represents the first-order correction to the approximate solution given by the MDM, Eqs. (3.13) and (3.14).

3.1.3 The Force-Derivative Method

Assuming sufficient regularity, Eq. (3.15) may be differentiated once with respect to time to obtain

$$\dot{z}_r(t) = \frac{1}{\lambda_r} \phi_r^T \dot{R}(t) - \frac{1}{\lambda_r} \dot{z}_r(t) \quad (3.26)$$

Substituting the above in Eq. (3.15) results in the following equation:

$$z_r(t) = \frac{1}{\lambda_r} \phi_r^T R(t) - \frac{1}{\lambda_r^2} \phi_r^T \dot{R}(t) + \frac{1}{\lambda_r} \dot{z}_r(t) \quad (3.27)$$

So Eq. (3.9) now becomes

$$T(t) = \sum_{r=1}^n \phi_r \frac{1}{\lambda_r} \phi_r^T R(t) - \sum_{r=1}^n \phi_r \frac{1}{\lambda_r^2} \phi_r^T \dot{R}(t) + \sum_{r=1}^n \phi_r \frac{1}{\lambda_r} \dot{z}_r(t) \quad (3.28)$$

Again, based on the orthogonality of the modes, the following identity can be established:

$$K^{-1} C K^{-1} = \Phi \frac{1}{\Lambda^2} \Phi^T \quad (3.29)$$

or

$$K^{-1} C K^{-1} = \sum_{r=1}^n \phi_r \frac{1}{\lambda_r^2} \phi_r^T \quad (3.30)$$

so that

$$T(t) = \mathbf{K}^{-1} \mathbf{R}(t) - \mathbf{K}^{-1} \mathbf{C} \mathbf{K}^{-1} \dot{\mathbf{R}}(t) + \sum_{r=1}^n \phi_r \frac{1}{\lambda_r^2} \ddot{z}_r(t) \quad (3.31)$$

If the forcing function is C^1 continuous, employ the Leibnitz's rule for differentiation, Eq. (3.21), to evaluate $\ddot{z}_r(t)$ given in Eq. (3.31) results in

$$\ddot{z}_r(t) = -\lambda_r \phi_r^T \mathbf{R}(t) + \phi_r^T \dot{\mathbf{R}}(t) + \lambda_r^2 z_{r0} e^{-\lambda_r t} + \lambda_r^2 \int_0^t e^{-\lambda_r(t-\tau)} \phi_r^T \mathbf{R}(\tau) d\tau \quad (3.32)$$

Using Eq. (3.32) in Eq. (3.31) and rearranging results in

$$T(t) = \sum_{r=1}^n \phi_r z_r(t) + \left(\mathbf{K}^{-1} - \sum_{r=1}^n \phi_r \frac{1}{\lambda_r} \phi_r^T \right) \mathbf{R}(t) + \left(-\mathbf{K}^{-1} \mathbf{C} \mathbf{K}^{-1} + \sum_{r=1}^n \phi_r \frac{1}{\lambda_r^2} \phi_r^T \right) \dot{\mathbf{R}}(t) \quad (3.33)$$

Again, approximating the response by using a subset of the modes for the summation terms in Eq. (3.33) one obtains:

$$\begin{aligned} T(t) \equiv & \sum_{r=1}^p \phi_r z_r(t) + \left(\mathbf{K}^{-1} - \sum_{r=1}^p \phi_r \frac{1}{\lambda_r} \phi_r^T \right) \mathbf{R}(t) \\ & + \left(-\mathbf{K}^{-1} \mathbf{C} \mathbf{K}^{-1} + \sum_{r=1}^p \phi_r \frac{1}{\lambda_r^2} \phi_r^T \right) \dot{\mathbf{R}}(t) \end{aligned} \quad (3.34)$$

or, in matrix form

$$\begin{aligned} T(t) \equiv & \hat{\Phi} \hat{\mathbf{Z}}(t) + \left(\mathbf{K}^{-1} - \hat{\Phi} \frac{1}{\hat{\Lambda}} \hat{\Phi}^T \right) \mathbf{R}(t) \\ & + \left(-\mathbf{K}^{-1} \mathbf{C} \mathbf{K}^{-1} + \hat{\Phi} \frac{1}{\hat{\Lambda}^2} \hat{\Phi}^T \right) \dot{\mathbf{R}}(t) \end{aligned} \quad (3.35)$$

Equation (3.34) or (3.35) is the response by the second-order FDM, where the third term represents the second-order correction to the approximate solution given by the MAM, Eqs. (3.24) and (3.25).

In general, for a C^j continuous forcing function, the highest $(j+1)$ th order FDM for approximating the response is given as follows:

$$T(t) \equiv \hat{\Phi} \hat{Z}(t) + \sum_{m=1}^{j+1} \left[\left((-K^{-1}C)^{m-1} K^{-1} + \hat{\Phi} (-\hat{\Lambda})^{-m} \hat{\Phi}^T \right) R^{(m-1)}(t) \right] \quad (3.36)$$

where the superscript in parentheses of $R(t)$ denotes the order of differentiation with respect to time.

The major advantage in using the analytical solution, Eq. (3.12), of the uncoupled modal equations is that when the load vector is available as a function of time such that exact integration is possible, the solution at any time can be obtained directly with time $t = 0$ as the initial condition. Furthermore, the only source of error is the truncation of modes which can be alleviated by the proper selection of modes. However, when the heat load vector is a function of time that cannot be integrated exactly, numerical time integration is required and the time step size for a desired accuracy will depend on the order of the numerical integration method used. The following section describes how to obtain the modal coordinates for a specific type of load.

3.2 Modal Coordinates for a Linearly Time-Varying Load

If the applied load varies linearly with time and has a constant slope over the entire time domain as shown in Fig. 3.1, then the modal coordinates given by Eq. (3.12) can be obtained by exact integration. Rewriting Eq. 3.12 for this case one obtains:

$$z_r(t) = z_{r0} e^{-\lambda_r t} + \int_0^t e^{-\lambda_r(t-\tau)} \phi_r^T R(\tau) d\tau \quad (3.37)$$

where

$$R(\tau) = R(0) + \dot{R}(0) \tau; \quad 0 \leq \tau \leq t \quad (3.38)$$

It is clear from Fig. (3.1) that $R(0)$ is the initial load vector and $\dot{R}(0)$ represents the constant slope. Substituting Eq. (3.38) in Eq. (3.37) and expanding results in:

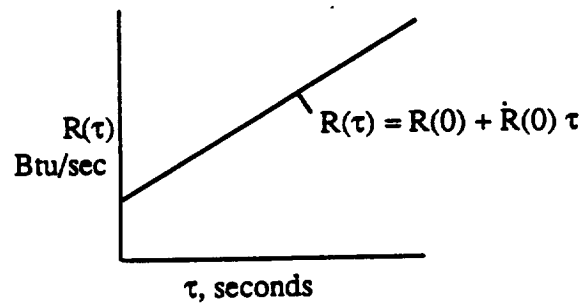


Fig. 3.1 Forcing function that varies linearly with time.

$$\begin{aligned}
z_r(t) = & z_{r0} e^{-\lambda_r t} + \phi_r^T R(0) \int_0^t e^{-\lambda_r(t-\tau)} d\tau \\
& + \phi_r^T \dot{R}(0) \int_0^t \tau e^{-\lambda_r(t-\tau)} d\tau
\end{aligned} \tag{3.39}$$

Using integration by parts and regrouping the terms, one has

$$z_r(t) = z_{r0} e^{-\lambda_r t} + \frac{\phi_r^T}{\lambda_r} \left\{ R(0) \left(1 - e^{-\lambda_r t} \right) + \dot{R}(0) \left(t - \frac{1 - e^{-\lambda_r t}}{\lambda_r} \right) \right\} \tag{3.40}$$

Now consider a more general case where the applied load vector can be treated as a series of piecewise linear functions of time with varying slopes over the entire time domain. Then Eq. (3.40) can be applied individually to each time interval, dt , using the modal coordinates obtained at the end of the previous time interval as the initial condition. Accordingly, Eq. (3.37) may be modified as follows:

$$z_{n,r} = z_{n-1,r} e^{-\lambda_r dt} + \int_0^{dt} e^{-\lambda_r(dt-\tau)} \phi_r^T R(\tau) d\tau \tag{3.41}$$

where
$$R(\tau) = R_{n-1} + \dot{R}_{n-1}\tau \quad 0 \leq \tau \leq dt \tag{3.42}$$

Similarly, it can be shown that eq. (3.40) now becomes

$$z_{n,r} = z_{n-1,r} e^{-\lambda_r dt} + \phi_r^T \left\{ \left(R_{n-1} - \frac{1}{\lambda_r} \dot{R}_{n-1} \right) \left(\frac{1 - e^{-\lambda_r dt}}{\lambda_r} \right) + \frac{dt}{\lambda_r} \dot{R}_{n-1} \right\} \tag{3.43}$$

3.3 A Priori Estimate of the Required Number of Modes

To minimize the computational costs associated with the complete solution of the EVP, some guidelines are presented below on selecting the number of modes prior to the actual solution process. These guidelines are limited to linear transient thermal problems.

The error introduced in solving Eq. (3.1) by the MDM, Eq. (3.13), can be evaluated based on the level of approximation of the heat load vector represented by that

subset of modes [65]. The participation factor of the r th mode, η_r , at time, t , is defined as follows:

$$\eta_r(t) = \phi_r^T R(t) \quad (3.44)$$

which gives a measure of the significance of that mode in representing the total load and hence the response. Pre-multiplying Eq. (3.44) by $C\phi_r$, and using the orthogonal property of the modes with respect to C , the approximate load vector is given by

$$\hat{R}(t) \equiv \sum_{r=1}^p C\phi_r \eta_r(t); \quad p < n \quad (3.45)$$

Once a desired level of approximation of the load vector has been attained, the generation of modes may be terminated. The error, e_1 , in the load vector represented by the truncated set of modes is given by

$$e_1 = \sqrt{\frac{R(t)^T (R(t) - \hat{R}(t))}{R(t)^T R(t)}} \quad (3.46)$$

If a direct relationship between the errors in the solution and the load vectors can be established then Eq. (3.46) may be used to obtain a priori estimate of the number of modes required by the MDM to achieve a desired degree of solution accuracy.

To determine the truncation of modes for the higher-order methods, which has not been studied in the past, the corrections offered by these methods to the MDM is considered. The full-system solution may be split into two parts given as follows:

$$T(t) = \sum_{r=1}^p \phi_r z_r(t) + \sum_{r=p+1}^n \phi_r z_r(t) \quad (3.47)$$

where the first term is the approximate solution given by the MDM, and the second term represents the contribution of the higher modes neglected by the MDM. As before, using the orthogonality conditions and assuming the transient load vector has continuous derivatives up to order j , it can be shown that

$$\begin{aligned} \sum_{r=p+1}^n \phi_r z_r(t) &= \sum_{r=p+1}^n \phi_r \frac{1}{\lambda_r} \phi_r^T R(t) - \sum_{r=p+1}^n \phi_r \frac{1}{\lambda_r^2} \phi_r^T \dot{R}(t) + \sum_{r=p+1}^n \phi_r \frac{1}{\lambda_r^3} \phi_r^T \ddot{R}(t) \\ &\quad - \dots + \sum_{r=p+1}^n (-1)^j \phi_r \frac{1}{(\lambda_r)^{j+1}} R^{(j)}(t) + \sum_{r=p+1}^n (-1)^{j+1} \phi_r \frac{1}{(\lambda_r)^{j+1}} z^{(j+1)}(t) \end{aligned} \quad (3.48)$$

For the specific case where the load vector has non-zero derivatives up to first-order only, that is, $j = 1$ in Eq. (3.48), neglecting the last term in Eq. (3.48), one has:

$$\sum_{r=p+1}^n \phi_r z_r(t) \equiv \sum_{r=p+1}^n \phi_r \frac{1}{\lambda_r} \phi_r^T R(t) - \sum_{r=p+1}^n \phi_r \frac{1}{\lambda_r^2} \phi_r^T \dot{R}(t) \quad (3.49)$$

It is easily recognized that the first term on the right-hand side of Eq. (3.49) is the correction offered by the MAM, Eq. (3.24), and will hereafter be referred to as CMAM for brevity. That is

$$\text{CMAM} = \sum_{r=p+1}^n \phi_r \frac{1}{\lambda_r} \phi_r^T R(t) \quad (3.50)$$

or

$$\text{CMAM} = \mathbf{K}^{-1} R(t) - \sum_{r=1}^p \phi_r \frac{1}{\lambda_r} \phi_r^T R(t) \quad (3.51)$$

Thus, by adding the contribution of the higher modes as well to the pseudo steady-state response, the MAM yields a better approximation of the total transient response than the MDM.

In a given spectrum, the magnitude of the eigenvalues successively increases. Examination of Eq. (3.50) indicates that at a given time, the significance of CMAM should decrease when higher modes are included in the MDM, as the eigenvalue appears in the denominator. In other words, the lower modes play a more important role in approximating the pseudo steady-state response. Based on this fact, the number of modes required to realize the maximum benefits of the MAM can be determined when the pseudo steady-state response has been approximated within a desired accuracy.

Alternatively, similar to Eq. (3.46), a measure of the error, e_2 , in the representation of $\mathbf{K}^{-1} \mathbf{R}(t)$ by the lower modes can be obtained as follows:

$$e_2 = \sqrt{\frac{(\mathbf{K}^{-1} \mathbf{R}(t))^T \left(\mathbf{K}^{-1} \mathbf{R}(t) - \hat{\Phi} \frac{1}{\hat{\Lambda}} \hat{\Phi}^T \mathbf{R}(t) \right)}{(\mathbf{K}^{-1} \mathbf{R}(t))^T \mathbf{K}^{-1} \mathbf{R}(t)}} \quad (3.52)$$

The second term on the right-hand side of Eq. (3.49) can be identified as the correction offered by the second-order FDM, Eq. (3.34), to the MAM and will be referred to as CFDM for brevity, that is,

$$\text{CFDM} = - \sum_{r=p+1}^n \phi_r \frac{1}{\lambda_r^2} \phi_r^T \dot{\mathbf{R}}(t) \quad (3.53)$$

or

$$\text{CFDM} = - \mathbf{K}^{-1} \mathbf{C} \mathbf{K}^{-1} \dot{\mathbf{R}}(t) + \sum_{r=1}^p \phi_r \frac{1}{\lambda_r^2} \phi_r^T \dot{\mathbf{R}}(t) \quad (3.54)$$

By including the contribution of the higher modes in approximating the first-order transient response, $-\mathbf{K}^{-1} \mathbf{C} \mathbf{K}^{-1} \dot{\mathbf{R}}(t)$, derived from the pseudo steady-state solution, the FDM enhances the MAM. At a given time, the magnitude of CFDM declines at a faster rate than that of CMAM since the square of the eigenvalue appears in the denominator. This makes the selection of modes more and more distinct as the order of the method increases. Similar to the MAM, the number of modes necessary for the convergence of the FDM is determined when $-\mathbf{K}^{-1} \mathbf{C} \mathbf{K}^{-1} \dot{\mathbf{R}}(t)$ is approximated by the lower modes within a specified tolerance, or the error norm, e_3 , given below becomes acceptable:

$$e_3 = \sqrt{\frac{(\mathbf{K}^{-1} \mathbf{C} \mathbf{K}^{-1} \dot{\mathbf{R}}(t))^T \left(\mathbf{K}^{-1} \mathbf{C} \mathbf{K}^{-1} \dot{\mathbf{R}}(t) - \hat{\Phi} \frac{1}{\hat{\Lambda}^2} \hat{\Phi}^T \dot{\mathbf{R}}(t) \right)}{(\mathbf{K}^{-1} \mathbf{C} \mathbf{K}^{-1} \dot{\mathbf{R}}(t))^T (\mathbf{K}^{-1} \mathbf{C} \mathbf{K}^{-1} \dot{\mathbf{R}}(t))}} \quad (3.55)$$

Although higher-order corrections involve the eigenvalues raised to successively higher negative exponents, they need not necessarily be negligible compared to the

lower-order corrections at all times, because they are dependent on the transient nature of the load as well. With just one mode included in the solution, a comparison of the norm of CMAM and CFDM, Eqs. (3.51) and (3.54) respectively, indicates their relative importance at that particular time. This rate of convergence with respect to modes depends on the nature of the variation of the eigenvalues within the spectrum. For a linear thermal problem subject to a specified transient load, it is thus possible to select the higher-order method which can achieve the maximum reduction at any given time.

Chapter 4

METHOD OF SOLUTION FOR NONLINEAR TRANSIENT THERMAL PROBLEMS

4.1 Linearization of the System of Equations

After a brief introduction to the Newton-Raphson scheme, its application to the nonlinear, transient heat transfer equation is described and the simplifying assumptions made in this study are highlighted. Although the final linearized form can be obtained by a direct application of the fixed-point iteration scheme, the details are presented here to aid in the future use of a rigorous form of the Newton-Raphson scheme.

4.1.1 Derivation of the Newton-Raphson Method

Consider a typical nonlinear set of equations of the form

$$F(T) = 0 \quad (4.1)$$

If \bar{T} is the exact solution vector, then Eq. (4.1) is satisfied identically. However, often one cannot compute the exact solution, but can obtain an approximate solution so that the unbalance in a typical equation is smaller than a specified tolerance. This is achieved by the Newton-Raphson scheme which is derived below by an intuitive approach based upon the Taylor polynomial [66].

Suppose that F is twice continuously differentiable in the interval $[a,b]$. Let $T \in [a,b]$ be an approximation to \bar{T} such that $F'(T)$ is non-singular and the difference between \bar{T} and T is small. Considering the second-degree polynomials for $F(\bar{T})$, expanded about T one has:

$$F(\bar{T}) = F(T) + F'(T)(\bar{T}-T) + \frac{(\bar{T}-T)^2}{2} F''(\xi(T))(\bar{T}-T) \quad (4.2)$$

where $\xi(T)$ lies between \bar{T} and T . But $F(\bar{T}) = 0$, and since the difference between \bar{T} and T is assumed to be small, square of the difference is even smaller and can be assumed negligible. Then,

$$0 = F(T) + F'(\bar{T})(\bar{T}-T) \quad (4.3)$$

which gives

$$\bar{T} = T - F'(\bar{T})^{-1} F(T) \quad (4.4)$$

which is a better approximation to \bar{T} than T . This sets the stage for the Newton-Raphson method, which involves generating the sequence of iterates T^i defined by

$$T^i = T^{i-1} - F'(T^{i-1})^{-1} F(T^{i-1}), \quad i \geq 1 \quad (4.5)$$

which may be rewritten as

$$J^{i-1} \Delta T^i = -F^{i-1} \quad (4.6)$$

where

$$J^{i-1} = F'(T^{i-1}) = \left(\frac{\partial F}{\partial T} \right)_{T^{i-1}} \quad (4.7)$$

is called the Jacobian matrix and

$$\Delta T^i = T^i - T^{i-1} \quad (4.8)$$

It is clear that Newton's method cannot be continued if the Jacobian is singular for some i . The method is most effective when J is bounded away from zero near the fixed point. Although Newton's method will sometimes converge even with a very poor initial approximation, in many cases it is imperative that a good initial approximation be chosen. Also, Newton's method will converge quadratically under suitable conditions on F . In fact, Newton's method can be derived as a special case of the fixed-point iteration scheme which exhibits linear convergence in general.

In practice, the method is generally performed in a two-step manner. First a vector ΔT^i is found which satisfies Eq. (4.6). Once this is accomplished, the new approximation T^i is obtained from Eq. (4.8). A difficulty in this method arises from the necessity to invert the Jacobian matrix during each iteration which involves reforming and factorization at each iteration, making the method computationally expensive for large sets of equations. In a modified form of the method, the Jacobian is formed and factored only once and is held constant throughout the balance of the iteration process [18]. More iterations are required with the modified method, but usually net computational costs are reduced.

4.1.2 Application of the Newton-Raphson Method with Simplifications

The discrete nonlinear transient heat conduction equation at any time t , Eq. (2.11) is reproduced below:

$$C(T) \dot{T} + K(T,t) T(t) = R(T,t) \quad (4.9)$$

The residual or unbalanced load in the nonlinear system of equations at the $(i-1)$ th iteration is given by,

$$F(T^{i-1}, T^{i-1}) = C(T^{i-1}) \dot{T}^{i-1} + K(T^{i-1}, t) T^{i-1}(t) - R(T^{i-1}, t) \quad (4.10)$$

Simplifying the notation, a typical p th equation of this system is given by,

$$F_p^{i-1} = C_{pm}^{i-1} \dot{T}_m^{i-1} + K_{pm}^{i-1}(t) T_m^{i-1}(t) - R_p^{i-1}(t); \quad p = 1, 2 \dots n \quad (4.11)$$

where m is a dummy summation index, and n is the total number of equations. The sequence of successive iterates generated by Newton's method for the temperature and its time derivative increments is then given by

$$J_{1ps}^{i-1} \Delta T_s^i + J_{2ps}^{i-1} \Delta \dot{T}_s^i = -F_p^{i-1} \quad (4.12)$$

where J_1 and J_2 are the Jacobians associated with temperature and its time derivative, respectively, and are defined according to Eq. (4.7) as follows:

$$J_{1ps}^{i-1} = \left(\frac{\partial F_p}{\partial T_s} \right)_{T}^{i-1} \text{ and } J_{2ps}^{i-1} = \left(\frac{\partial F_p}{\partial T_s} \right)_{T}^{i-1} \quad (4.13)$$

The new values of the unknowns at the end of the current iteration will then be

$$T_s^i = T_s^{i-1} + \Delta T_s^i \text{ and } T_m^i = T_m^{i-1} + \Delta T_m^i \quad (4.14)$$

While the right hand side of Eq. (4.12) is given directly in Eq. (4.10), the product terms involving the Jacobians on the left hand side of Eq. (4.12) are derived from Eqs. (4.13) and (4.10) using the chain rule of differentiation as follows

$$J_{1ps}^{i-1} \Delta T_s^i = C_{pm}^{i-1} \left(\frac{\partial T_m}{\partial T_s} \right)^{i-1} \Delta T_s^i = C_{pm}^{i-1} \delta_{ms} \Delta T_s^i = C_{ps}^{i-1} \Delta T_s^i \quad (4.15)$$

and

$$\begin{aligned} J_{2ps}^{i-1} \Delta T_s^i &= \left(\frac{\partial C_{pm}}{\partial T_s} \right)^{i-1} T_m^{i-1} \Delta T_s^i + K_{pm}^{i-1} \left(\frac{\partial T_m}{\partial T_s} \right)^{i-1} \Delta T_s^i \\ &+ \left(\frac{\partial K_{pm}}{\partial T_s} \right)^{i-1} T_m^{i-1} \Delta T_s^i - \left(\frac{\partial R_p}{\partial T_s} \right)^{i-1} \Delta T_s^i \end{aligned} \quad (4.16)$$

Equation (4.12) now becomes

$$C_{ps}^{i-1} \Delta T_s^i + [\Delta C_{ps} + K_{ps} + \Delta K_{ps} - \Delta R_{ps}]^{i-1} \Delta T_s^i = -F_p^{i-1} \quad (4.17)$$

The incremental temperature-dependent system matrices and load vector are given by

$$\Delta C_{ps}^{i-1} = \left(\frac{\partial C_{pm}}{\partial T_s} \right)^{i-1} T_m^{i-1} \quad (4.18)$$

$$\Delta K_{ps}^{i-1} = \left(\frac{\partial K_{pm}}{\partial T_s} \right)^{i-1} T_m^{i-1} \quad (4.19)$$

$$\Delta R_{ps}^{i-1} = \left(\frac{\partial R_p}{\partial T_s} \right)^{i-1} \quad (4.20)$$

Dropping the indicial notation, Eq. (4.17) may be rewritten as follows:

$$C^{i-1} \Delta T^i + [\Delta C + K + \Delta K - \Delta R]^{i-1} \Delta T^i = -F^{i-1} \quad (4.21)$$

It is seen that the Jacobian associated with temperature involves the increments in the system nonlinear capacitance, conductance matrices and load vector, namely ΔC , ΔK

and ΔR . These increments reflect the change in material properties with temperature, and generally have a minor effect on the accuracy of the Jacobian J_2 [24]. The matrix ΔR includes the effect of radiation exchange as well. The evaluation of these incremental matrices is cumbersome and prohibitively expensive. Even though the system matrices C and K are symmetric their increments are not, and ΔR is unsymmetric as well. Consequently, the iterative solution requires an unsymmetric solver. Moreover, evaluation of the true Jacobian requires additional knowledge about the nature of nonlinearities and identification of element types. Therefore, for ease of implementation, the Jacobian is approximated by the conductance matrix alone neglecting the incremental quantities, which is exact if material properties are not temperature-dependent and there is no radiation exchange. This makes computation of the Jacobian, as well as the solution of the linearized system of equations easier as matrix symmetry is maintained, albeit convergence could be slower. Introducing this modification in Eq. (4.21), we now have

$$C^{i-1} \Delta T^i + K^{i-1} \Delta T^i = -F^{i-1} \quad (4.22)$$

where

$$K = K_c + K_h + 4 K_r \quad (4.23)$$

Substituting for ΔT^i and ΔT^i from Eq.(4.14), using Eq. (4.10) and simplifying, one obtains the linearized equations given as follows:

$$C^{i-1} T^i + K^{i-1}(t) T^i(t) = R^{i-1}(t) \quad (4.24)$$

where the temperatures at the current iteration, and not their increments, are the unknowns.

4.2 The Force-Derivative Method for the Transient Response

4.2.1 One-Step Approach

For constant or linearly varying transient loads, the approach used to obtain the transient response for linear problems in chapter 3 can be readily extended to solve

Eq. (4.24). Thereby, the response is computed at the time of interest in one step, with time $t = 0$ as the initial condition. The initial eigenvalue problem of Eq. (4.24) is given by,

$$\mathbf{K}_0 \Phi_0 - \Lambda_0 \mathbf{C}_0 \Phi_0 = 0 \quad (4.25)$$

where

$$\mathbf{K}_0 = \mathbf{K}(T_0) \quad \text{and} \quad \mathbf{C}_0 = \mathbf{C}(T_0) \quad (4.26)$$

However, due to the nonlinear nature of the system matrices, the eigensolution is varying with time as well. The eigenvalue problem at time t is

$$\mathbf{K}^{i-1} \Phi^{i-1} - \Lambda^{i-1} \mathbf{C}^{i-1} \Phi^{i-1} = 0 \quad (4.27)$$

which needs to be updated during the iteration process.

Assume a solution to Eq. (4.24) in the form of a modal summation

$$\mathbf{T}^i(t) = \sum_{r=1}^n \phi_r^{i-1} z_r^i(t) \quad (4.28)$$

which yields the uncoupled modal equations given as follows:

$$\dot{z}_r^i(t) + \lambda_r^{i-1} z_r^i(t) = \phi_r^{i-1 T} \mathbf{R}^{i-1}(t) \quad (4.29)$$

with initial condition

$$z_r(0) = z_{r0} = \phi_{r0}^T \mathbf{C}_0 T_0 \quad (4.30)$$

The solution to Eq. (4.29) analogous to Eq. (3.12) is given by,

$$z_r^i(t) = z_{r0} e^{-\lambda_r^{i-1} t} + \int_0^t e^{-\lambda_r^{i-1} (t-\tau)} \phi_r^{i-1 T} \mathbf{R}^{i-1}(t, \tau) d\tau \quad (4.31)$$

It is important to note that for nonlinear problems, the load vector and the system matrices, and hence the eigensolution, are functions of temperature and are therefore continually changing as the temperature distribution evolves with time. Careful inspection of Eq. (4.31) reveals that a major approximation is embedded in that equation.

Since the solution is not computed at intermediate times, the nonlinear quantities are evaluated directly as a function of $T^{i-1}(t)$, the current estimate of the temperature at the desired time of response. This essentially ignores the variation of the integrand with time due to nonlinearity, and includes only the explicit time-dependence when evaluating the integral in Eq. (4.31). Such an approximation could result in large errors for highly nonlinear problems. It is therefore imperative to introduce a time-stepping scheme so that the transient variation of the nonlinear quantities are well represented when obtaining the modal coordinates. If the transient variation of the load is of a complex nature, the one-step approach is not applicable in the first place, similar to linear problems.

4.2.2 Multi-Step Approach

Since Eq. (4.24) holds true at any instant of time, the temperature T_n^i at the current iteration at time t_n must satisfy the following equation

$$C_n^{i-1} T_n^i + K_n^{i-1} T_n^i = R_n^{i-1} \quad (4.32)$$

where, the subscript n denotes the current computation time, and the superscript i denotes the current iteration number, and the following simplifying notations are used, namely

$$K_n^{i-1} = K(T_n^{i-1}, t_n) \quad (4.33)$$

$$C_n^{i-1} = C(T_n^{i-1}) \quad (4.34)$$

$$R_n^{i-1} = R(T_n^{i-1}, t_n) \quad (4.35)$$

The solution is marched out in time from the initial temperature at time $t = 0$, and the time step is defined as follows:

$$dt = t_n - t_{n-1} \quad (4.36)$$

The initial condition to start the iteration process at each time step is given by,

$$T_n^i = T_{n-1}; \quad i = 1 \quad (4.37)$$

Although the temperature-dependent thermal properties and load vector are allowed to vary during the iterations at each time step, the eigensolution, which is determined from the converged temperature at the end of the previous time step, is held constant until convergence at the current time step. To accommodate this piecewise linear approximation of the eigensolution, the left-hand side of Eq. (4.32) is modified and the change is moved over to the right-hand side to form a corrective heat load vector $Q_{NL_n}^{i-1}$. Accordingly, we now have

$$C_{n-1} \dot{T}_n^i + K_{n-1} T_n^i = R_n^{i-1} + Q_{NL_n}^{i-1} \quad (4.38)$$

where

$$Q_{NL_n}^{i-1} = - ([K_n^{i-1} - K_{n-1}] T_n^{i-1} + [C_n^{i-1} - C_{n-1}] \dot{T}_n^{i-1}) \quad (4.39)$$

In a more general approach, Eqs. (4.38) and (4.39) may be rewritten as follows:

$$C_{n-k} \dot{T}_n^i + K_{n-k} T_n^i = R_n^{i-1} + Q_{NL_n}^{i-1} \quad (4.40)$$

and

$$Q_{NL_n}^{i-1} = - ([K_n^{i-1} - K_{n-k}] T_n^{i-1} + [C_n^{i-1} - C_{n-k}] \dot{T}_n^{i-1}) \quad (4.41)$$

where k is an integer greater than zero. Here the eigensolution is held constant over a period of several time steps, say m , depending on the severity of the nonlinearity; k indicates the number of time steps since the previous update. The applied load vector may be split into a linear component, R_{L_n} , (which may be time-dependent) and a nonlinear component $R_{NL_n}^{i-1}$. The entire right-hand side of Eq. (4.40) may be considered as a generalized heat load vector which is defined as follows:

$$Q(T_n^{i-1}, t_n) = Q_n^{i-1} = R_{L_n} + R_{NL_n}^{i-1} + Q_{NL_n}^{i-1} \quad (4.42)$$

Another major variation between the linear and nonlinear solutions is in the definition of the right-hand side load vector Eq. (4.42). For linear problems, it comprises the linear applied load vector alone, while it is rather complicated for nonlinear applications where

a nonlinear applied load vector may exist and additional corrective nonlinear terms are involved as well. The eigenvalue problem associated with Eq. (4.40) is given by,

$$\mathbf{K}_{n-k} \Phi_{n-k} - \Lambda_{n-k} \mathbf{C}_{n-k} \Phi_{n-k} = 0 \quad (4.43)$$

The modal equations now become

$$\dot{z}_{n,r}^i + \lambda_{n-k,r} z_{n,r}^i = \phi_{n-k,r}^T Q_n^{i-1} \quad (4.44)$$

with initial condition

$$z_{n-1,r} = \phi_{n-k,r}^T \mathbf{C}_{n-k} T_{n-1} \quad (4.45)$$

The solution to Eq. (4.44) is given as follows:

$$z_{n,r}^i = z_{n-1,r} e^{-\lambda_{n-k,r} t} + \int_0^t e^{-\lambda_{n-k,r} (t-\tau)} \phi_{n-k,r}^T Q(T_n^{i-1}, \tau) d\tau \quad (4.46)$$

In light of the discussion following Eq. (4.31), the error in Eq. (4.46) is expected to be small compared to the one-step solution, Eq. (4.31), for sufficiently small time steps. A truncated modal summation solution for this problem, similar to Eq. (3.13) for linear problems, is given by,

$$T_n^i \equiv \sum_{r=1}^p \phi_{n-k,r} z_{n,r}^i \quad p \ll n \quad (4.47)$$

or, in matrix form

$$T_n^i \equiv \hat{\Phi}_{n-k} \hat{Z}_n^i \quad (4.48)$$

Noting from Eq. (4.43) that the modes are now normalized with respect to \mathbf{K}_{n-k} and \mathbf{C}_{n-k} , the response given by the MAM is obtained by modifying Eq. (3.25) to yield

$$T_n^i \equiv \hat{\Phi}_{n-k} \hat{Z}_n^i + \left[\mathbf{K}_{n-k}^{-1} - \hat{\Phi}_{n-k} \frac{1}{\Lambda_{n-k}} \hat{\Phi}_{n-k}^T \right] Q_n^{i-1} \quad (4.49)$$

while that of the second-order FDM is obtained by modifying Eq. (3.35) as follows:

$$\begin{aligned}
T_n^i &\equiv \widehat{\Phi}_{n-k} \widehat{Z}_n^i + \left[K_{n-k}^{-1} - \widehat{\Phi}_{n-k} \frac{1}{\widehat{\Lambda}_{n-k}} \widehat{\Phi}_{n-k}^T \right] Q_n^{i-1} \\
&+ \left[-K_{n-k}^{-1} C_{n-k} K_{n-k}^{-1} + \widehat{\Phi}_{n-k} \frac{1}{\widehat{\Lambda}_{n-k}^2} \widehat{\Phi}_{n-k}^T \right] \dot{Q}_n^{i-1}
\end{aligned} \tag{4.50}$$

The exact first-order time derivative used in Eq. (4.50) is obtained from Eq. (4.42) as

$$\dot{Q}(T_n^{i-1}, t_n) = \dot{Q}_n^{i-1} = \dot{R}_{L_n} + \left(\frac{d(R_{NL} + Q_{NL})}{dT} \right)_n^{i-1} \tag{4.51}$$

For the purpose of easy implementation, \dot{Q}_n^{i-1} has been approximated in this study as

$$\dot{Q}_n^{i-1} \equiv \dot{R}_{L_n} \tag{4.52}$$

The truncation of modes and the replacement of \dot{Q}_n^{i-1} by \dot{R}_{L_n} are the two numerical errors in the current form of the FDM. The former can be minimized by a proper selection of $\widehat{\Phi}$ based on the discussion in Sec. (3.3). The latter can be reduced by a frequent update of $\widehat{\Phi}$ when necessary, that is, by maintaining a small value for k in Eq. (4.40).

4.3 Modal Coordinates For a Piecewise Linear Time-Varying Load

Recall that in Eq. (4.46), the nonlinear part of the generalized heat load vector is assumed constant during each time interval, and the integration is performed only for the explicit time-dependent portion. Accordingly, for a nonlinear problem when the linear part of the heat load vector, R_L , varies linearly with time Eq. (3.43) may be modified to yield,

$$\begin{aligned}
z_{n,r}^i &= z_{n-1,r} e^{-\lambda_{n-k,r} dt} + \Phi_{n-k,r}^T \left\{ \left(R_{L_{n-1}} - \frac{1}{\lambda_{n-k,r}} \dot{R}_{L_{n-1}} \right) \left(\frac{1 - e^{-\lambda_{n-k,r} dt}}{\lambda_{n-k,r}} \right) + \left(\frac{dt}{\lambda_{n-k,r}} \dot{R}_{L_{n-1}} \right) \right\} \\
&+ \Phi_{n-k,r}^T \left\{ (R_{NL_n}^{i-1} + Q_{NL_n}^{i-1}) \left(\frac{1 - e^{-\lambda_{n-k,r} dt}}{\lambda_{n-k,r}} \right) \right\}
\end{aligned} \tag{4.53}$$

The first two terms in Eq. (4.53) comprise the linear component of the modal coordinates while the third term represents the nonlinear contribution.

4.4 Convergence Criterion and Distribution Error Norm

The convergence criterion used to terminate the iteration process at any time t_n is given by,

$$\sqrt{\frac{(T_n^i - T_n^{i-1})^T (T_n^i - T_n^{i-1})}{T_n^i T_n^i}} \leq \epsilon \quad (4.54)$$

where ϵ is the specified tolerance. The distribution error norm of an approximation to the temperature vector is given by

$$e = \sqrt{\frac{(T - T^a)^T (T - T^a)}{T^T T}} \quad (4.55)$$

where T represents a full-system solution based on a well-refined mesh, and T^a is an approximation based on the first p thermal modes. Note that this error norm can only be used to evaluate a method a posteriori, and is not intended to be used to predict the number of modes necessary for convergence of the modal solution.

4.5 A Note on the Required Number of Modes

The guidelines provided in Sec. 3.3 to estimate the number of modes required for linear problems cannot be applied directly to nonlinear problems. When the system matrices and hence the eigenmodes depend on the solution vector, which in turn depends on the number of modes included and the order of the method used, the issue becomes too complex for analysis. For linear problems, the improvement in the response obtained by the MAM as compared to the MDM is given directly by the pseudo steady-state term, CMAM, Eq. (3.51). For nonlinear problems, this linear superposition of the correction terms to obtain the response by the higher-order methods is not appropriate. It is therefore necessary to get the responses by the MDM, MAM, and FDM individually,

using their respective solution vectors to evaluate the nonlinear quantities. Then the correction made by the MAM, CMAM, is given by the difference between the entire right-hand sides of Eqs. (4.49) and (4.48), that is, by the difference between the responses of the MAM and the MDM. Similarly, CFDM is obtained from Eqs. (4.50) and (4.49) as the difference between the solutions of the FDM and the MAM. For the same reasons, it can be said that the superposition of the contribution of each successive higher mode to compute the total response of all the modes is permissible only for linear problems.

4.6 A Note on the Computational Effort Involved

The three modal methods presented in Sec. 4.2.2 for solving nonlinear thermal problems have been implemented in the COMET [63] on the CONVEX C220 high-performance computer at NASA Langley Research Center. The details of the implementation, which include the construction of the execution control file, the development of independent programs called processors, etc., following the rules and syntax of the COMET, can be found in Ref. [67]. The step-by-step procedure to be followed in the solution process using the modal methods is illustrated in Appendix A. The computational effort involved in the different steps for a nonlinear problem and the simplifications that occur for a linear problem are summarized below.

The basic advantages of using the modal methods to solve thermal problems are:

1. The need to solve much fewer equations than in the full system.
2. The modal equations are uncoupled.
3. The use of the convolution integral form of the solution for the modal coordinates.

The skyline form of the symmetric conductance matrix, \mathbf{K} , is used which requires less computer storage and also less computing time for all matrix operations involving \mathbf{K} .

The main computationally intensive step for nonlinear problems is the solution of the EVP for intermediate basis updates, the frequency of which is problem-dependent. The product term $\mathbf{K}_{n-k}^{-1} \mathbf{Q}_n^{i-1}$ (Eqs. 4.49 and 4.50) involves the inverse of \mathbf{K} . It is computed, however, without actually inverting the \mathbf{K} matrix but by solving the linear set of equations $\mathbf{K}_{n-k} \mathbf{r} = \mathbf{Q}_n^{i-1}$ whose solution, \mathbf{r} , yields $\mathbf{K}_{n-k}^{-1} \mathbf{Q}_n^{i-1}$ directly. Similarly, the term $\mathbf{K}_{n-k}^{-1} \mathbf{C} \mathbf{K}_{n-k}^{-1} \mathbf{Q}_n^{i-1}$ (Eq. 4.50) involves the solution of two sets of linear equations and a matrix-vector multiplication. Note also that in this study, $\dot{\mathbf{Q}}_n^{i-1}$ has been approximated as $\dot{\mathbf{R}}_{L_n}$ in the FDM. The evaluation of $\mathbf{Q}_{NL_n}^{i-1}$, (Eq. (4.41)) and the products $\hat{\Phi} \frac{1}{\hat{\Lambda}} \hat{\Phi}^T \mathbf{Q}_n^{i-1}$ (Eqs. 4.49 and 4.50) and $\hat{\Phi} \frac{1}{\hat{\Lambda}^2} \hat{\Phi}^T \mathbf{Q}_n^{i-1}$ (Eq. 4.50) involve two matrix-vector products

each. Conventional implicit algorithms need to form and factor the left-hand side coefficient matrix and solve simultaneous algebraic equations at every time step for nonlinear problems. Although explicit algorithms avoid the solution of simultaneous equations, they require much smaller time steps so that the solution remains stable. Modal methods, however, entail only the forward reduction and backward substitution stages in the solution of simultaneous equations, as the \mathbf{K} matrix needs to be factored only with every eigenmode update and is held constant until the next update. The forward reduction and backward substitution processes could amount to significant computational effort though, when the solution is obtained in a large number of time steps.

For the FDM, \mathbf{Q}_n^{i-1} and $\dot{\mathbf{Q}}_n^{i-1}$ can be treated as multiple loads and hence $\mathbf{K}_{n-k}^{-1} \mathbf{Q}_n^{i-1}$ and $\mathbf{K}_{n-k}^{-1} \dot{\mathbf{Q}}_n^{i-1}$ can be computed in parallel. Also for any method, the modal loads $\hat{\Phi}_{n-k,r}^T \mathbf{Q}_n^{i-1}$ as well as the various matrix-vector products are good candidates for fine-grain parallel processing.

For linear problems, the procedure is much simpler. Since all system matrices are assumed time-independent for the linear case, only one eigensolution and one factorization of \mathbf{K} need to be performed. The guidelines presented in Sec. 3.3 can be

used to solve only for the desired number of eigenmodes. No iterations are required. Furthermore, if the applied load is constant or varies linearly in time at a constant rate, then no time-stepping is required either, as discussed already in Sec. 3.4, unlike nonlinear problems. Also, for the linear case, the response of the MDM and the MAM are obtained directly as by-products from the FDM. Nonlinear problems necessitate an independent run for each modal method, so that the response of that particular method is used to compute the temperature-dependent quantities which in turn affect the response.

Chapter 5

LINEAR TRANSIENT EXAMPLE PROBLEMS

Literature survey indicates that the MDM is unsuccessful in the efficient solution of transient linear thermal problems, since excitement of higher frequencies in the wide spectrum response necessitates the inclusion of almost all modes for an accurate solution [54]. On the other hand, by representing approximations of the higher eigenmodes with few vectors in the basis, the Lanczos vectors are effective in the reduction process [56]. From the derivation of the higher-order modal methods presented in chapter 3, it is clear that these methods include an increasingly better approximation of the higher modes neglected by the MDM. It is therefore expected that the MAM and the FDM are more effective reduced-basis methods than the MDM for transient thermal problems and has been demonstrated for a linear one-dimensional problem [50].

This chapter introduces the application of the modal methods to linear thermal analysis before embarking on nonlinear analysis. In the following numerical study, the methods are evaluated based on the efficiency which is measured by the number of modes necessary to represent an accurate response. The accuracy of a solution is determined based on the distribution error norm, Eq. (4.55). Since the applied load varies linearly in time, the exact modal coordinates given in Eq. (3.40) were used to predict the response at any time in one step.

5.1 Rod Subject to Convection at One End

This simple linear transient example was chosen to introduce the modal methods to thermal problems and to demonstrate the improved efficiency of the higher-order methods compared to the MDM. The rod shown in Fig. 5.1 is initially at a uniform

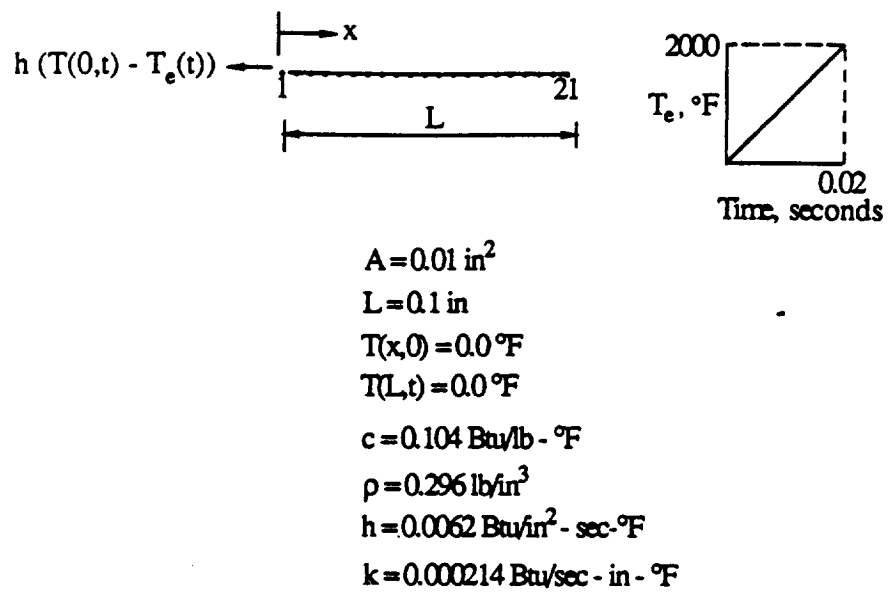


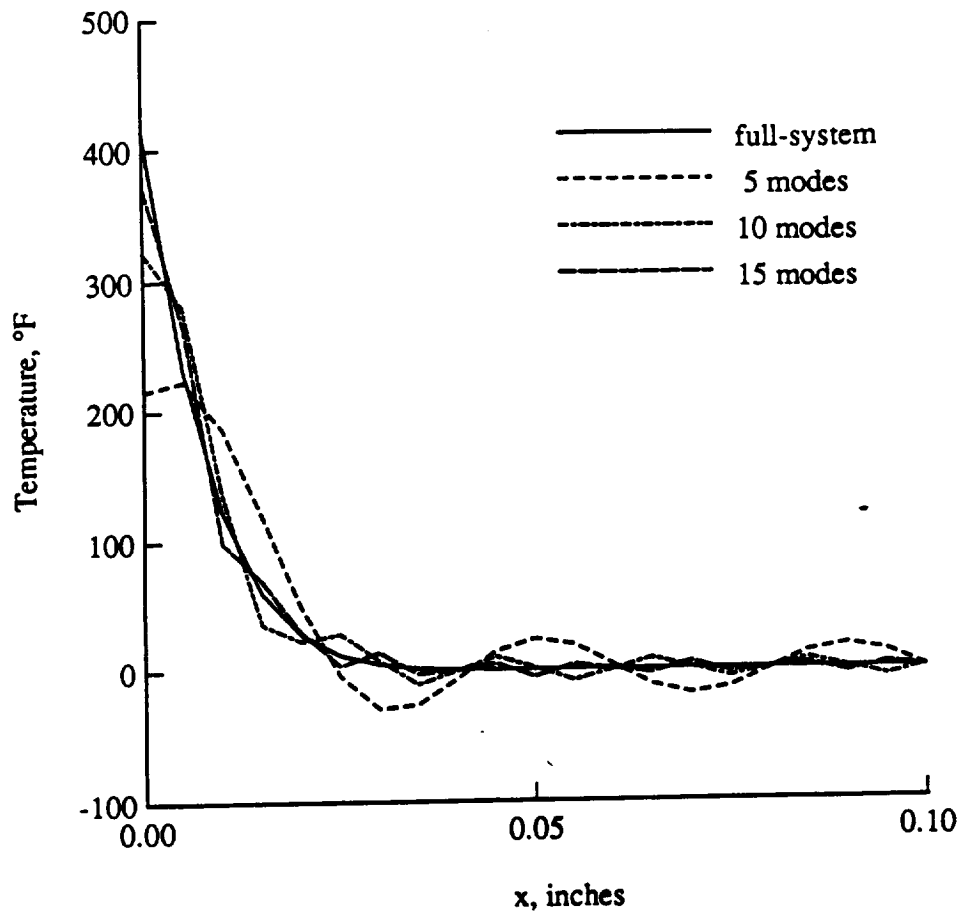
Fig. 5.1 Thermal finite element model of a rod subject to transient convective heating at one end (Linear example problem 1).

temperature of 0° F. Beginning at time zero, the left end is heated by convection while the right end is maintained at 0° F. A total of twenty elements was used to discretize the model. A forcing function that varies linearly with time was selected so that up to the second-order FDM could be applied.

Temperature distribution at an early time $t = 0.02$ sec (when the gradient is still very steep) was obtained by the three modal methods (Figs. 5.2a - 5.2c). The response predicted by the MDM is shown in Fig. 5.2a. The full-system solution, denoted by the solid line in Fig. 5.2a, results from using all twenty modes. The acceptable error corresponds to a distribution that is fairly close to the exact solution. The solution approximated by using a reduced number of five modes underpredicts the peak temperature (417° F at left end) by 49%, and the distribution along the rod is also very oscillatory in nature. When the number of modes is increased to 10 and 15, the peak temperature is underpredicted by 23% and 11% respectively. Eighteen out of the 20 modes are required by the MDM to yield a response with an acceptable error, Eq. (4.55), of 0.083.

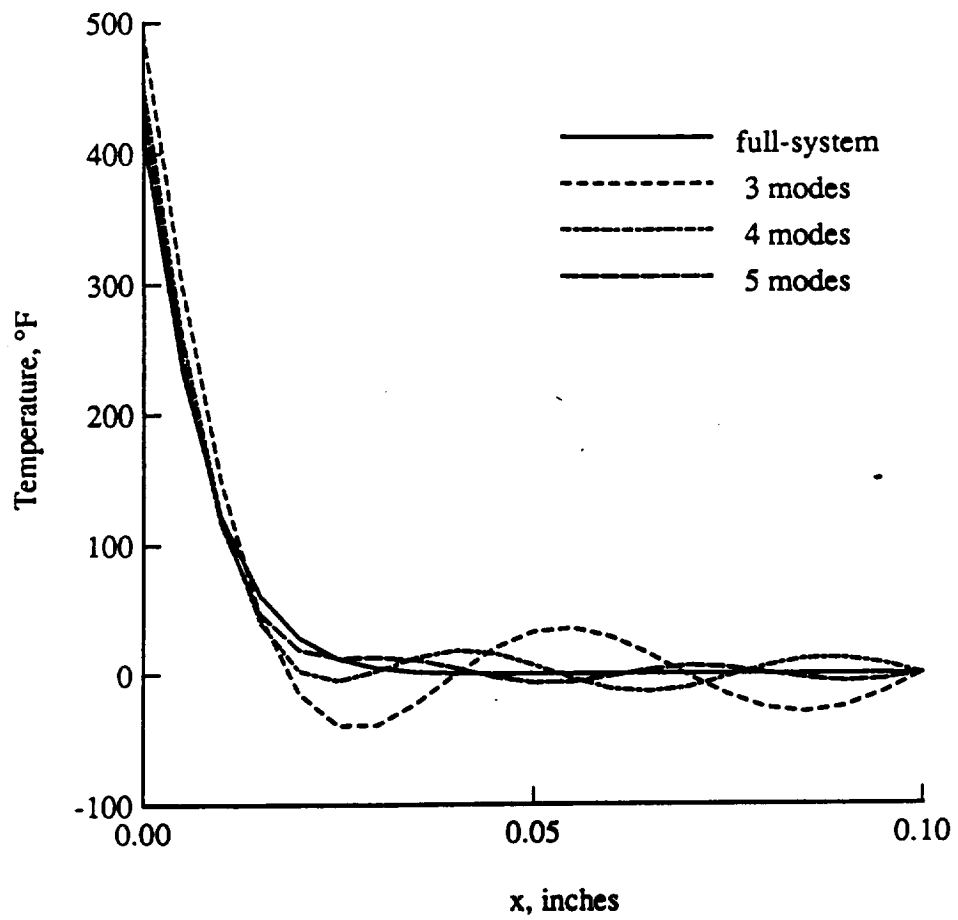
Figure 5.2b shows that the MAM overpredicts the peak temperature by 18% when using three modes and by 9% with four modes. However, with five modes the error falls within 0.08 and the oscillations in the distribution along the rod are mild. This faster convergence of the MAM compared to the MDM is due to the pseudo steady-state term which includes a first-order approximation of the higher modes that are neglected by the MDM.

A higher rate of convergence is exhibited by the FDM which has the highest error with one mode but captures the distribution accurately with as few as three modes, Fig. 5.2c. It is evident that the derivative-related term in the FDM has further improved the approximation of the higher modes compared to the MAM. The rates of convergence of the three modal methods for this linear example with a C^1 continuous applied load are



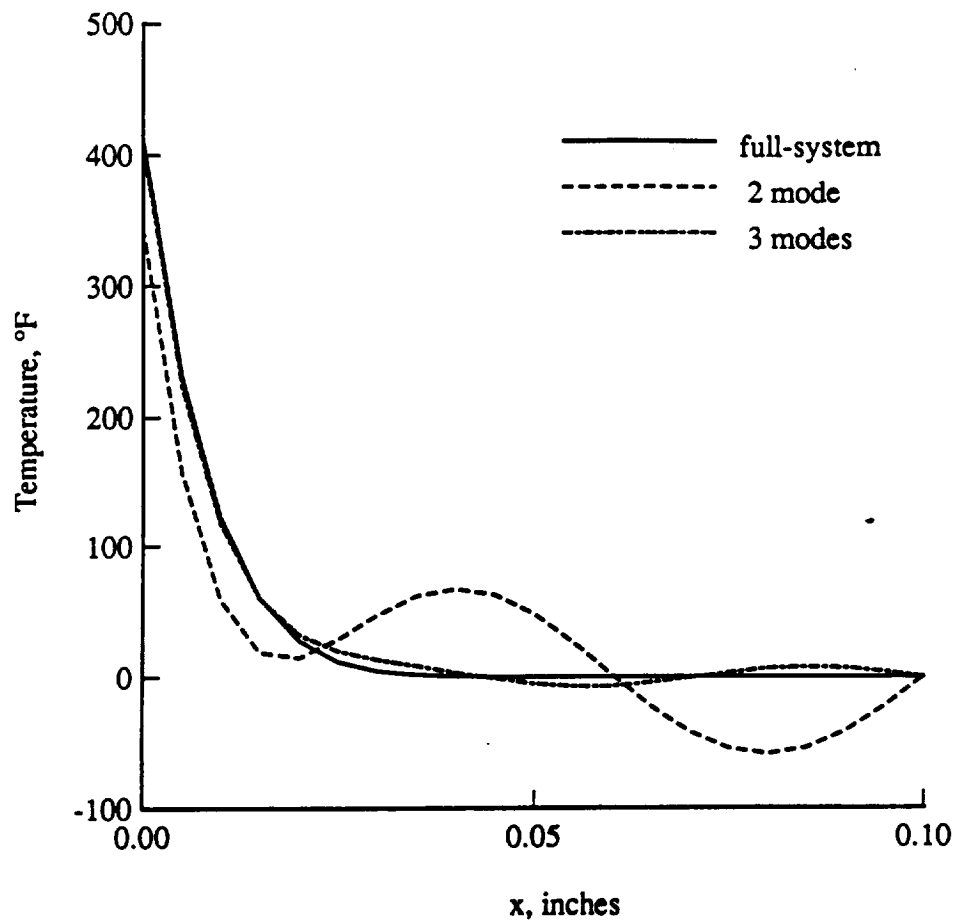
a) Mode-displacement method (MDM).

Fig. 5.2 Temperature distribution along a rod subject to transient convection at one end at time $t = 0.02$ sec (Linear example problem 1).



b) Mode-acceleration method (MAM).

Fig. 5.2 Continued.



c) Force-derivative method (FDM).

Fig. 5.2 Concluded.

compared in Fig. 5.3. While the FDM requires just 15% of the modes (3 out of 20), which means a reduction of the problem size by 85%, the MAM and the MDM have achieved a reduction in problem size of 75% and 10%, respectively.

5.2. Plate Subject to Uniform Surface Heating

This problem was chosen to demonstrate the reliability of the measures presented in Sec. 3.3 to predict the number of modes required for linear problems.

The plate shown in Fig. 5.4 is subject to a uniform specified heat load which increases linearly with time. The initial temperature of the plate is 0°F . All four edges of the boundary convect to the environment which is at a temperature $T_e = 0^\circ\text{F}$.

The full plate was analyzed although this is a symmetric problem and only a quarter of the plate needs to be considered. The finite element mesh used for the modal analysis consists of 165 DOF with 140 uniform rectangular elements. This mesh is considered adequate for this problem since the full-system solution compares very well with that of a much finer mesh with 561 DOF. Since the load varies linearly with time, the modal solution at any time can be computed in one step.

The guidelines listed in Sec. 3.3 are used to estimate a priori the number of modes that are required by the MDM, MAM, and the FDM at two different times $t = 2$ sec and 9 sec, respectively. The norm of CMAM and CFDM were used to obtain the results presented herein.

Estimate for the Required Number of Modes at Time $t = 2$ sec

The mode participation factor, Eq. (3.44), which indicates the component of the applied load that contributes to the response of the corresponding eigenvector, provides a measure of the significance of that vector in the total response. The participation factor of each mode is used to compute the error in the load vector, e_1 , Eq. (3.46), for increasing number of modes in the subset as shown in Fig. 5.5. Likewise, the errors, e_2 and e_3 ,

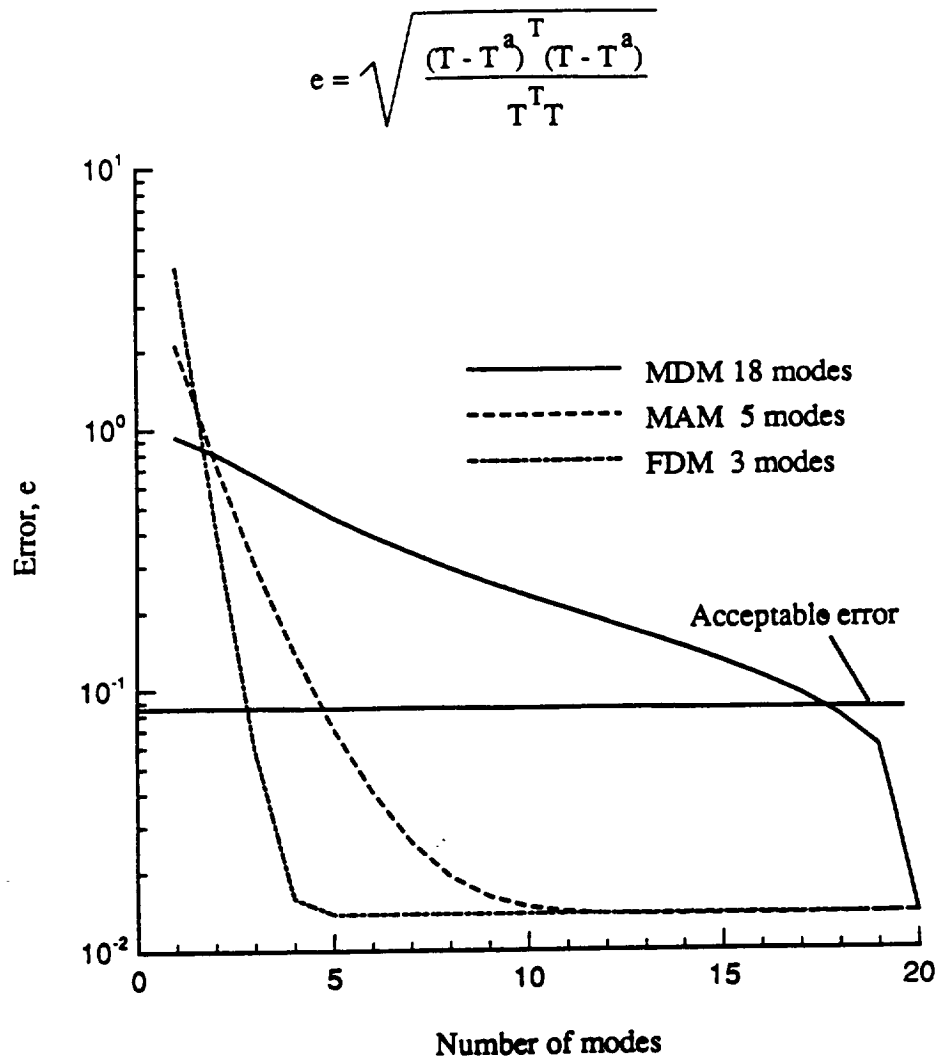


Fig. 5.3 Convergence of the modal methods at time $t = 0.02$ sec (Linear example problem 1).

$$\begin{aligned}
 T(x,y,0) &= 0.0^{\circ}\text{F} & q_s &= 200t \text{ Btu/in}^2\text{-sec} \\
 k_x &= 0.02 \text{ Btu-in/in}^2\text{-sec-}^{\circ}\text{F} & h &= 10.0 \text{ Btu/in}^2\text{-sec-}^{\circ}\text{F} \\
 k_y &= 0.01 \text{ Btu-in/in}^2\text{-sec-}^{\circ}\text{F} & T_s &= 0.0^{\circ}\text{F} \\
 \rho &= 1.0 \text{ lb/in}^3 \\
 c &= 1.0 \text{ Btu/lb-}^{\circ}\text{F}
 \end{aligned}$$

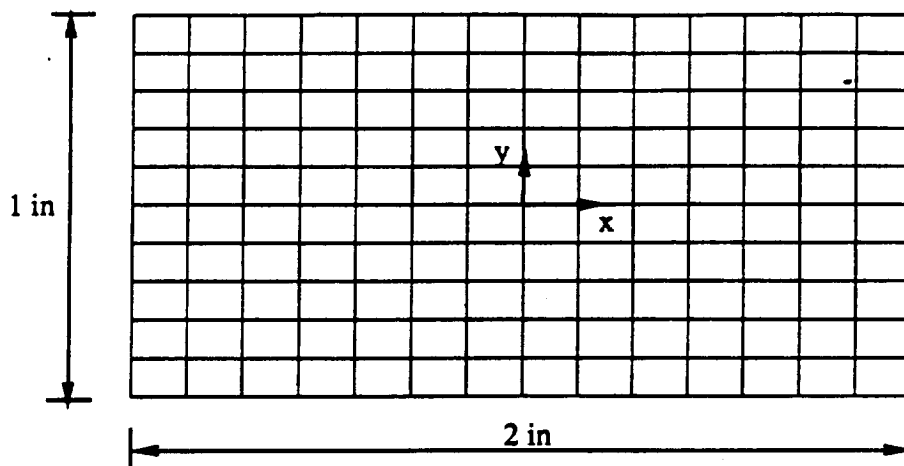


Fig. 5.4 Thermal finite element model (165 DOF) of a plate subject to uniform, transient heating over the surface and convection along the entire boundary (Linear example problem 2).

$$e_1 = \sqrt{\frac{\mathbf{R}(t)^T (\mathbf{R}(t) - \hat{\mathbf{R}}(t))}{\mathbf{R}(t)^T \mathbf{R}(t)}}$$

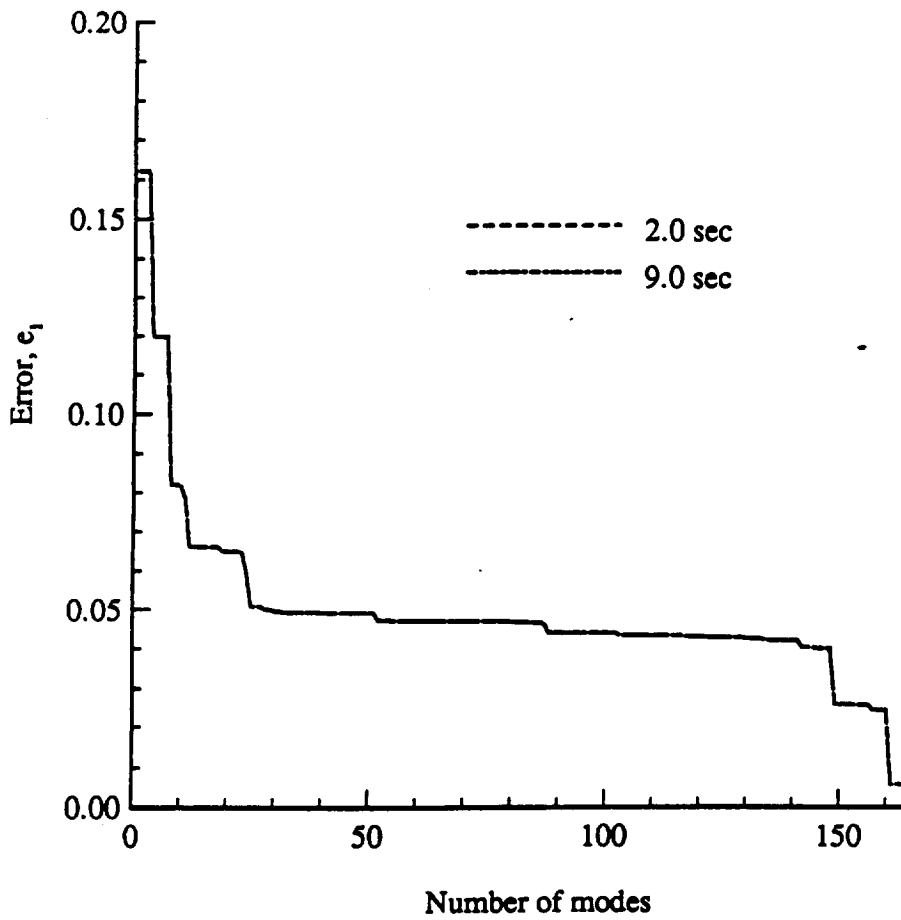


Fig. 5.5 Convergence of the error, e_1 , in the load vector used to predict the number of modes required by the MDM at times $t = 2.0$ sec and 9.0 sec (Linear example problem 2).

given by Eqs. (3.52) and (3.55), respectively, are computed for each additional mode and are shown in Figs. 5.6 and 5.7. The error converges in a step-like manner as seen in Fig. 5.5 indicating no change due to the addition of the second and third modes and then drops sharply with the inclusion of the fourth mode. This step-like convergence occurs because the second and third modes are asymmetric and therefore orthogonal to the uniform load and hence produce a negligible modal load. The step-like convergence over the entire spectrum is listed in Table 5.1. The wide range of modes 25 to 148 have negligible participation, but the 149th and the 161st modes cause a dramatic reduction in the error, thus confirming the importance of the higher modes in the MDM solution.

Table 5.1 A priori estimate of the required number of modes at time $t = 2$ sec
(Linear example problem 2)

Number of modes	Error e_1	Number of modes	Error e_2	Number of modes	Error e_3
1	0.162908	1	0.598 E-02	1	0.383 E-03
90	0.443 E-01	12-18	0.138 E-03	4-7	0.452 E-04
149	0.261 E-01	19-23	0.126 E-03	8	0.578 E-05
160	0.246 E-01	24	0.927 E-04		
161	0.576 E-02	25-27	0.284 E-04		

On the other hand, the error e_2 , Eq. (3.52), in the representation of the pseudo steady-state response, $K^{-1} R(t)$, also converges in a step-like manner, Fig. 5.6, but decreases rapidly due to the increasing magnitude of the higher eigenvalue appearing in the denominator. This also explains the faster rate at which the error e_3 , Eq. (3.55), approaches zero (Fig. 5.7) due to the square of the eigenvalue appearing in the denominator. The number of modes required by each of the methods is determined when the error approaches zero. From Figs. 5.5 - 5.7, it is estimated that up to 160 modes are required by the MDM whereas only 25 and 8 modes are required by the MAM and the FDM respectively. Referring to Table 5.1, these modes correspond to errors approximately two orders of magnitude less than the maximum error in each case.

$$e_2 = \sqrt{\frac{(\mathbf{K}^{-1}\mathbf{R}(t))^T \left(\mathbf{K}^{-1}\mathbf{R}(t) - \hat{\Phi} \frac{1}{\hat{\Lambda}} \hat{\Phi}^T \mathbf{R}(t) \right)}{(\mathbf{K}^{-1}\mathbf{R}(t))^T \mathbf{K}^{-1}\mathbf{R}(t)}}$$

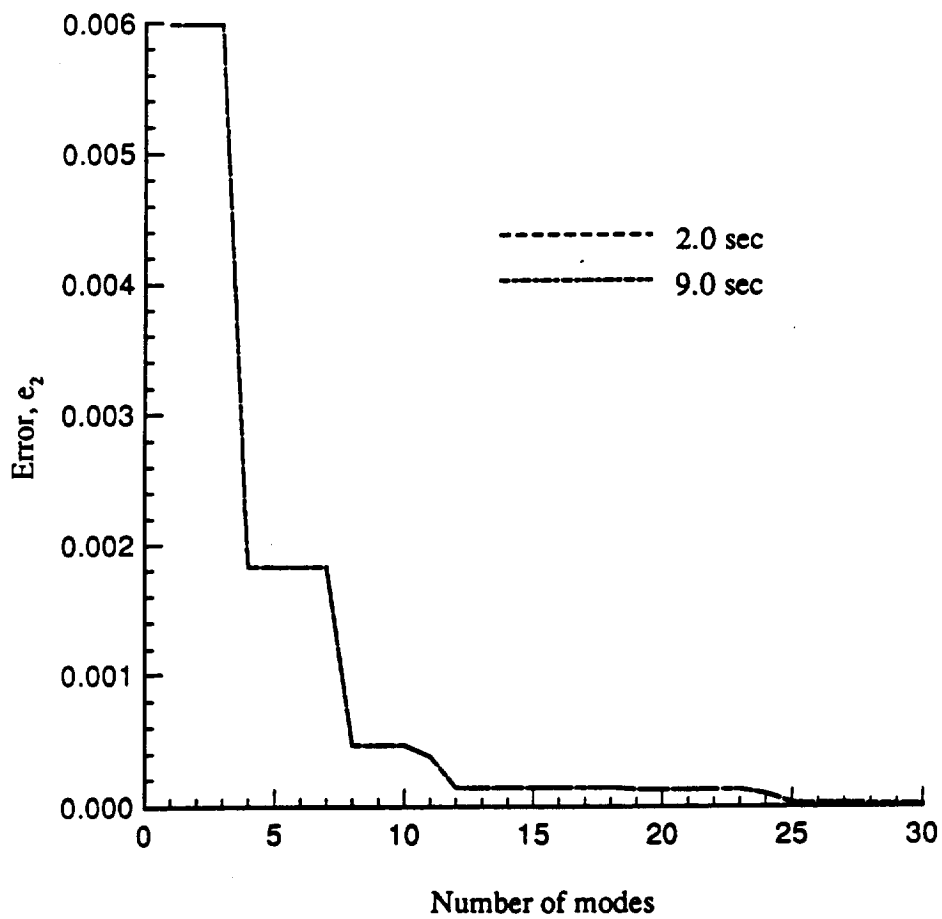


Fig. 5.6 Convergence of the error, e_2 , in the pseudo steady-state response used to predict the number of modes required by the MAM at times $t = 2.0$ sec and 9.0 sec (Linear example problem 2).

$$e_3 = \sqrt{\frac{(\mathbf{K}^{-1} \mathbf{C} \mathbf{K}^{-1} \dot{\mathbf{R}}(t))^T (\mathbf{K}^{-1} \mathbf{C} \mathbf{K}^{-1} \dot{\mathbf{R}}(t) - \frac{\hat{\Phi}}{\hat{\Lambda}^2} \hat{\Phi}^T \dot{\mathbf{R}}(t))}{(\mathbf{K}^{-1} \mathbf{C} \mathbf{K}^{-1} \dot{\mathbf{R}}(t))^T (\mathbf{K}^{-1} \mathbf{C} \mathbf{K}^{-1} \dot{\mathbf{R}}(t))}}$$

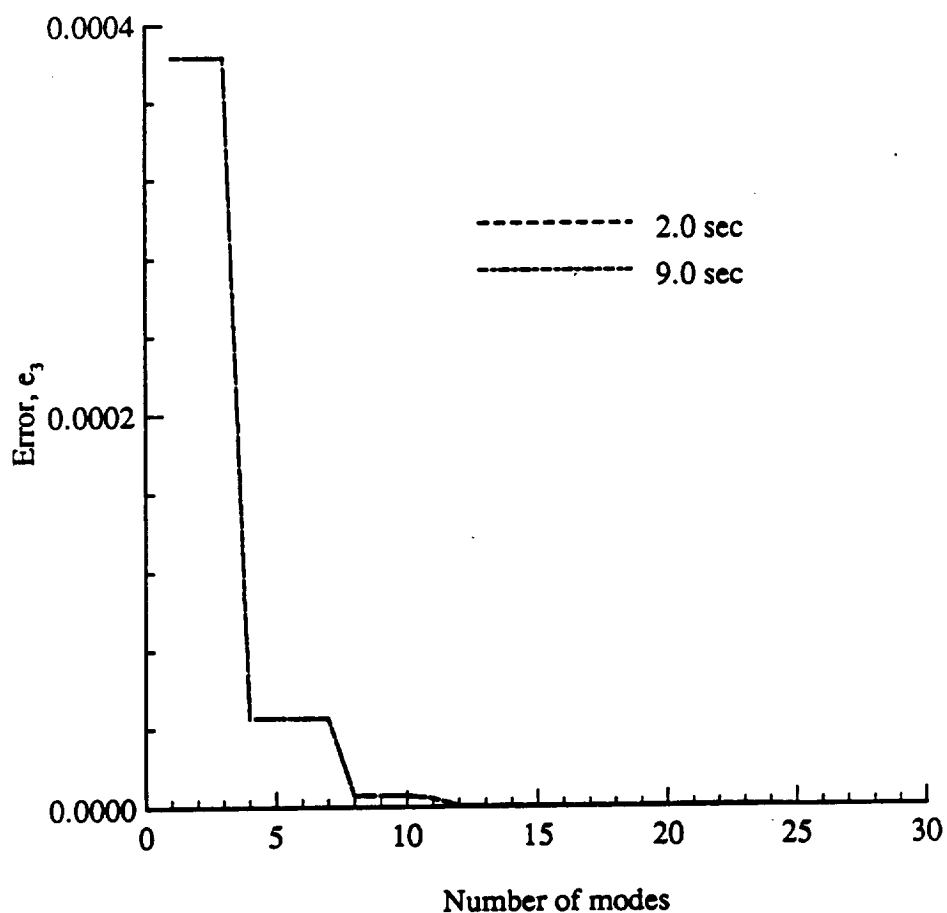


Fig. 5.7 Convergence of the error, e_3 , in the derivative form of the pseudo steady-state response used to predict the number of modes required by the FDM at times $t = 2.0$ sec and 9.0 sec (Linear example problem 2).

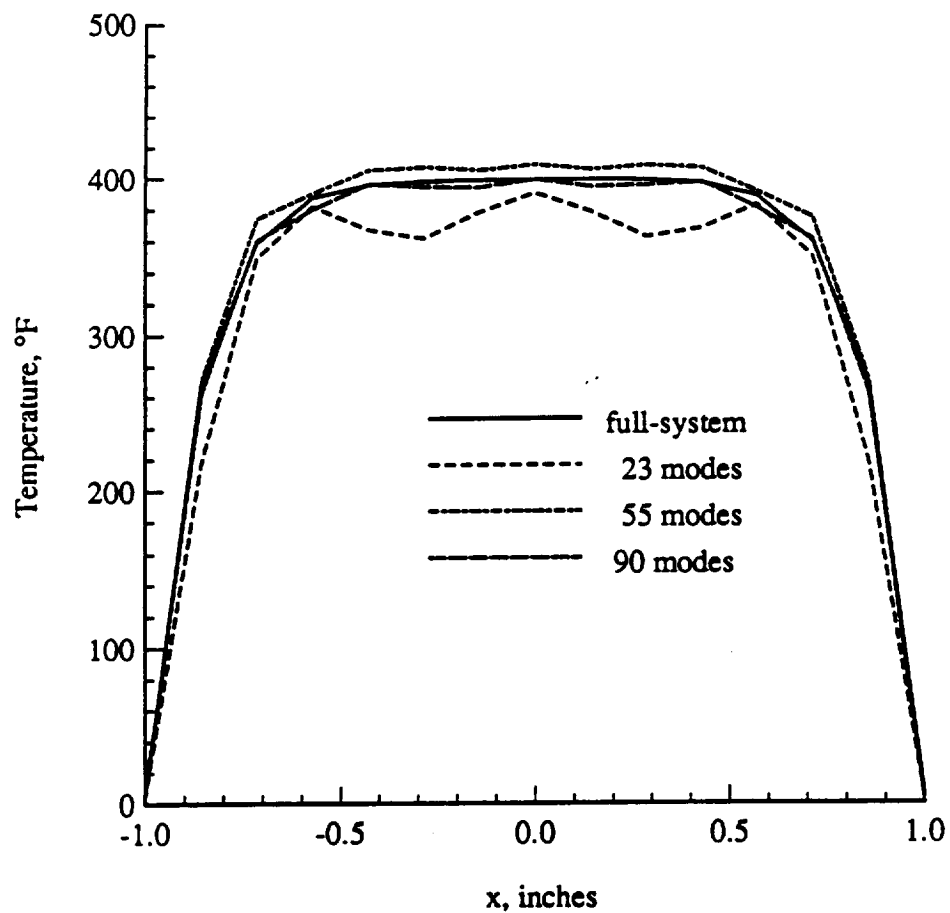
Table 5.1 highlights the selected modes which cause the rapid convergence of the methods.

Convergence of the Modal Methods at Time $t = 2$ sec

The modal solutions obtained using the estimated number of modes at time $t = 2$ sec are shown in Figs. 5.8a - 5.8c. To judge the reliability of these estimates, in the case of the MAM for example, the distribution along $y = 0$ in. obtained by 10, 23 and 25 modes are compared in Fig. 5.8b, since modes 13 through 23 are nearly orthogonal to the load. Similarly for the FDM the solutions from using eight and four modes are compared in Fig. 5.8c. Figures 5.8b and 5.8c demonstrate that 25 and 8 modes are indeed required by the MAM and the FDM respectively, and thus confirm that the corresponding estimates are accurate; whereas Fig. 5.8a shows that the MDM yields an acceptable solution even with about 90 modes, which is much fewer than the 160 modes estimated. This deviation from the estimate could possibly be due to the fact that the estimate is based on the error in the load vector and not the error in the solution vector itself.

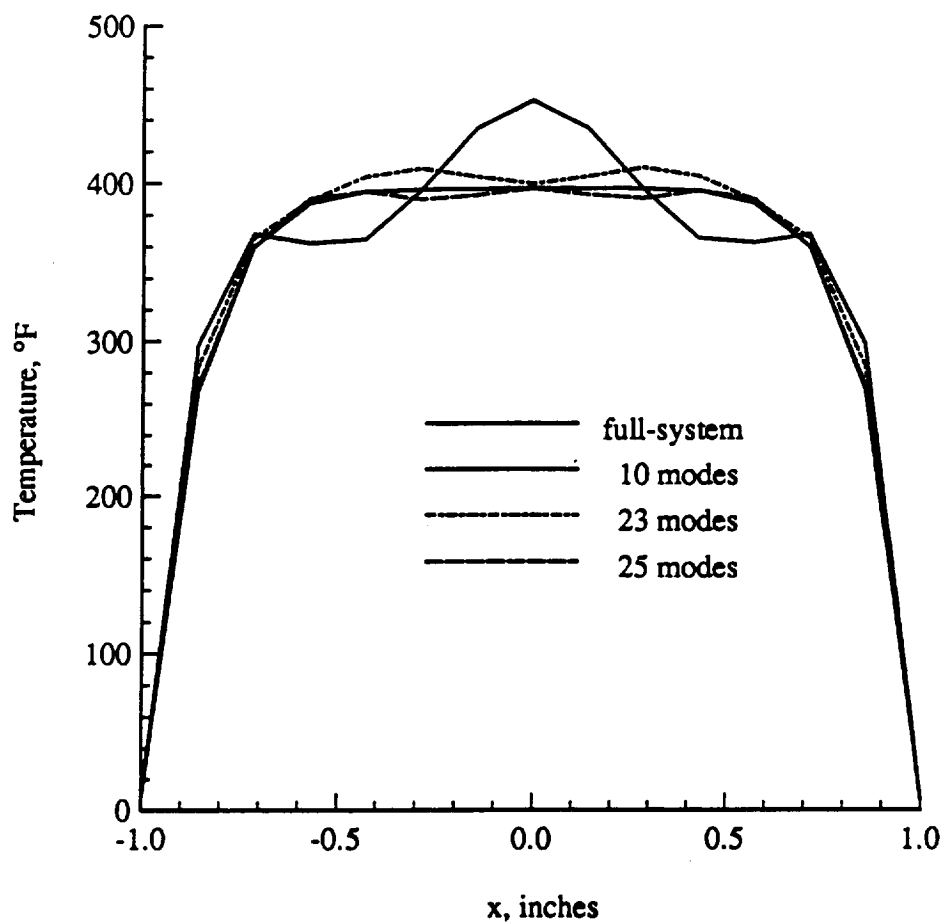
Estimate for the Required Number of Modes at Time $t = 9$ sec

The rates of convergence of the errors, e_1 , e_2 and e_3 , remain the same at this time. This is because the error e_2 , for instance, is essentially the error in the representation of \mathbf{K}^{-1} by the subset of modes used. Since the eigenmodes are constant for this problem, this approximation does not change with time. The correction offered by the MAM, CMAM (Eq. (3.50)), varies with time since the load varies with time, as seen in Fig. 5.9. Although CMAM decreases as more modes are included at a given time, the maximum value of CMAM (which occurs when only one mode is included) increases with time as $R(t)$ increases monotonically. For the given nature of the load, it is obvious from Fig. 5.9 that the MAM requires fewer modes to converge at time $t = 9$ sec than at time $t = 2$ sec. The rate of convergence of the correction of the FDM, CFDM (Eq. (3.53)), does not change with time (Fig. 5.10), since the applied load has a constant first



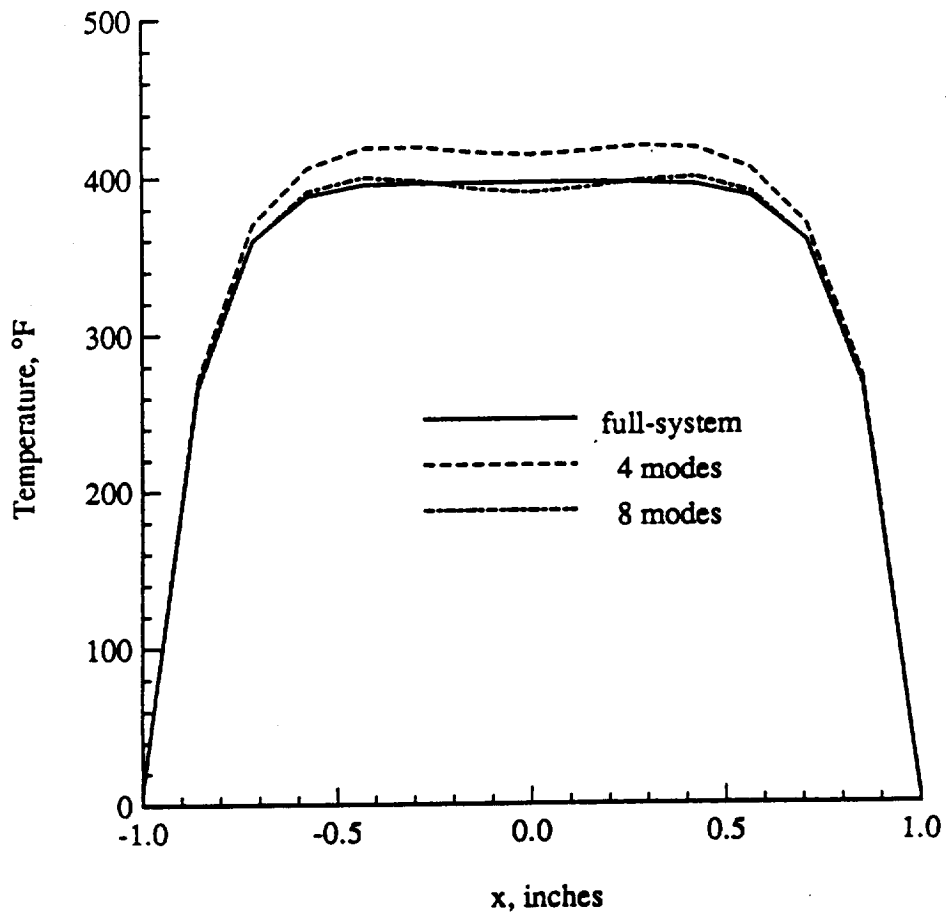
a) Mode-displacement method (MDM).

Fig. 5.8 Temperature distribution at time $t = 2.0$ sec along $y = 0.0$ in. (Linear example problem 2).



b) Mode-acceleration method (MAM).

Fig. 5.8 Continued



c) Force-derivative method (FDM).

Fig. 5.8 Concluded

$$\text{CMAM} = \mathbf{K}^{-1} \mathbf{R}(t) - \sum_{r=1}^p \phi_r \frac{1}{\lambda_r} \phi_r^T \mathbf{R}(t)$$

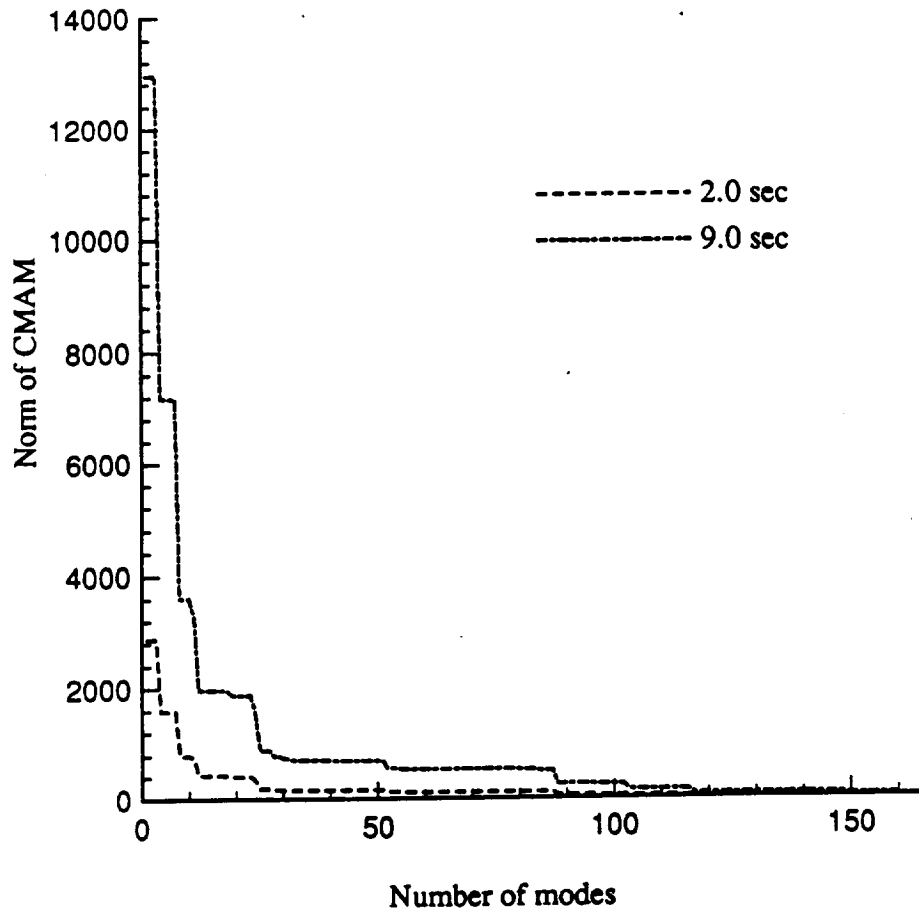


Fig. 5.9 Convergence of the correction offered by the MAM, CMAM, at times $t = 2.0$ sec and 9.0 sec (Linear example problem 2).

$$\text{CFDM} = -\mathbf{K}^{-1} \mathbf{C} \mathbf{K}^{-1} \dot{\mathbf{R}}(t) + \sum_{r=1}^p \phi_r \frac{1}{\lambda_r^2} \phi_r^T \dot{\mathbf{R}}(t)$$

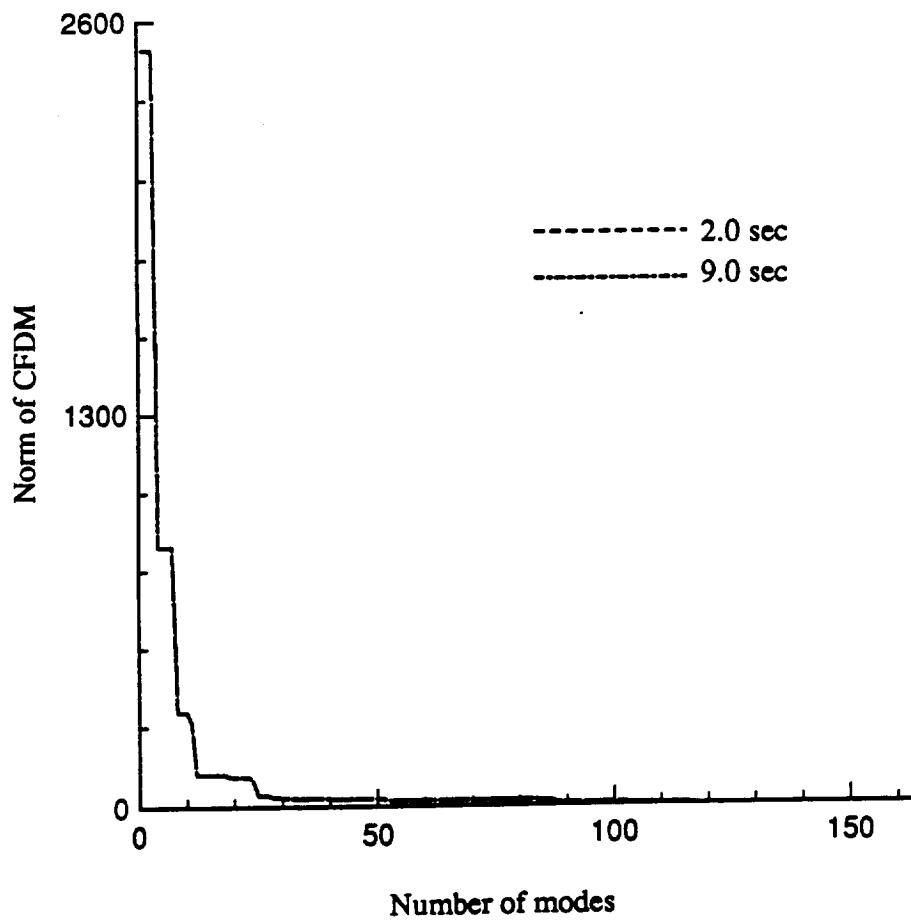


Fig. 5.10 Convergence of the correction offered by the FDM, CFDM, at times $t = 2.0$ sec and 9.0 sec (Linear example problem 2).

derivative with respect to time. Nevertheless, since the magnitude of CFDM is not negligible when compared to CMAM at time $t = 9$ sec, the FDM is expected to play an important role in the reduction process at this time also and hence converge with fewer modes than the MAM, albeit the difference is smaller at time $t = 2$ sec. The rate of convergence of the load vector, Eq. (3.45), is also expected to vary with time by realizing that the participation factor of the non-orthogonal modes is proportional to the load $R(t)$. Although the corrections indicate that each method individually converges faster at this time than at time $t = 2$ sec, additional work may be necessary to use these corrections to decide the cutoff value for the number of modes required at different times.

Convergence of the Modal Methods at Time $t = 9$ sec

The modal responses were computed at time $t = 9$ sec and it is found that the MDM, MAM, and the FDM converge with fewer modes at this time, namely 30, 8 and 1 respectively. The distributions shown in Fig. 5.11 or, alternatively, the distribution error norms compared in Fig. 5.12, confirm that all three methods converge with fewer modes at this time. For this problem with a monotonically time-varying load, the number of modes predicted based on the errors at time $t = 2$ sec is a conservative estimate, that is, guarantees convergence of the modal methods at all times but may not be necessary at all times, as the results at time $t = 9$ sec have shown.

The results demonstrate the potential of the higher-order methods to effectively improve the reduction achieved for transient thermal problems. Also the error estimates and the convergence of the correction terms show the potential to serve as useful tools in the prediction of the number of modes required at any given time.

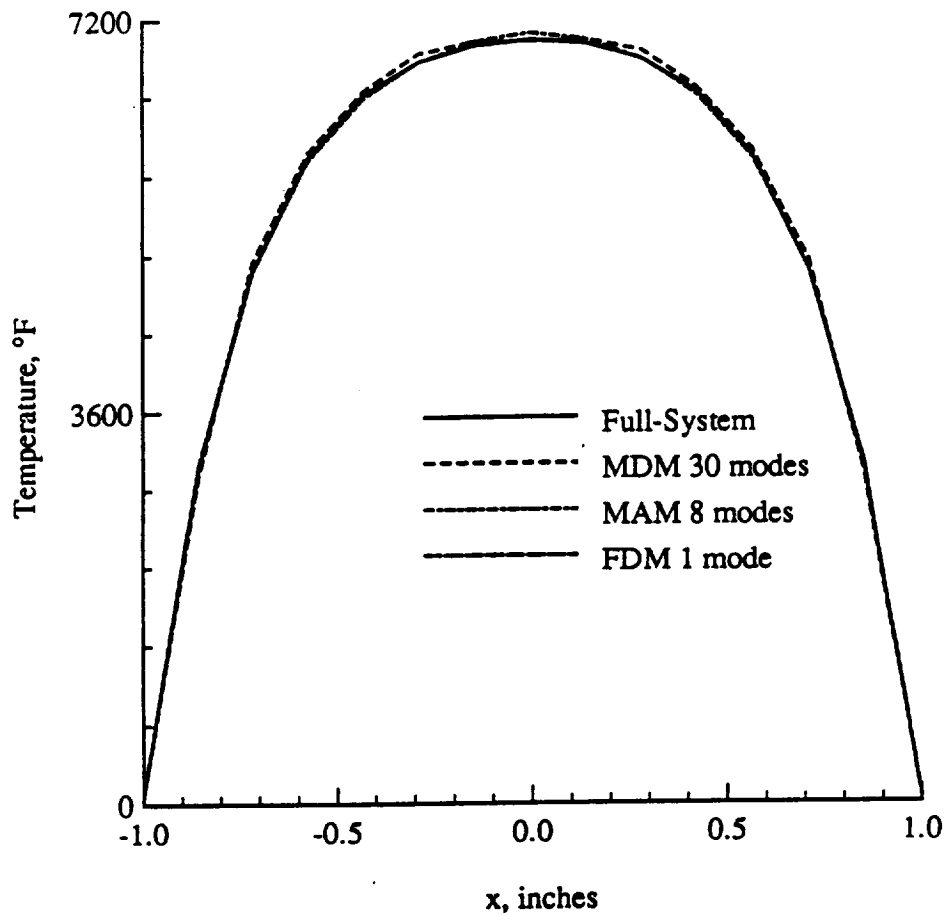


Fig. 5.11 Temperature distribution at time $t = 9.0$ sec along $y = 0.0$ in. (Linear example problem 2).

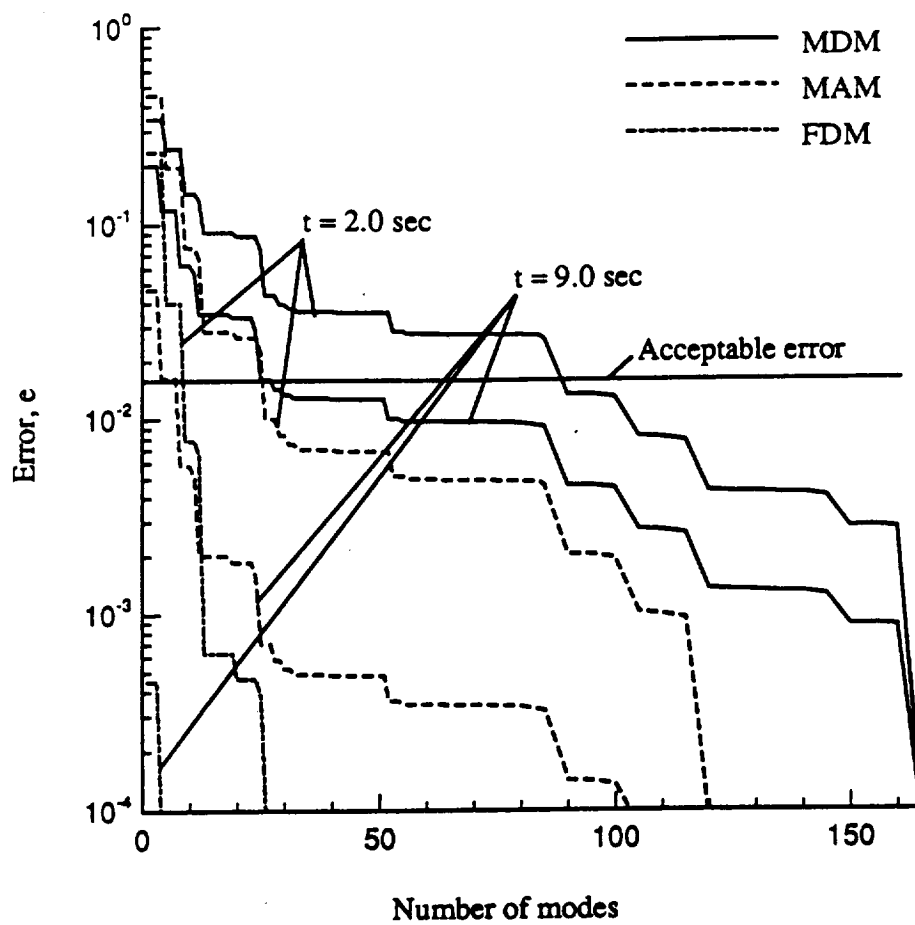


Fig. 5.12 Convergence of the modal methods at times $t = 2.0$ sec and 9.0 sec (Linear example problem 2).

Chapter 6

NONLINEAR TRANSIENT EXAMPLE PROBLEMS

To study the feasibility of using the modal methods as a reduction technique for nonlinear transient thermal problems, two nonlinear examples were analyzed. The results of these analyses are presented in this chapter. The relative performance of the methods is evaluated and the conditions that bring out their best performances are highlighted. The multi-step approach described in Sec. 4.2.2 was used even though the load varies linearly in time, to accommodate for the temperature-dependent load vectors and eigenmodes. Also, the modal coordinates given by Eq. (4.53) were used to solve the numerical examples that follow.

6.1 Rod Subject to Convection at One End

with Temperature-Dependent Thermal Conductivity

The problem statement for this simple example is shown in Fig. 6.1. It was primarily chosen to validate the new finite element algorithm for nonlinear problems which is presented in chapter 4. Two cases with different thermal conductivities are considered.

6.1.1 Case 1: $k(T) = 0.0001 + 0.5 E - 06 T$

Time for Eigensolution Update

Some trial runs were made to determine the time when an eigensolution update is necessary to adequately represent the change in the nonlinear basis vectors with time. The frequency of these updates requires a compromise between computation time and accuracy. The FDM was used to march the solution from time $t = 0$ sec when the initial

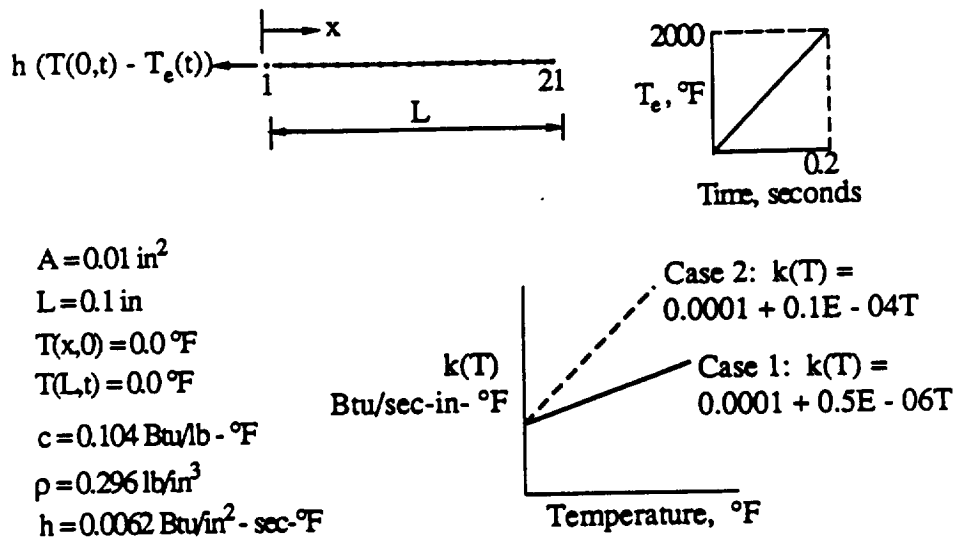


Fig. 6.1 Thermal finite element model of a rod subject to transient convective heating at one end with temperature-dependent thermal conductivity (Nonlinear example problem 1).

eigenvalue problem was solved. An arbitrarily chosen time step, $dt = 0.01$ sec, (Eq. (4.36)) and a minimum of two modes (which is discussed subsequently) were used. The number of iterations needed to achieve convergence, within a tolerance of $\epsilon = 0.01$, increases with time as seen in Fig. 6.2, until the solution does not converge at time $t = 0.08$ sec, regardless of the number of modes in the subset. Even though the solution converges at time $t = 0.07$ sec, the number of iterations increases when more modes are included in the solution. A similar behavior was observed even when the tolerance was increased to $\epsilon = 0.1$, or, when the time step was decreased to $dt = 0.005$ sec. However, with an EVP update at time $t = 0.05$ sec, the number of iterations reduces to three from nine or ten at time $t = 0.06$ sec, and the increase in number of iterations at a later time $t = 0.1$ sec is less with more modes. This confirms the need to update the temperature-dependent eigensolution in time for nonlinear problems. However, this approach based on the iterations required is not meant to be used for an a priori estimate of the time for an EVP update.

Convergence of Modal Methods

The solution at time $t = 0.1$ sec in the early transient period when the gradient is significant, is used to evaluate the performance of the modal methods. A time step $dt = 0.01$ sec was used for this analysis with the initial eigensolution updated only once at time $t = 0.05$ sec, that is, $m = 5$ (see discussion following Eq. 4.41). The converged solution used to compute the distribution error norm of the reduced-basis solutions was obtained with a fine mesh of 101 nodes using a small time step $dt = 0.001$ sec. The implicit transient thermal analyzer in COMET which uses the Crank-Nicholson algorithm for time integration was used for this purpose.

The MDM underpredicts the exact peak temperature of 373.7° F by 38%, 17% and 8.2% with 5 (25% of the number of degrees of freedom), 10 (50%) and 15 (75%) modes respectively. At least 16 modes are required by the MDM to yield a distribution

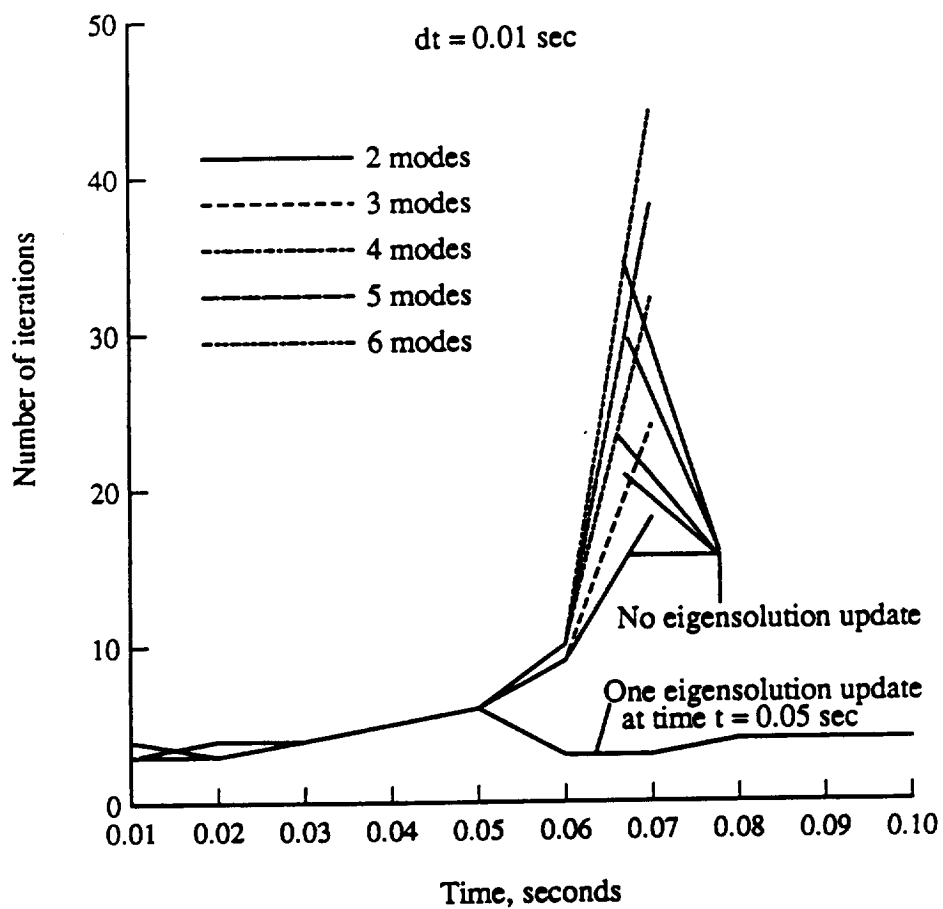


Fig. 6.2 History of iterations required by the FDM to determine the time for an EVP update (Case 1 of nonlinear example problem 1).

fairly close to exact. On the other hand, the MAM converges with a much smaller subset of four modes while the FDM exhibits a superior performance by predicting the peak temperature within 1.36% using just two modes as shown in Fig. 6.3. This is made possible by the large ratio (10) of the magnitude of the derivative of the load to that of the load itself (which varies linearly with time) at this early time. The rates of convergence of the three methods are compared in Fig. 6.4.

Effect of Time Step

The effect of the time step size on the performance of the FDM was studied. The responses obtained by the FDM using two modes are compared for two different time steps $dt = 0.01$ and 0.05 sec in Fig. 6.5 which have an error norm of 0.038 and 0.08 respectively. The smaller time step yields a distribution very close to the exact and helps to obtain a smooth temperature history when desired, as it computes the response at more instants of time. The advantages though, should justify the additional computational effort required to do the iterations at each of the intermediate times. Computations reveal that both time steps require the same total number of iterations, 17. The solution was further marched out in time to $t = 0.2$ sec. The solution at time $t = 0.1$ sec was used as the initial guess and the corresponding EVP was solved. The solution at time $t = 0.2$ sec obtained in one step (error = 0.09), is compared with that obtained in five steps using $dt = 0.02$ sec (error = 0.02) in Fig. 6.6. Again, the two analyses involve the same total number of iterations 7. These results are summarized in Table 6.1. By well-representing the transient variation of the nonlinear quantities, a smaller time step yields a better solution accuracy for a given computational effort.

Minimum Number of Modes

It is seen in Fig. 6.4 that the error from the FDM is shown for two modes and more only. For the chosen time step ($dt = 0.01$ sec), tolerance ($\epsilon = 0.1$) and EVP update ($m = 5$), it was determined by trial and error that a minimum of two modes were required

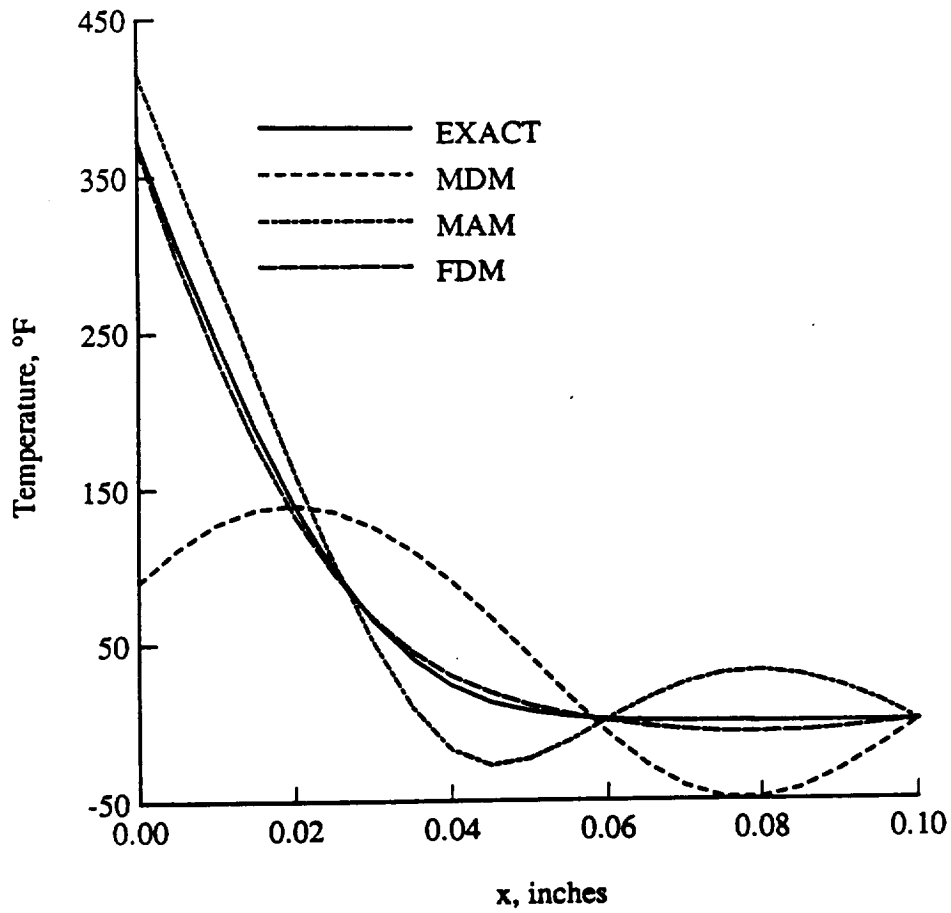


Fig. 6.3 Temperature distribution obtained by the MDM, MAM, and the FDM using two modes at time $t = 0.1$ sec (Case 1 of nonlinear example problem 1).

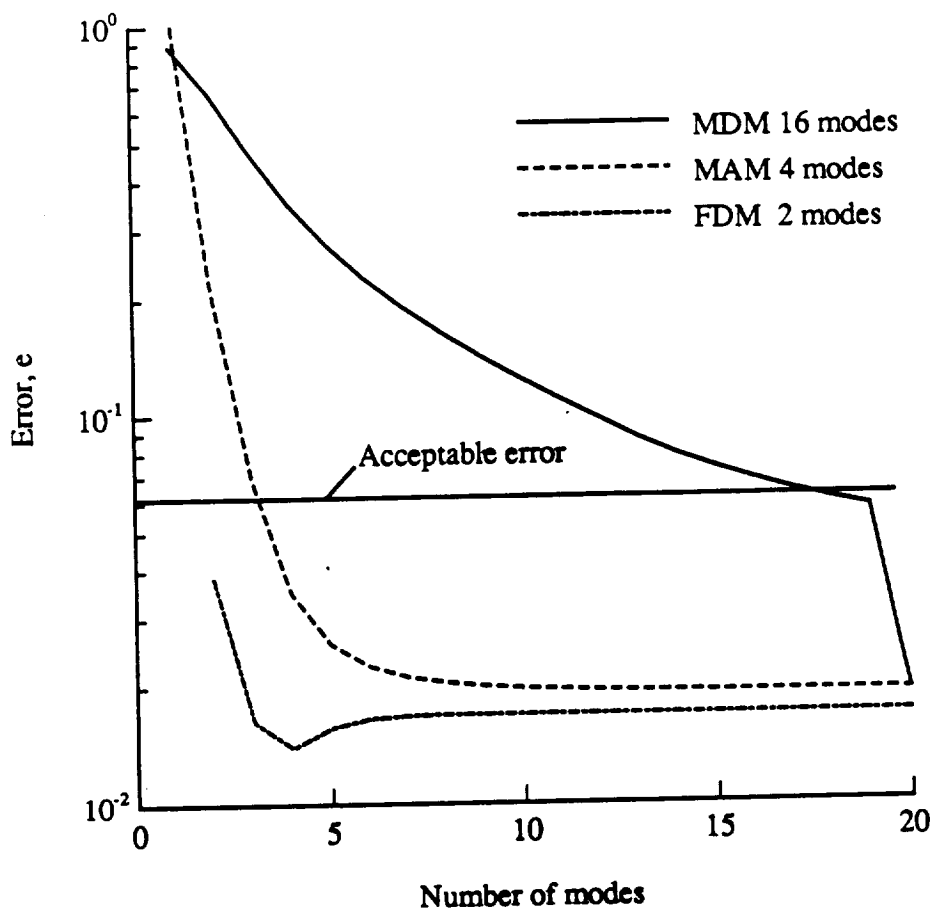


Fig. 6.4 Convergence of the modal methods at time $t = 0.1$ sec (Case 1 of nonlinear example problem 1).

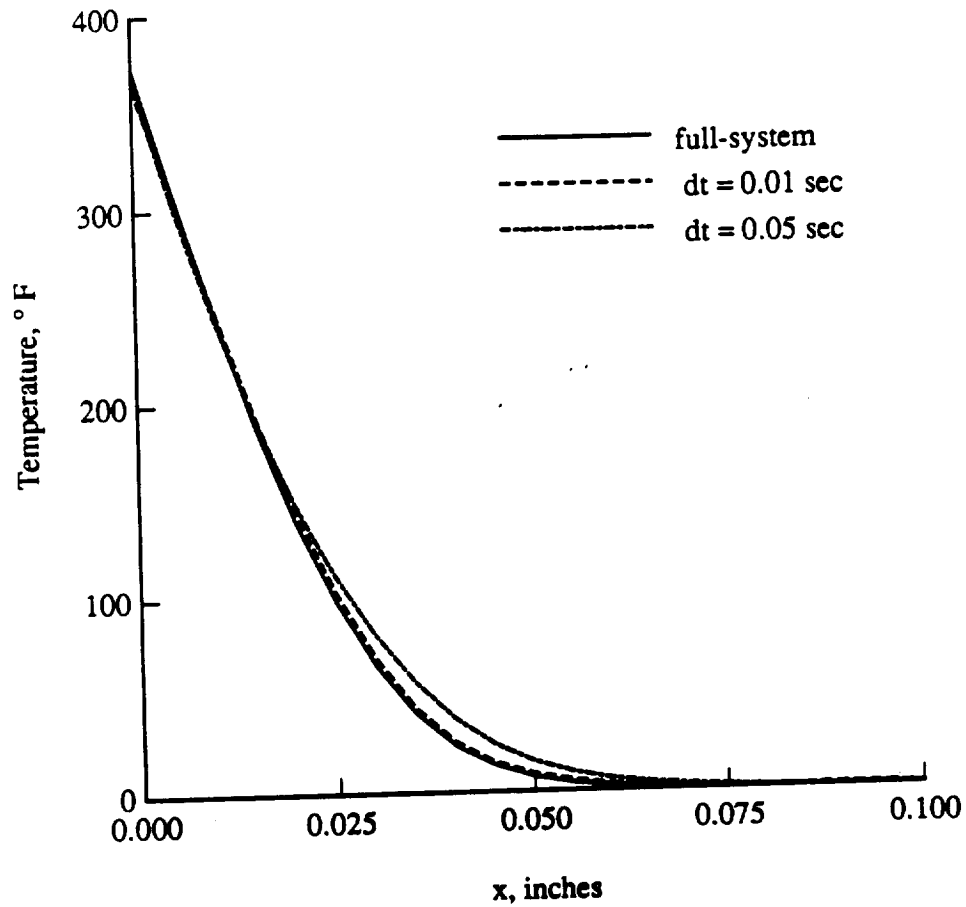


Fig. 6.5 Effect of time step on the response of the FDM at time $t = 0.1$ sec with initial condition at time $t = 0.0$ sec and one EVP update at time $t = 0.05$ sec (Case 1 of nonlinear example problem 1).

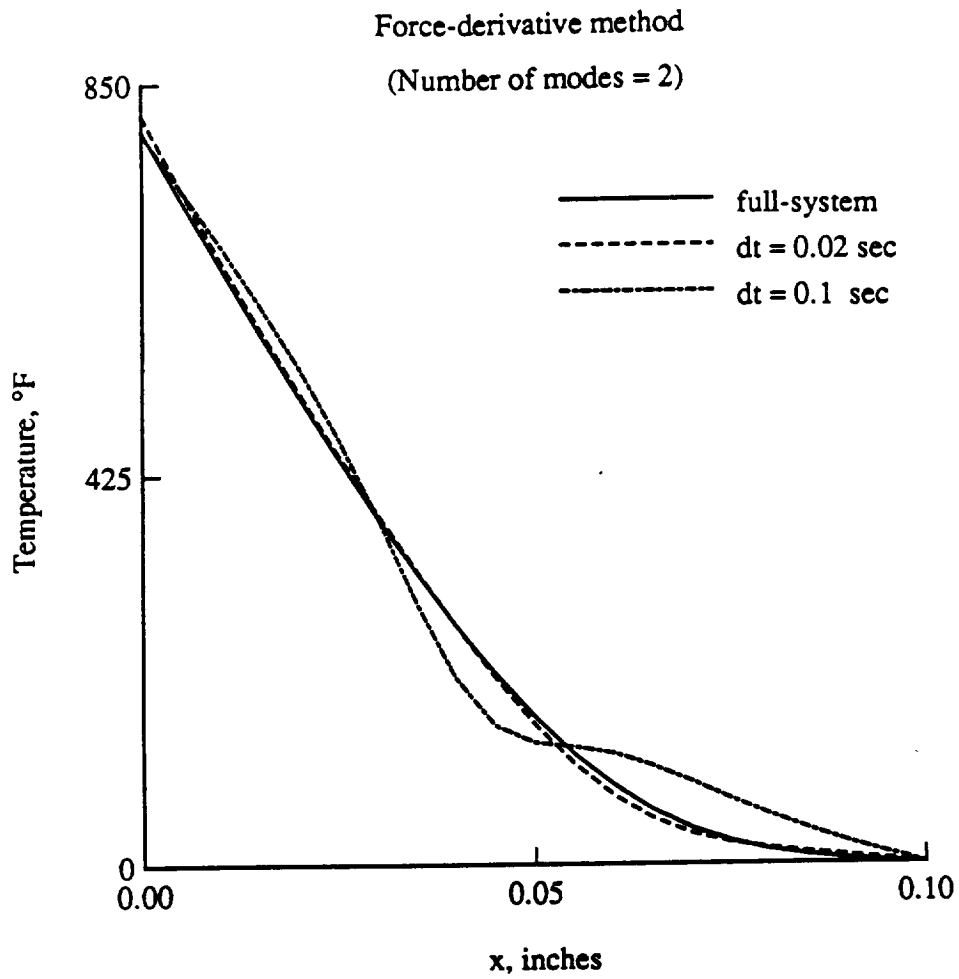


Fig. 6.6 Effect of time step on the response of the FDM at time $t = 0.2$ sec with initial condition at time $t = 0.1$ sec and no EVP update (Case 1 of nonlinear example problem 1).

Table 6.1 Effect of time step on the solution accuracy of the FDM
(Case 1 of nonlinear example problem 1)

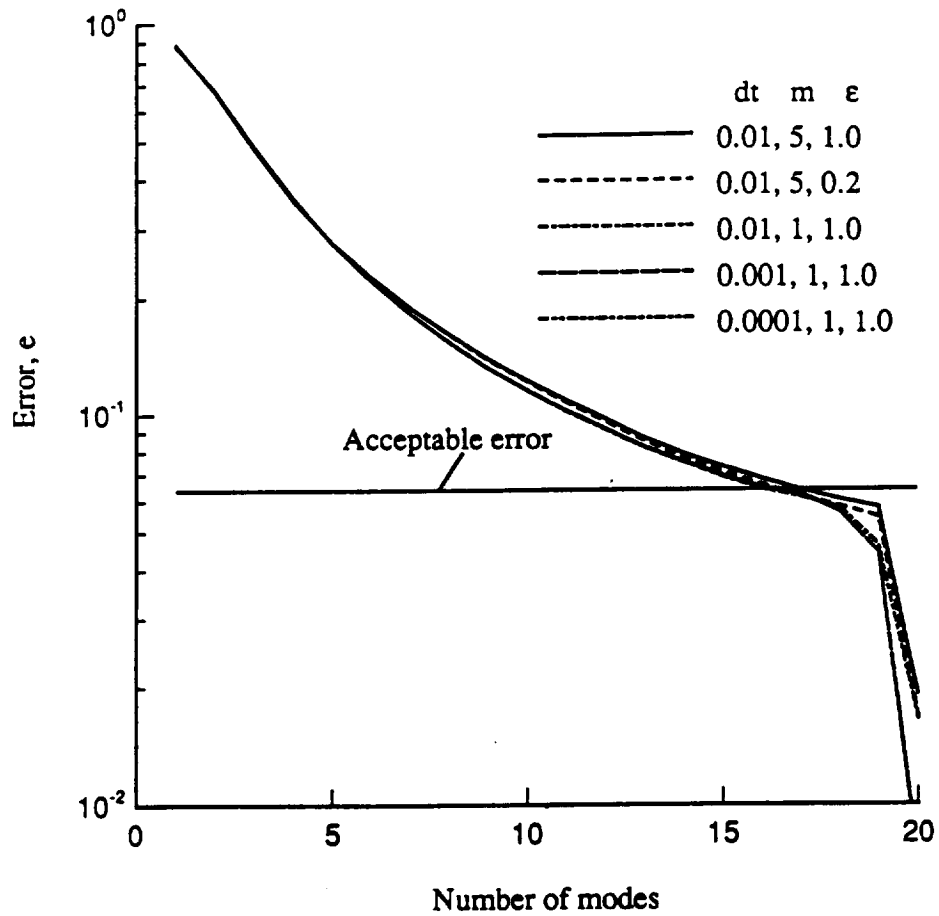
Time = 0.1 sec			Time = 0.2 sec		
Time step dt	Number of iterations	Error e	Time step dt	Number of iterations	Error e
0.01	17	0.038	0.02	7	0.02
0.05	17	0.08	0.1	7	0.09

by the FDM to obtain a solution (which is already converged), at $t = 0.1$ sec without any numerical instability or divergence at some intermediate time. A similar behavior was observed even with a fine mesh of 101 DOF. This minimum requirement for the number of modes did not arise for linear problems where the eigenmodes are independent of the solution and just one mode yields a solution even if highly erroneous.

The time-marching parameters were varied to study their effect on the minimum number of modes required by the modal methods at $t = 0.1$ sec. The results of this study are shown in Figs. 6.7a - 6.7c and are also summarized in Table 6.2. The MDM and the MAM yield a solution with one mode for all the parameters studied for this problem. The FDM also converges with one mode for the first set of parameters with only one EVP update and no iterations. Instead, when iterations are performed as with the second set of parameters, or, a piecewise linear approach (where the eigensolution is updated every time step, i.e., $m = 1$) is used with smaller time steps, the MAM converges with fewer modes (three instead of four) but the FDM requires more (two instead of one) for a minimum but the same number (two) to converge.

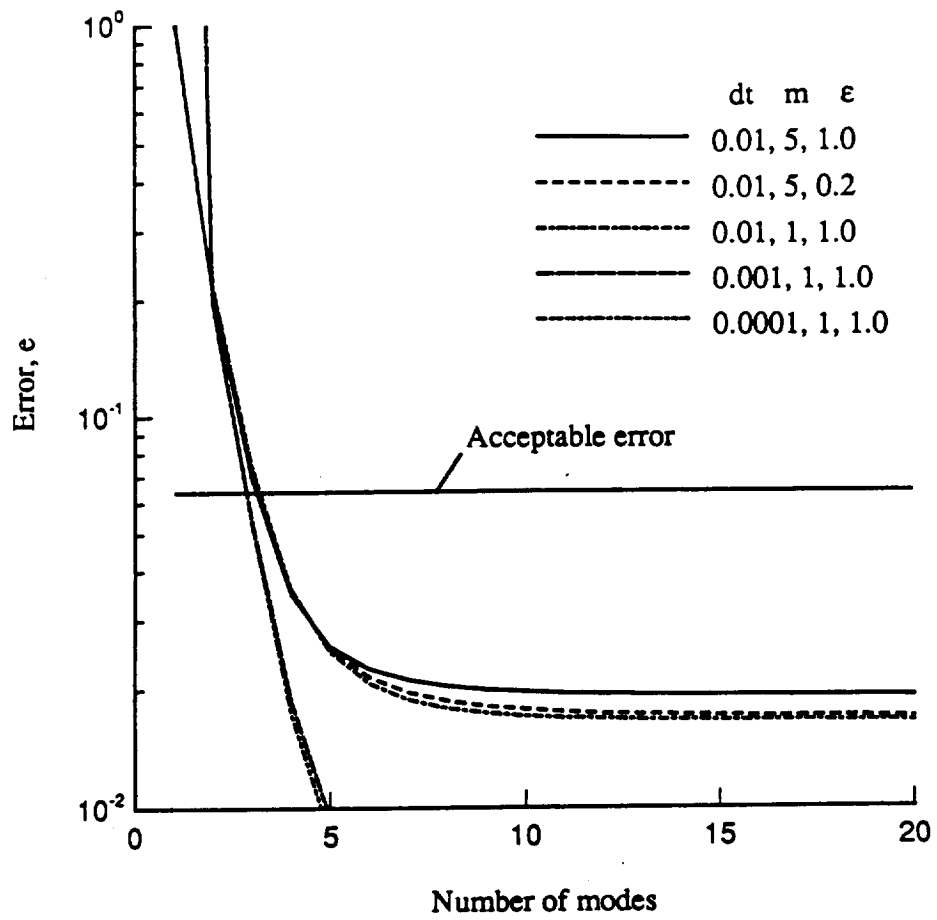
6.1.2 Case 2: $k(T) = 0.0001 + 0.1 E - 04 T$

To study the effect of variation of the nonlinear parameter $k(T)$, the slope of the conductivity curve was increased by a factor of 20. Although the heat load is identical in both cases, the diffusivity is very different. This is reflected in the temperature profiles at the same time $t = 0.05$ sec in Fig. 6.8. The temperature distribution in the first case has a



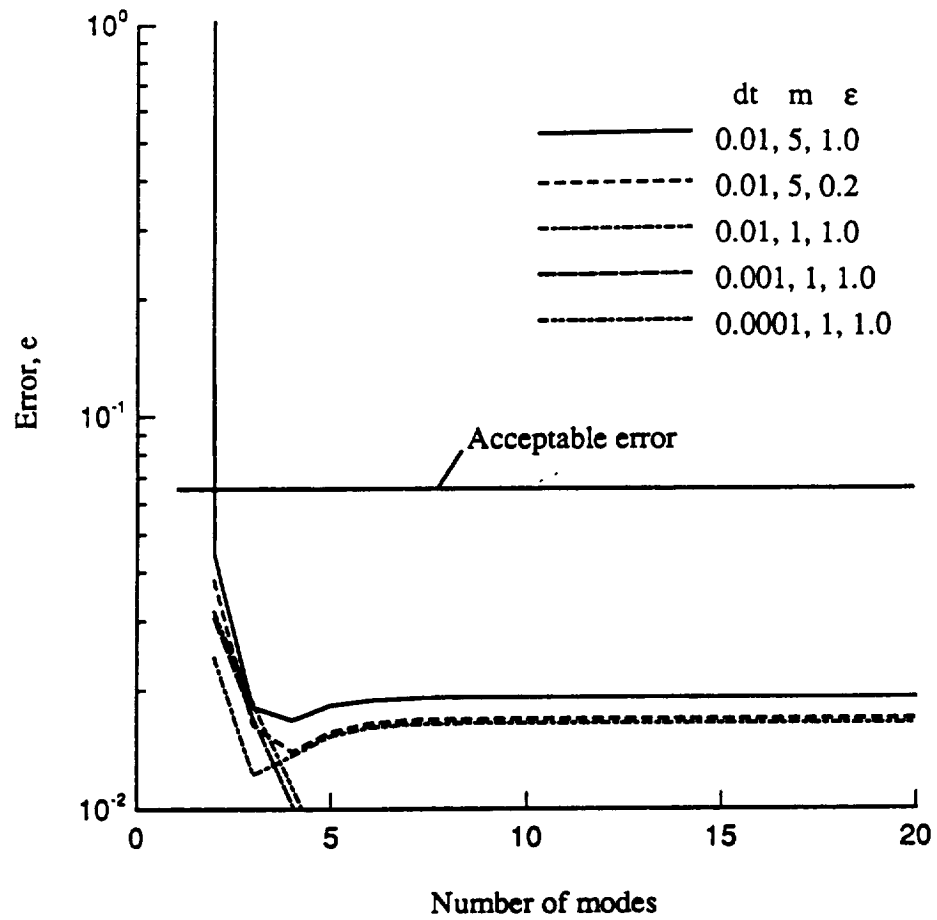
a) Mode-displacement method (MDM).

Fig. 6.7 Effect of time-marching parameters on the number of modes required by the MDM, MAM, and the FDM at time $t = 0.1$ sec (Case 1 of nonlinear example problem 1).



b) Mode-acceleration method (MAM).

Fig. 6.7 Continued.



c) Force-derivative method (FDM).

Fig. 6.7 Concluded.

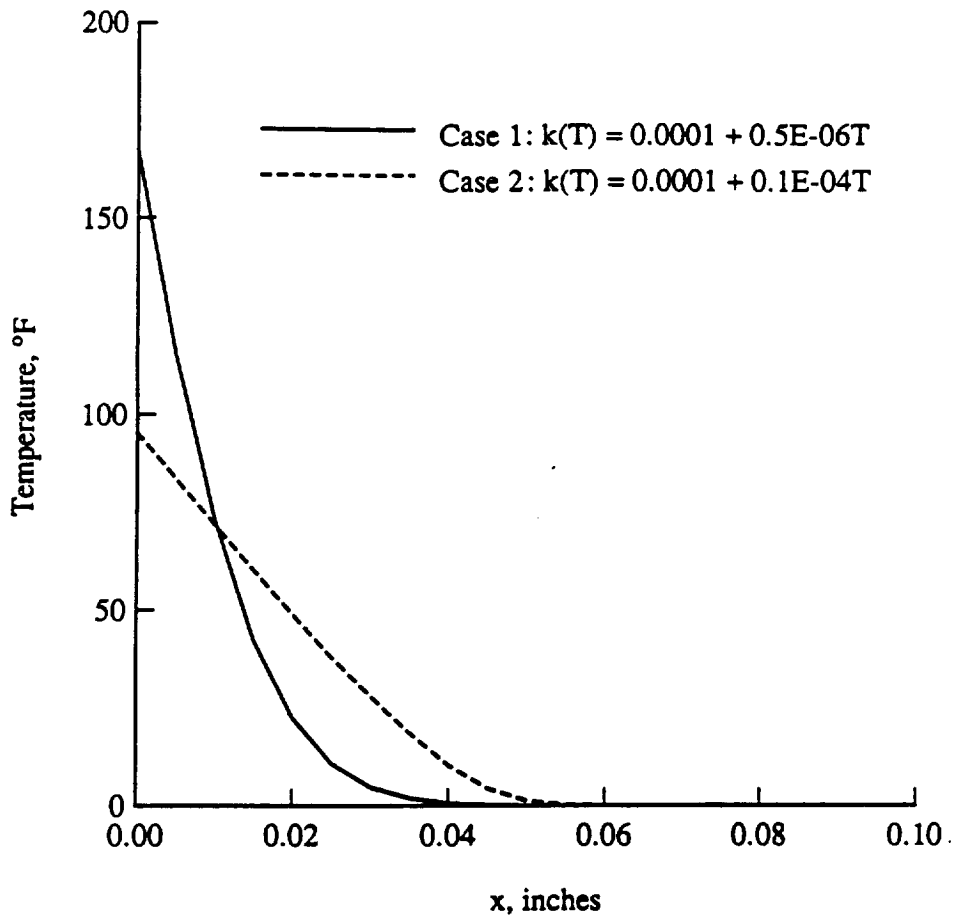


Fig. 6.8 Comparison of temperature distributions at time $t = 0.05$ sec for the two cases of nonlinear example problem 1.

relatively steep gradient compared to the second case, and the peak temperature is almost twice as well.

Table 6.2 Effect of time-marching parameters on the number of modes required at time $t = 0.1$ sec (Case 1 of nonlinear example problem 1)

Time-marching parameters			Minimum number of modes for a stable solution			Modes required to converge within the desired accuracy		
dt	m	ϵ	MDM	MAM	FDM	MDM	MAM	FDM
0.01	5	1.0	1	1	1	17	4	2
0.01	5	0.2	1	1	2	17	4	2
0.01	1	1.0	1	1	2	17	4	2
0.001	1	1.0	1	1	2	17	3	2
0.0001	1	1.0	1	1	2	17	3	2

Time for Eigensolution Update

As in Case 1, the FDM was used to obtain the transient response starting with time $t = 0.0$ as the initial condition. A time step $dt = 0.001$ sec was used which caused the solution to converge in only one iteration for a tolerance $\epsilon = 1.0$. A minimum of four modes were required in this case. As seen in Fig. 6.9, the error in the computed response progressively decreases from time $t = 0$ sec until it suddenly shoots up to prohibitive levels sometime after time $t = 0.025$ sec, even if more modes are included. With one EVP update at time $t = 0.025$ sec, the error at time $t = 0.05$ sec falls within an acceptable limit, confirming the need to update the nonlinear eigenmodes.

Convergence of Modal Methods

Using a time step $dt = 0.001$ sec and an EVP update at time $t = 0.025$ sec as determined above for the FDM, the solution at time $t = 0.05$ sec was obtained by the three methods. While the FDM required a minimum of four modes to converge, the MAM required seven. The MDM solution, though, became acceptable only with 16 modes. When the eigensolution was updated every 0.01 sec, the MAM also converged with only

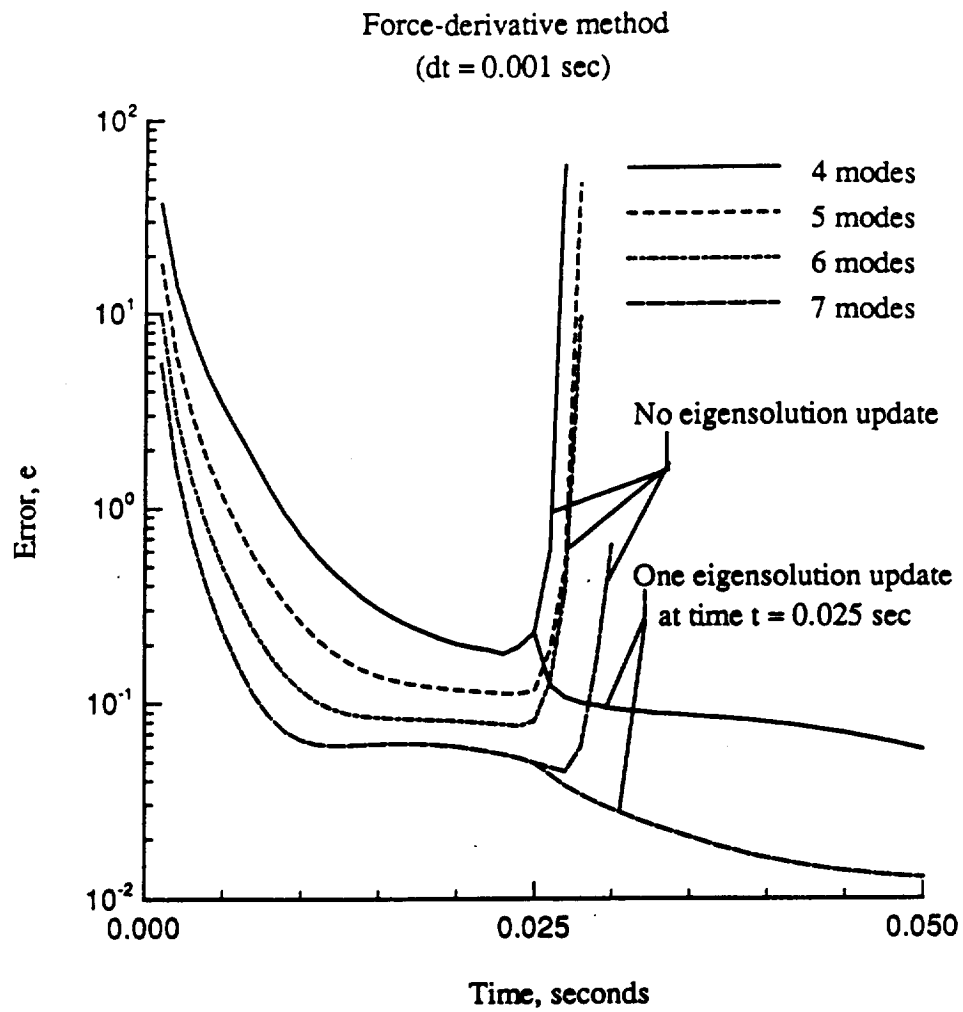


Fig. 6.9 Error history of the FDM to determine the time for an EVP update (Case 2 of nonlinear example problem 1).

four modes like the FDM. The rates of convergence of the three modal methods using $dt = 0.001$ sec and $m = 10$ are compared in Fig. 6.10 for this case.

Effect of Time Step

For the given EVP update at time $t = 0.025$ sec, the unacceptable error resulting from using a time step $dt = 0.025$ sec is dramatically reduced by decreasing the time step to $dt = 0.001$ sec as seen in Fig. 6.11. Also, this entails little additional computational effort, as the solution requires only one iteration per time step.

Minimum Number of Modes

Results of a parametric study conducted similar to Case 1 are shown in Figs. 6.12a - 6.12c and are summarized in Table 6.3. For this case, the MDM again needs just one mode for a well-behaved solution with any of the parameters. With the first set of parameters, the MAM requires up to seven modes as a minimum and also for convergence. When the time step is reduced, this minimum decreases for the MAM, which then converges with four modes itself like the FDM. So for this case of higher nonlinearity, the reduction achieved by the MAM and the FDM is identical even at this early time $t = 0.05$ sec. On the contrary, the minimum requirement for the FDM increases when the time step is decreased, similar to the first case.

In both cases of this example, the higher-order MAM and the FDM demonstrate superior convergence over the basic modal method, the MDM. Also the FDM is more effective than the MAM for a longer time in the first case with the less temperature-dependent conductivity. The difference in the convergence of the FDM relative to the MAM for the two cases is understood by studying the norm of the respective corrections obtained as discussed in Sec. 4.5. With two modes the proportion of the FDM

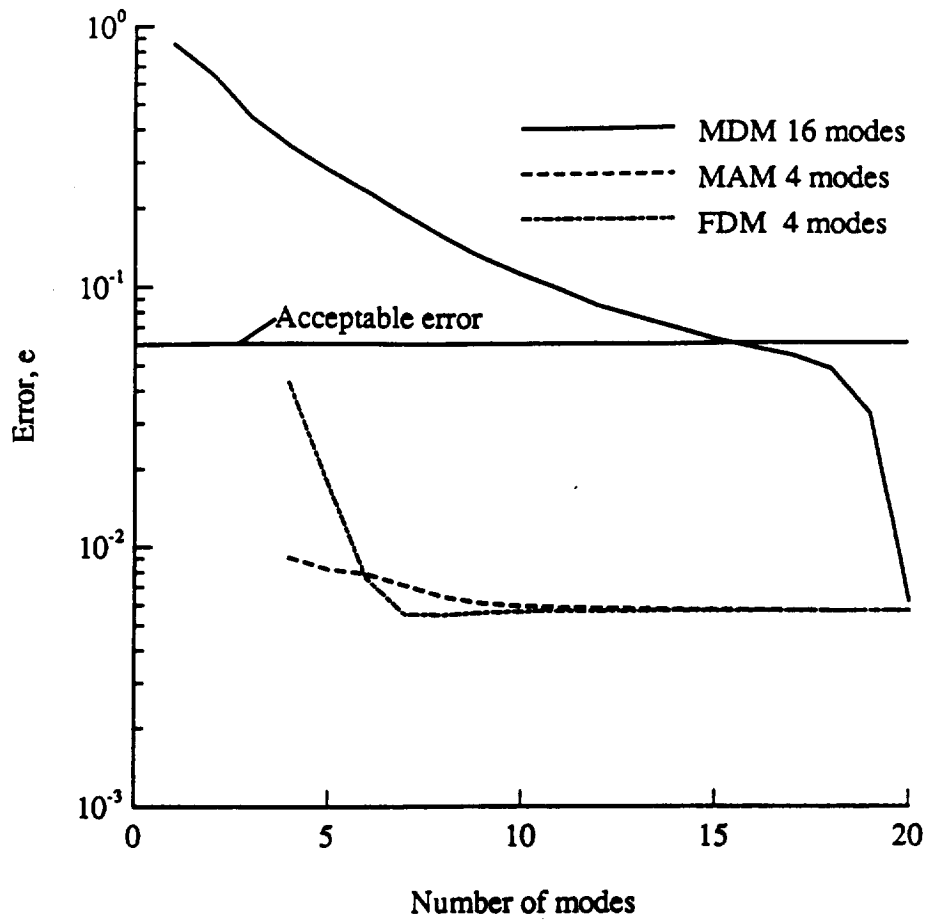


Fig. 6.10 Convergence of the modal methods at time $t = 0.05$ sec (Case 2 of nonlinear example problem 1).

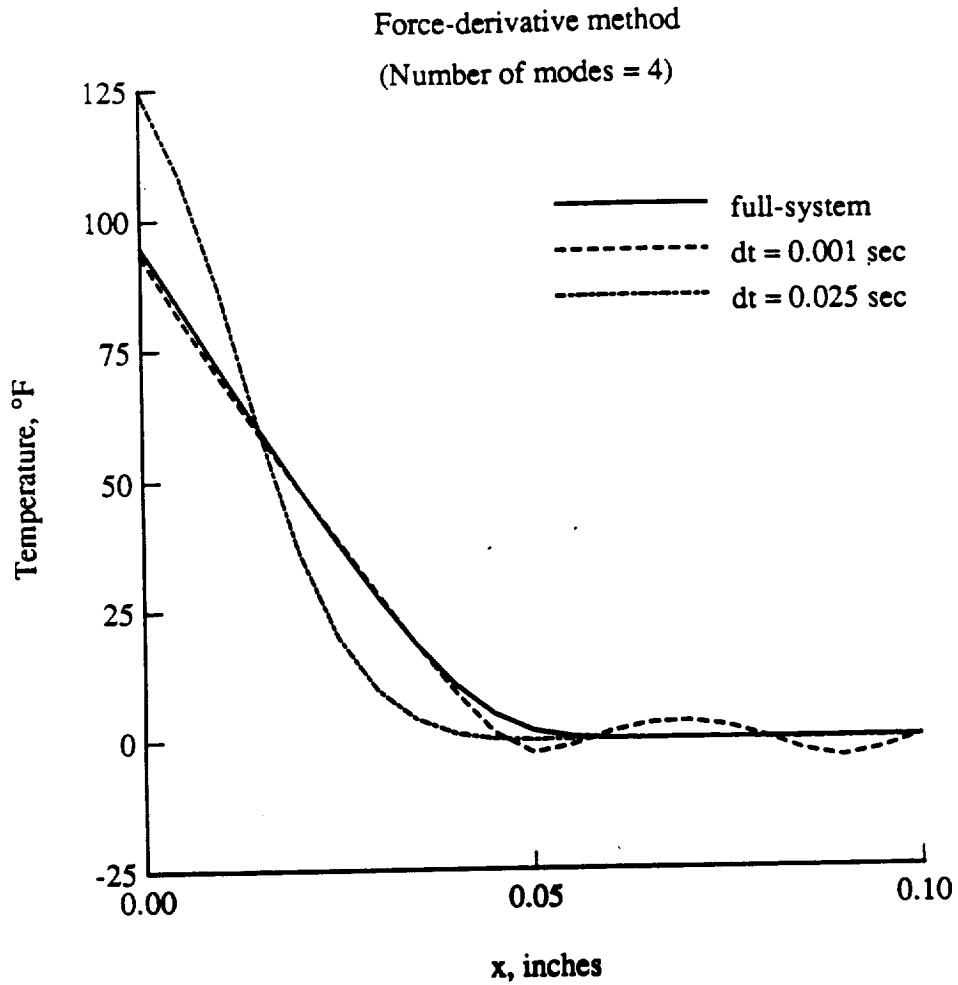
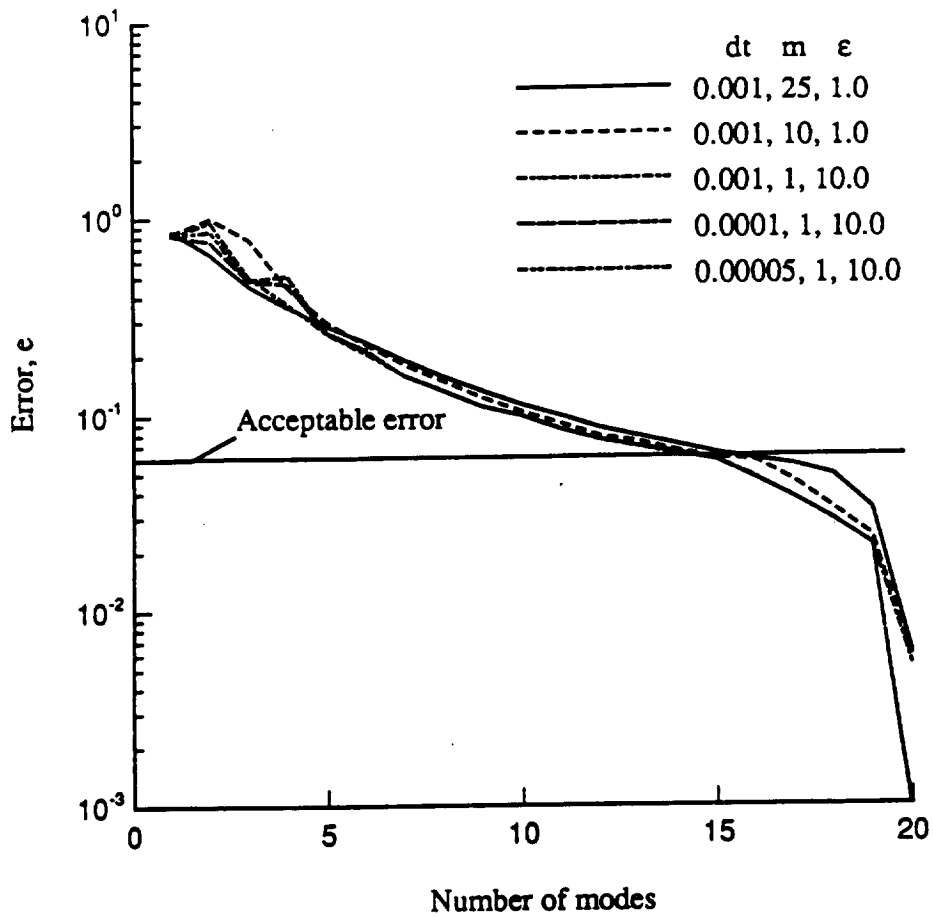
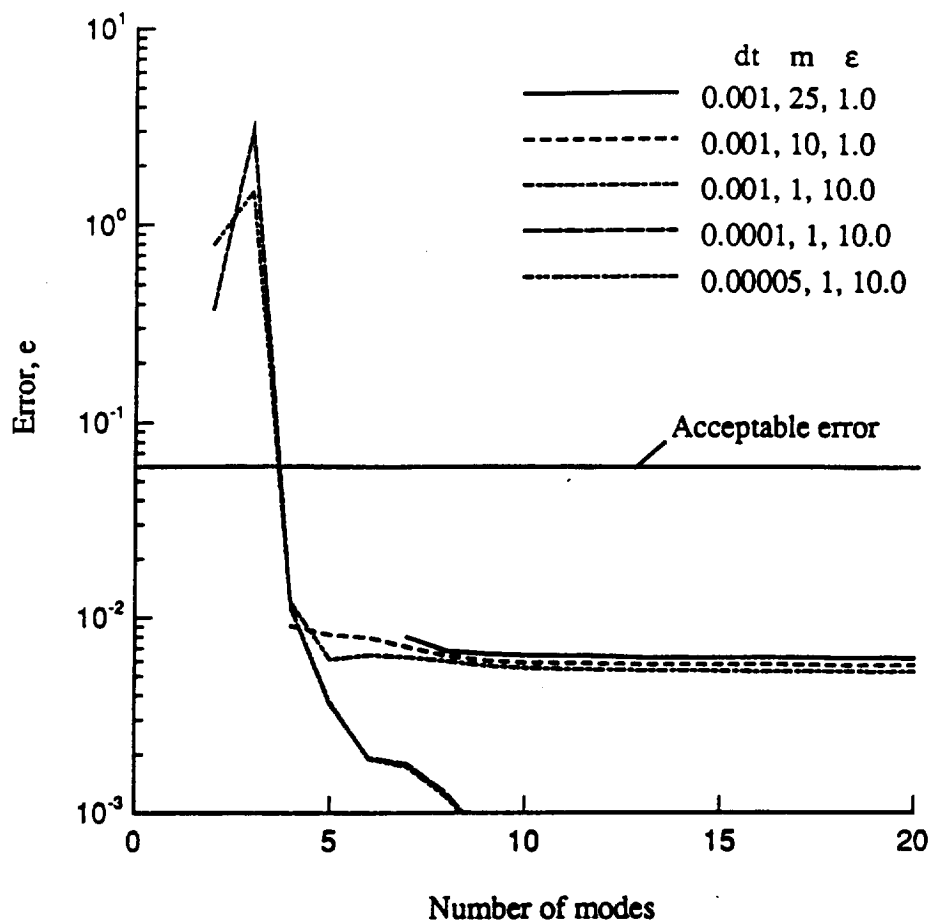


Fig. 6.11 Effect of time step on the response of the FDM at time $t = 0.05$ sec with initial condition at time $t = 0.0$ and one EVP update at time $t = 0.025$ sec (Case 2 of nonlinear example problem 1).



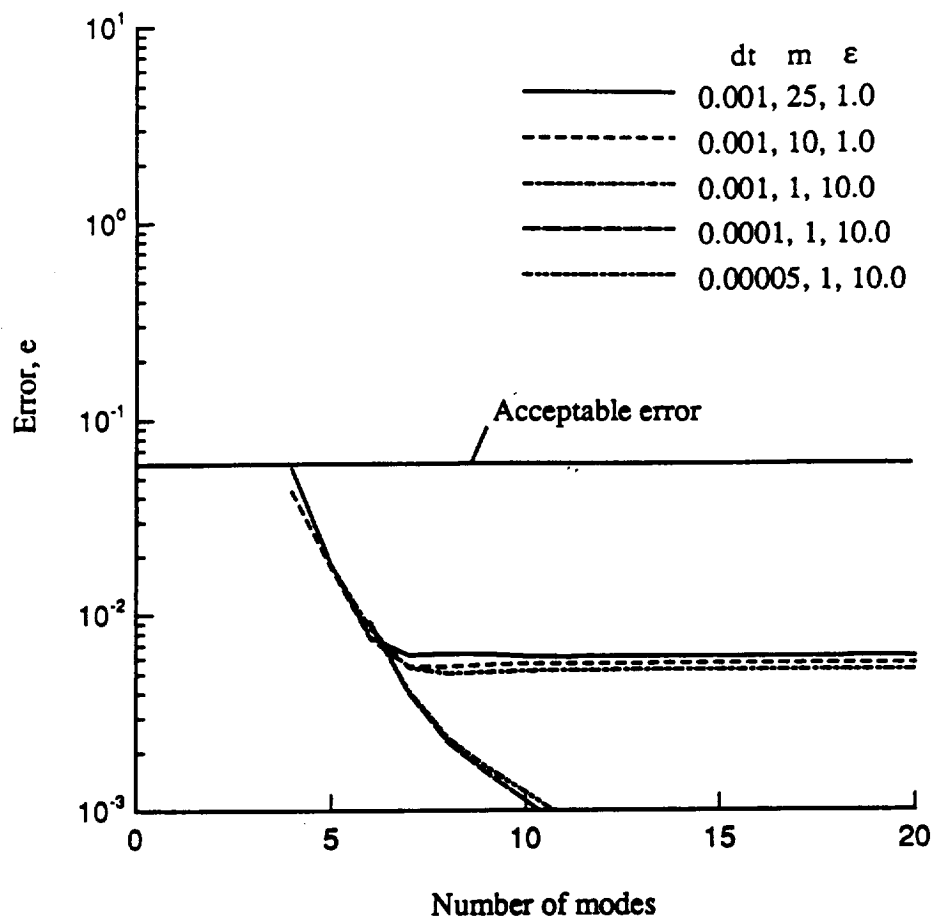
a) Mode-displacement method (MDM).

Fig. 6.12 Effect of time-marching parameters on the number of modes required by the MDM, MAM, and the FDM at time $t = 0.05$ sec (Case 2 of nonlinear example problem 1).



b) Mode-acceleration method (MAM).

Fig. 6.12 Continued.



c) Force-derivative method (FDM).

Fig. 6.12 Concluded.

Table 6.3 Effect of time-marching parameters on the number of modes required at time $t = 0.05$ sec (Case 2 of nonlinear example problem 1)

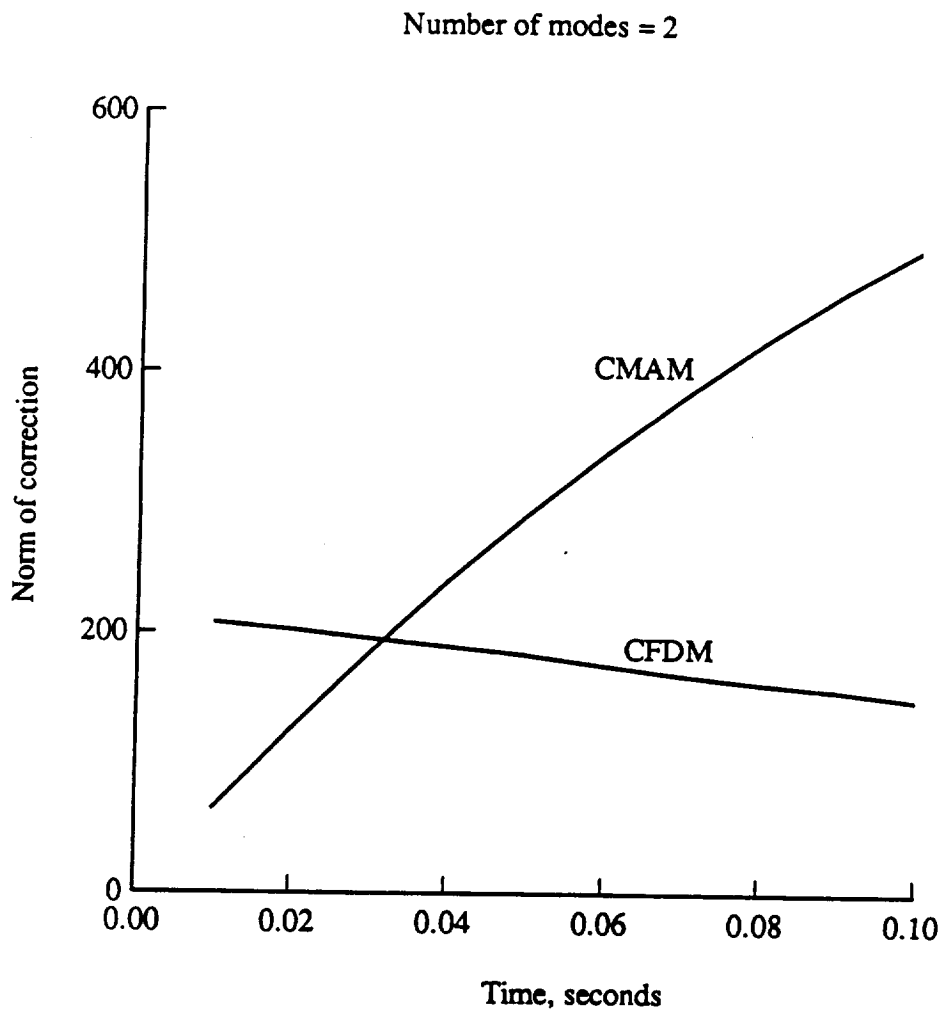
Time-marching parameters			Minimum number of modes for a stable solution			Modes required to converge within the desired accuracy		
dt	m	ϵ	MDM	MAM	FDM	MDM	MAM	FDM
0.001	25	1.0	1	7	4	16	7	4
0.001	10	1.0	1	4	4	16	4	4
0.001	1	10.0	1	4	5	16	4	5
0.0001	1	10.0	1	2	6	16	4	6
0.00005	1	10.0	1	2	6	16	4	6

correction to that of the MAM looks significant at time $t = 0.1$ sec in Fig. 6.13a (Case 1), whereas in Fig. 6.13b (Case 2), with four modes it is almost negligible at time $t = 0.05$ sec. That is, CFDM contributes very little compared to CMAM, to the solution of Case 2. Figures 6.13a and 6.13b also illustrate that the relative importance of the higher-order terms changes with time.

6.2 Lower Surface of Bay 3 of Shuttle Wing Segment

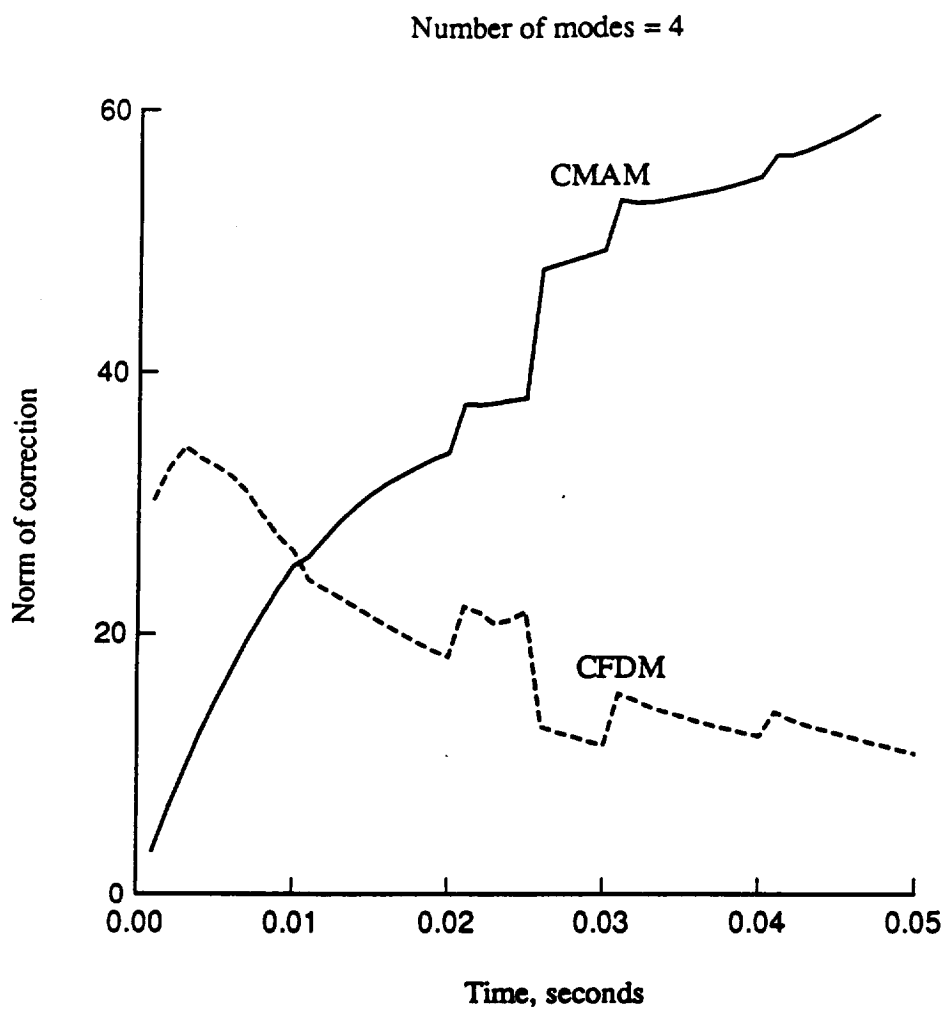
The specific objective of this research is to compare the efficiency of the modal methods, in terms of the reduction achieved, in performing the nonlinear transient thermal analysis of a realistic structure, such as the Shuttle wing segment shown in Fig. 6.14. The thermal model shown in Fig. 6.15 represents a 58 in. segment of the lower surface of bay 3 and consists of a 0.119 in. thick aluminum sheet (to represent the structure) covered by a 1.36 in. thick layer of high-temperature reusable surface insulation (HRSI). The 0.16 in. thick strain isolator pad (SIP) lies between the wing skin and the HRSI. The HRSI is bonded to the SIP and the SIP is bonded to the skin with room temperature vulcanized (RTV) adhesive.

The lateral edges and the aluminum structure are assumed to be adiabatic. The outer wing surface is subject to heat loads representative of Shuttle reentry. The nature of



a) Case 1 of nonlinear example problem 1.

Fig. 6.13 History of the corrections made by the MAM and the FDM.



b) Case 2 of nonlinear example problem 1.

Fig. 6.13 Concluded.

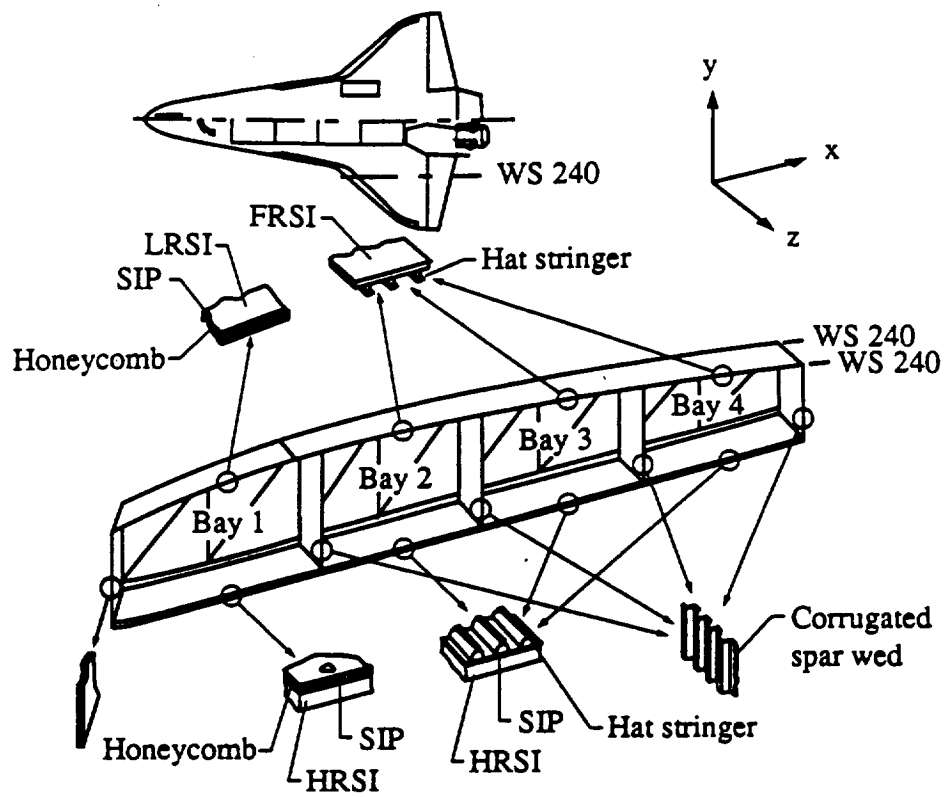


Fig. 6.14 Geometry of Shuttle wing segment at Wing Station 240.

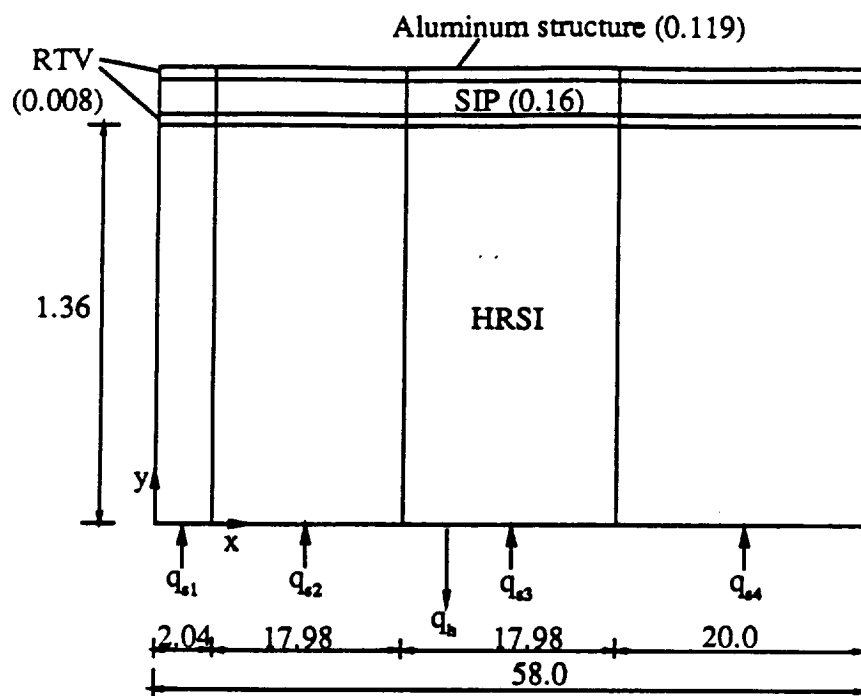


Fig. 6.15 Thermal model of the lower surface of bay 3 of Shuttle wing segment. (Not to scale; all dimensions in inches).

the heating history is significantly complex. As depicted in Figs. 6.16 and 6.17, in addition to the transient variation of the intensity, the spatial distribution of the load on the surface changes dramatically as well. This is a result of the air in the boundary layer over the wing undergoing transition from a laminar to a turbulent flow beginning at about 700 sec into the heating history. Radiation loss from the surface is modeled using an equivalent nonlinear convection coefficient whose variation with temperature is shown in Fig. 6.18a. The thermal properties (specific heat and thermal conductivity) of the HRSI are highly temperature-dependent and their variation is shown in Fig. 6.18b. The various materials involved whose properties considerably differ between them, coupled with the complex imposed heating, result in a nonsymmetric temperature distribution.

6.2.1 Simplified One-Dimensional Model

In a preliminary analysis, the spatial variation in the applied heat load was ignored and uniform specified heating was assumed. This resulted in a simplified one-dimensional model across the thickness of the HRSI. Two-node conduction elements were used to model the HRSI, SIP, RTV and aluminum skin, and zero-length or point elements were used to represent the external heating and convection. The purpose of this analysis is to characterize the finite element discretization necessary across the HRSI thickness, so that the entire thermal response (not only the peak temperature) can be predicted with reasonable accuracy and minimal computational effort throughout the load history. Studies based on the simplified model are used to gain insight into the physics of this problem and to understand how it affects the performance of the modal methods. These preliminary results are expected to be useful in the subsequent finite element modeling of the actual two-dimensional problem.

Mesh Convergence

A series of meshes were generated starting with a relatively coarse mesh (Fig. 6.19) consisting of 16 nodes with ten uniform-length elements through the HRSI

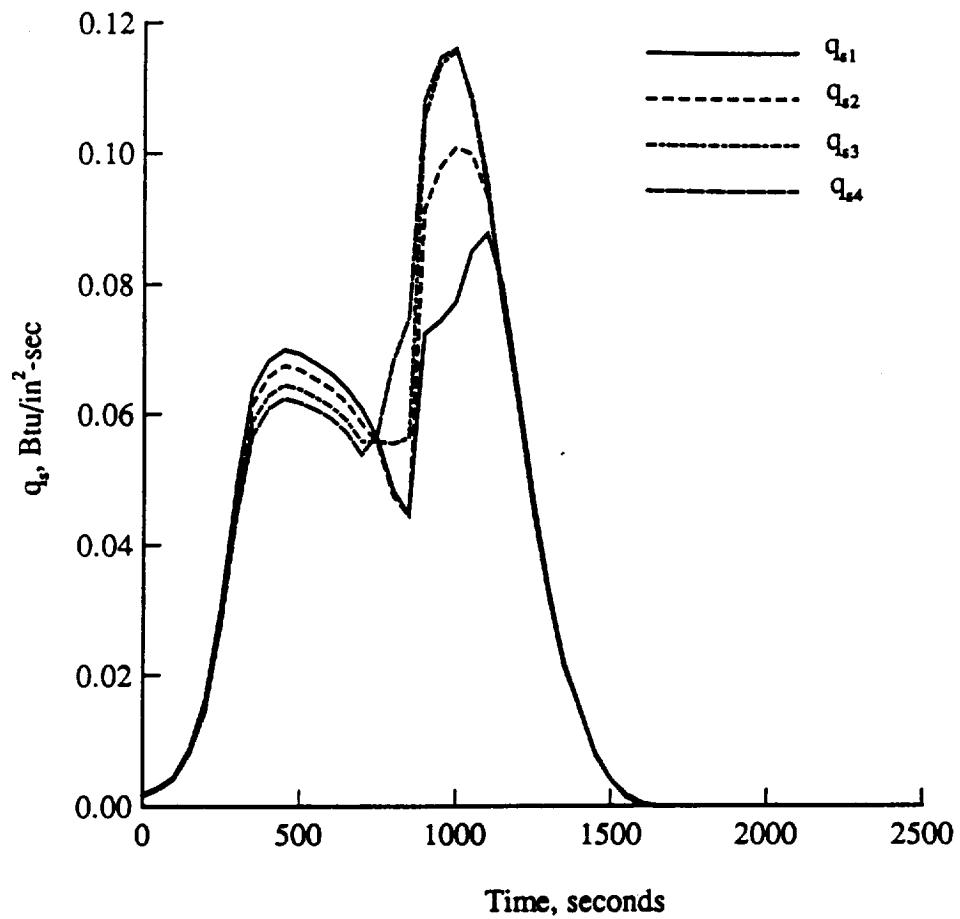


Fig. 6.16 Heating history for the lower surface of bay 3 of Shuttle wing segment (Also see Fig. 6.15).

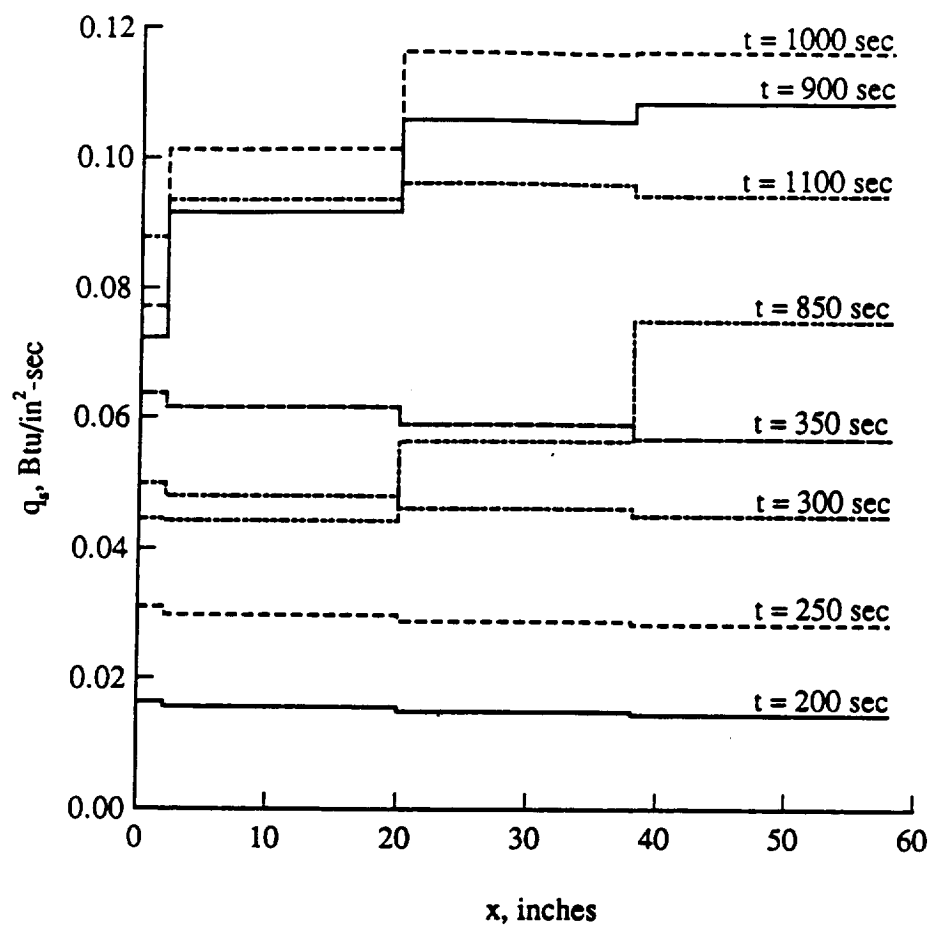
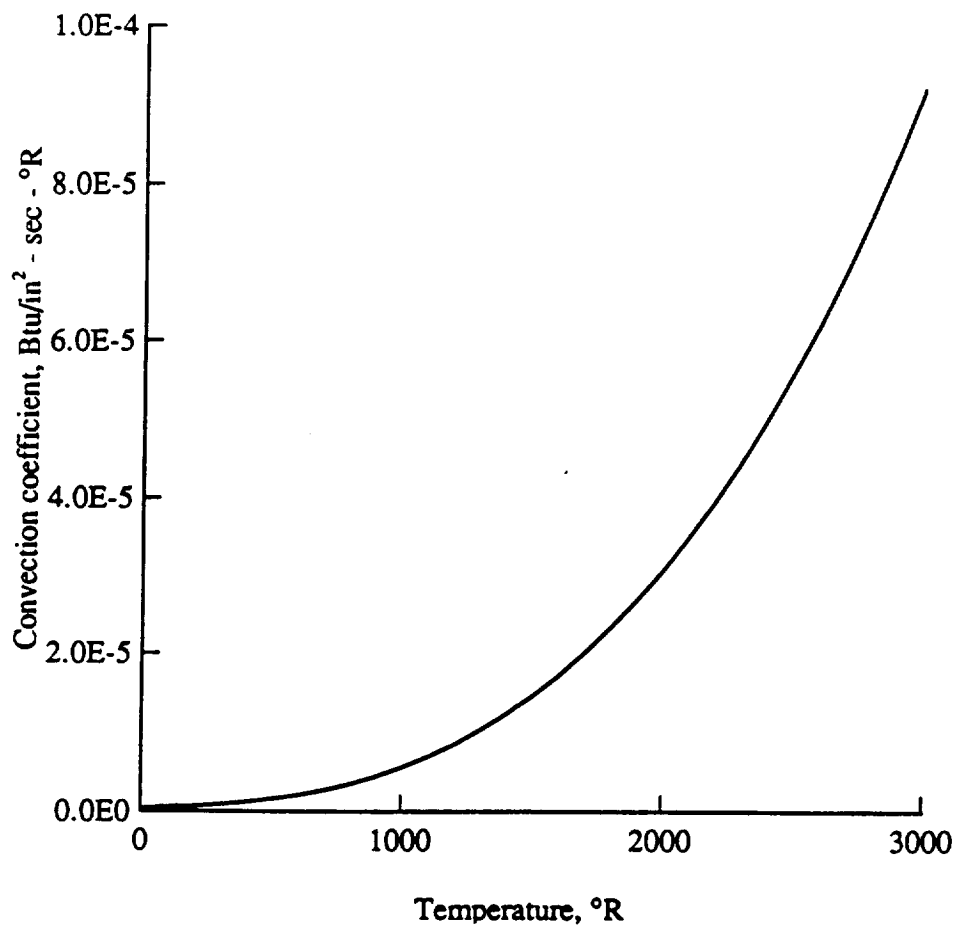
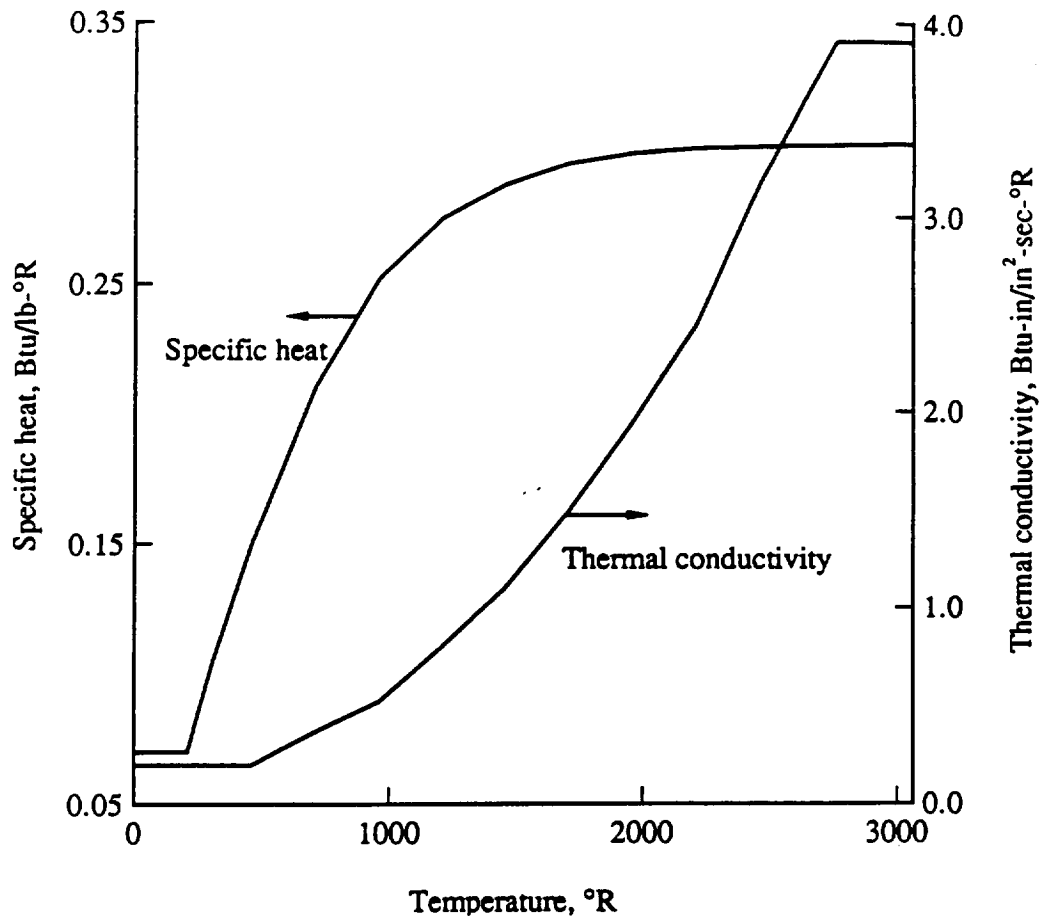


Fig. 6.17 Spatial distribution of discontinuous heat load on the lower surface of bay 3 at selected times (Also see Figs. 6.15 and 6.16).



a) Convection coefficient.

Fig. 6.18 Temperature-dependent quantities.



b) HRSI thermal properties.

Fig. 6.18 Concluded.

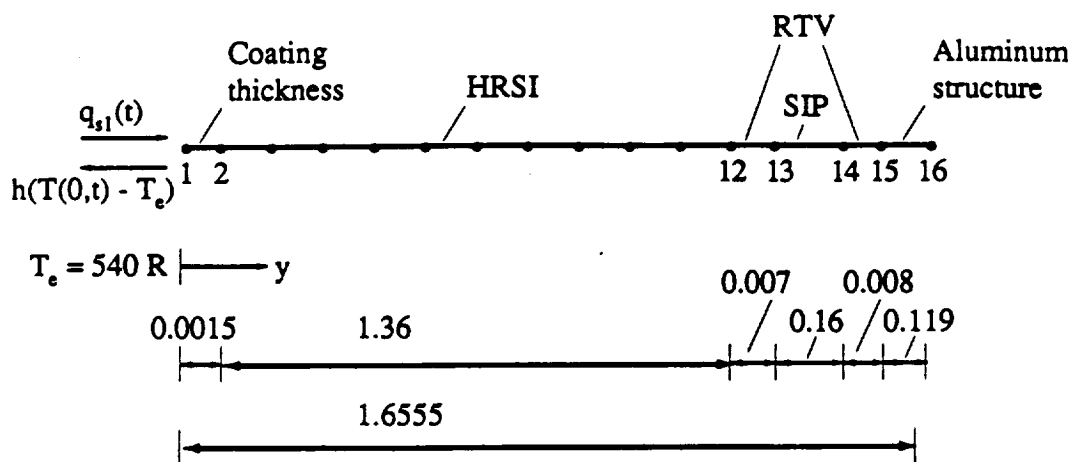


Fig. 6.19 Finite element mesh (16 DOF, uniform) for Shuttle one-dimensional thermal model. (Not to scale; all dimensions in inches).

thickness. Successively refined meshes include 26, 46, 80 and 166 DOF with 20, 40 50 and 160 uniform elements, respectively, to represent the HRSI. Finally, based on the nature of the problem, the 16 DOF mesh with ten uniform elements was modified to have ten graduated elements with an arbitrary stretching factor of 2. This gives a large range of element sizes, with fine elements in the region near the heated end and very large elements in the interior.

The full-system solutions were obtained using a relatively small time step $dt = 0.5$ sec with the eigensolution updated every time step. The well-refined 166 DOF system yields a very smooth solution as depicted by the solid lines in Figs. 6.20 and 6.21. The temperature at the HRSI surface rises very rapidly as the heating is applied and diffuses rather slowly through the HRSI thickness and SIP to the aluminum skin as shown in Fig. 6.20. After peak heating occurs at time $t = 1100$ sec, the surface begins to cool while the temperatures of the interior of the HRSI and the aluminum skin continue to rise. The temperature distribution pattern in Fig. 6.21 shows steep gradients at early time due to the low conductivity of the HRSI. A good modal solution should capture this nonlinear behavior accurately with as few modes as possible.

The 166 DOF solution is considered to be converged and is used to compute the distribution error norm of the other full-system solutions, to determine the adequacy of the meshes. As expected, the coarse 16 DOF systems both uniform and graded, have the highest error norm over the entire time period with a maximum of 0.008 and 0.017 respectively at times $t = 275$ sec and $t = 475$ sec. The corresponding full-system solutions denoted by triangles and circles respectively (Fig. 6.21), are compared with the converged solution at discrete times when the errors are high. The distribution of the uniform mesh is not as smooth as those of the finer uniform meshes (not shown); nevertheless the nodal temperatures match those of the 166 DOF mesh at corresponding locations. The full-system solution of the graded mesh is far from smooth. The error at

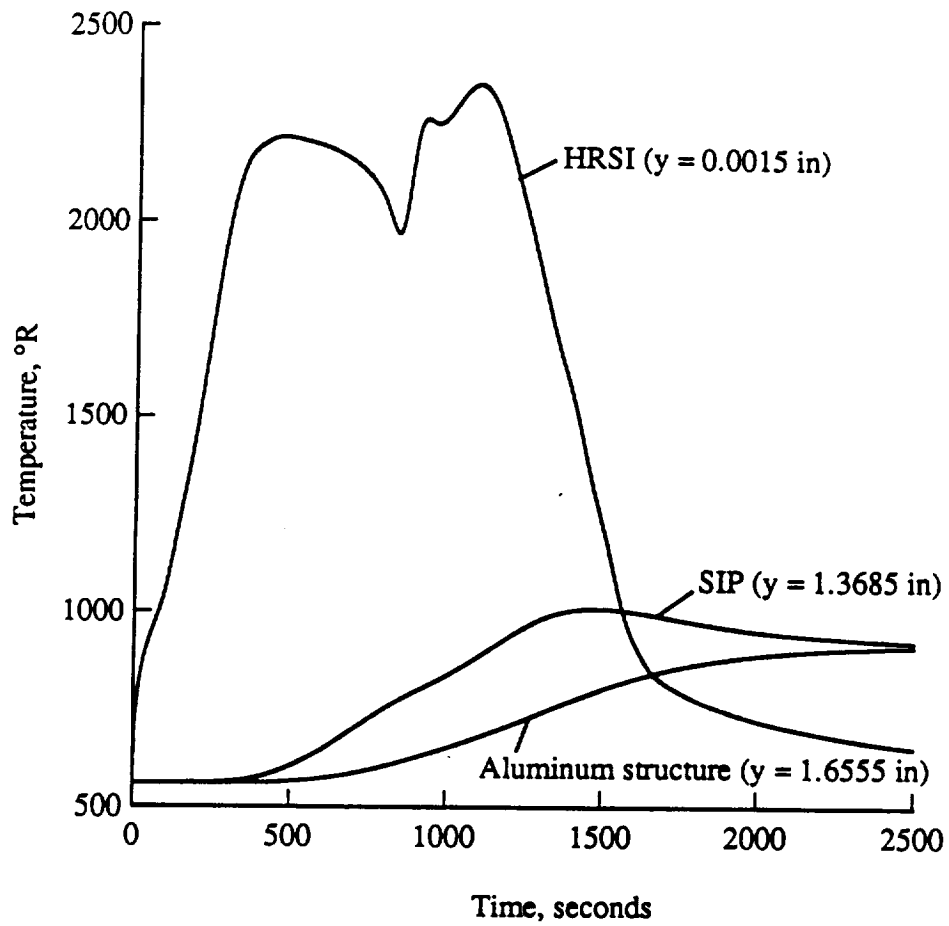


Fig. 6.20 Temperature histories at different locations through a Shuttle tile and substructure obtained from a one-dimensional thermal model (Also see Fig. 6.19).

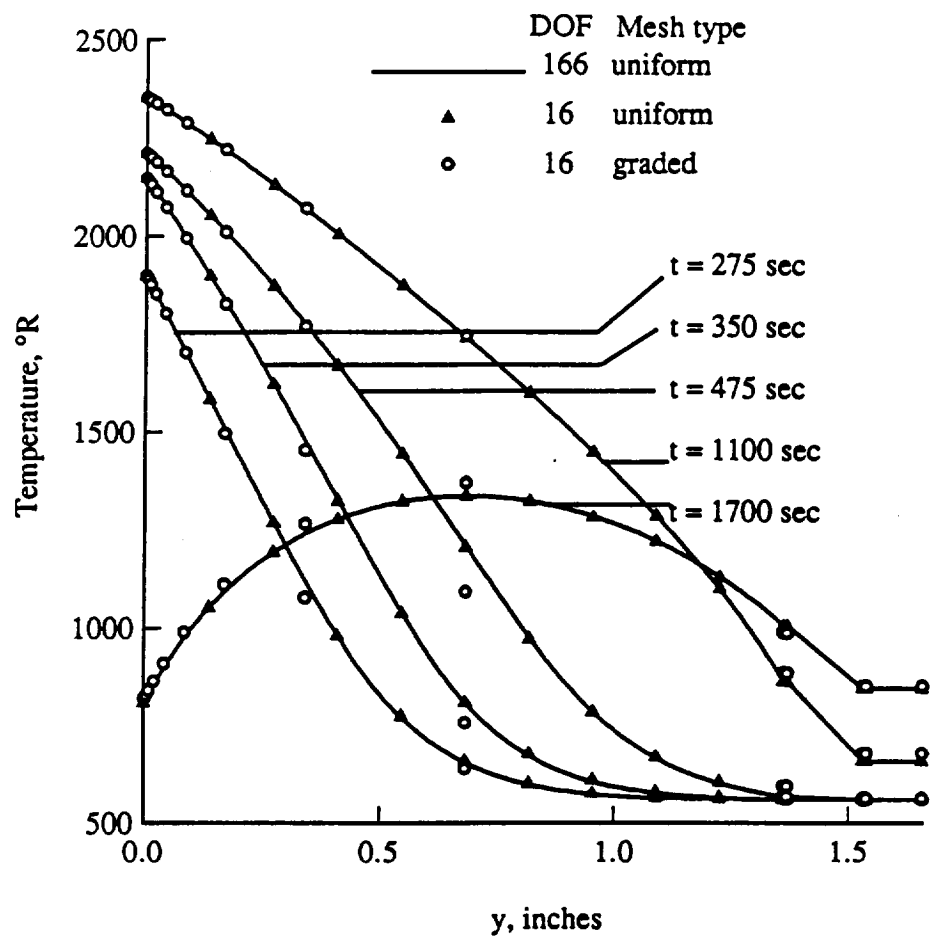


Fig. 6.21 Comparison of full-system solutions of different meshes for Shuttle one-dimensional thermal model.

the location of the mid-HRSI thickness starts increasing around time $t = 350$ sec and reaches a maximum at time $t = 475$ sec (temperature distribution at intermediate times are not shown), when the peak temperature is almost reached but the temperature penetrates at a fast rate due to increase in conductivity, but the nodes are too far apart to capture this nonlinear behavior. Notwithstanding this error, the peak temperature as well as the gradient at the heated end are captured accurately at all times. The 46 DOF and 80 DOF solutions are very smooth and agree with the converged solution.

Convergence of Modal Methods for the Various Meshes

Having determined the limitations of the various meshes used and the accuracy of the respective full-system solutions, the modal solutions were obtained to identify the effect of the mesh on the eigensolution and hence on the efficiency of the modal methods. Although the transient variation of the load is curvilinear (Fig. 6.16), the thermal analyzer assumes linear variation between the specified input times so that the highest order modal method that can be used is the second-order FDM. For the purpose of a one-to-one comparison, a time step of 2 sec (determined by some trial and error) was used in all of the following analyses, (except where indicated otherwise) and the eigensolution was updated every 50 sec (that is, $m = 25$).

With the crude 16 DOF uniform mesh, each of the three methods requires 12 (75%) modes to converge, yielding a reduction of only 25%. While in the case of the graded mesh, the coarseness produces an inadequate solution accuracy in the interior of the HRSI, in the uniform mesh it decreases the efficiency of the MAM. The MAM converges with 20 modes on all other uniform meshes. This yields a steady increase in the percentage of reduction achieved with refinement beyond the 26 DOF mesh as seen in Fig. 6.22. It is noteworthy that with the 16 DOF coarse but graded mesh, the MAM shows a dramatic convergence with just 6 modes, 50% less modes than the uniform mesh, subject to the error bound of the full-system solution. This reduction is

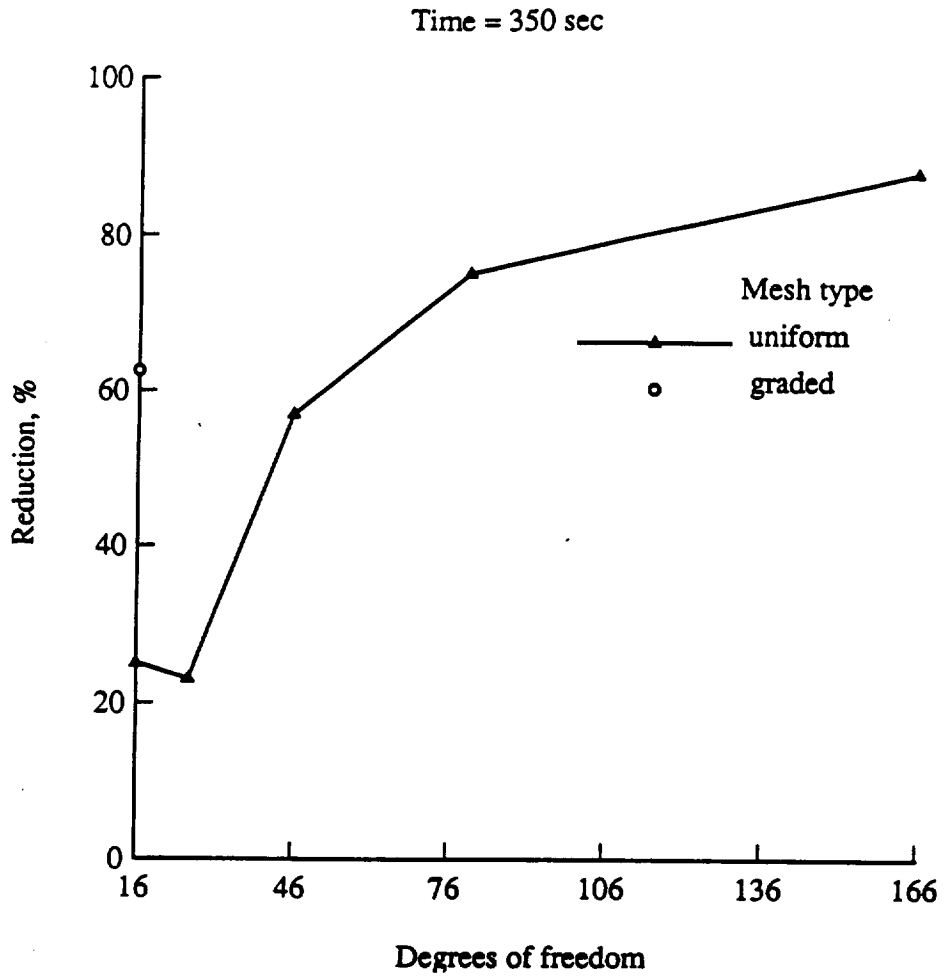


Fig. 6.22 Effect of finite element mesh on efficiency of the MAM for Shuttle one-dimensional thermal model.

comparable to that of the much finer 46 DOF uniform mesh. The increase in efficiency of the MDM is observed to be far less with the graded mesh which requires 11 modes (instead of 12 modes for the uniform mesh) and even with the finest 166 DOF mesh which still needs to retain 70 (42%) modes. Based on the requirement for convergence throughout the heating history, the FDM has not performed better than the MAM with any mesh (this issue is discussed later). Table 6.4 summarizes some of these results below.

Table 6.4. Comparison of reduction achieved by the MDM and the MAM for Shuttle 1-D model

Mesh description	Required number of modes		Reduction %	
	MDM	MAM, FDM	MDM	MAM, FDM
16, uniform	12	12	25.0	25.0
16, graded	11	6	31.25	62.5
166, uniform	70	20	58.0	88.0

Figure 6.23 compares the eigenvalues of the meshes at time $t = 350$ sec and clearly shows how the mesh affects the distribution of the eigenvalues within the spectrum. The relative position of the fourth eigenvalue corresponding to the 16 DOF meshes, for instance, is given by 0.25 on the x-axis in Fig. 6.23. Mesh refinement enhances the rate of increase of the eigenvalues at the lower end of the spectrum, although the degree of enhancement decreases as the mesh becomes finer. A higher magnitude for the eigenvalues has been attained more efficiently, that is, by retaining fewer DOF in the mesh, by a suitable grading of the element sizes. This explains why the efficiency of the MAM with the 16 DOF graded mesh is comparable to the efficiency with the much finer 46 DOF mesh, and is much higher than that with the 16 DOF uniform mesh. A comparison of the mode shapes of the 16 DOF uniform and graded meshes shown in Figs. 6.24a and 6.24b shows how the steep gradients can be well-captured by fewer modes of the graded mesh.

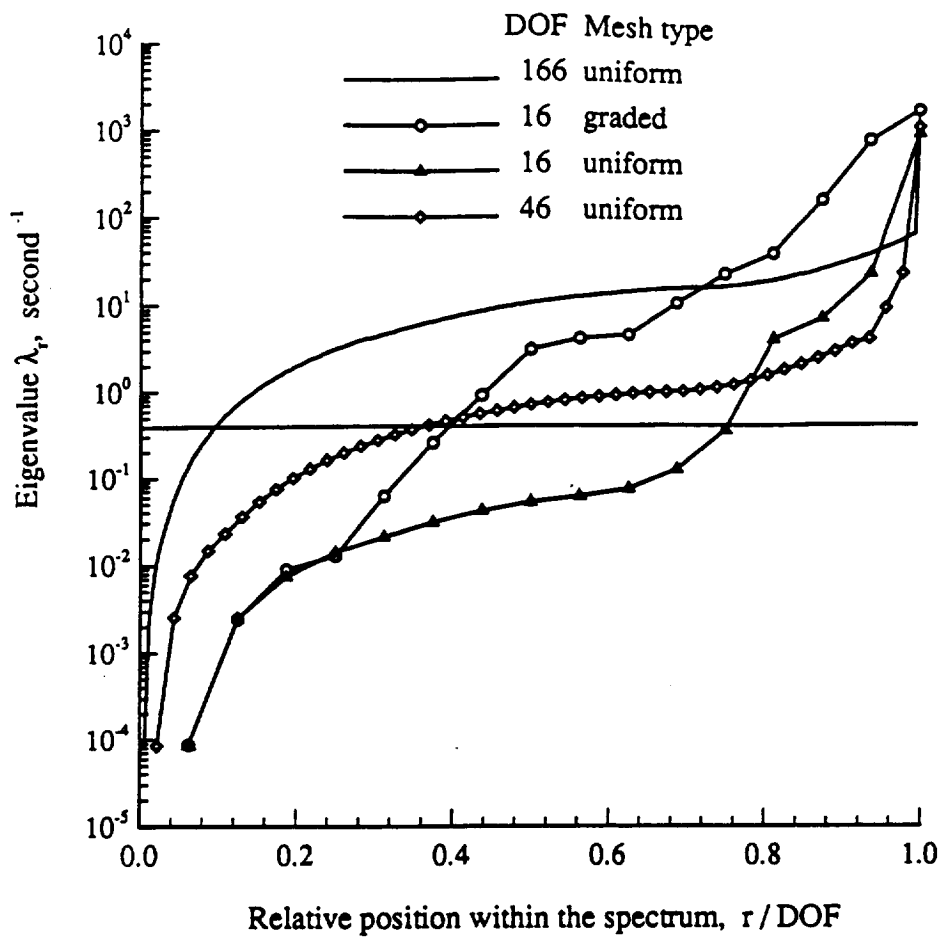
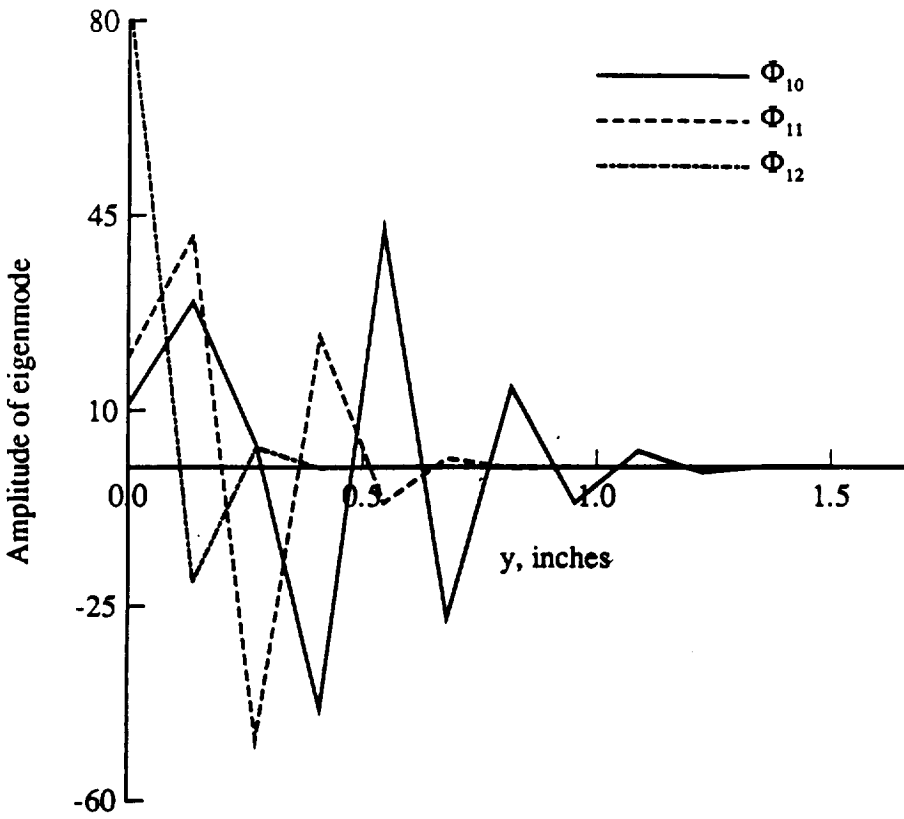
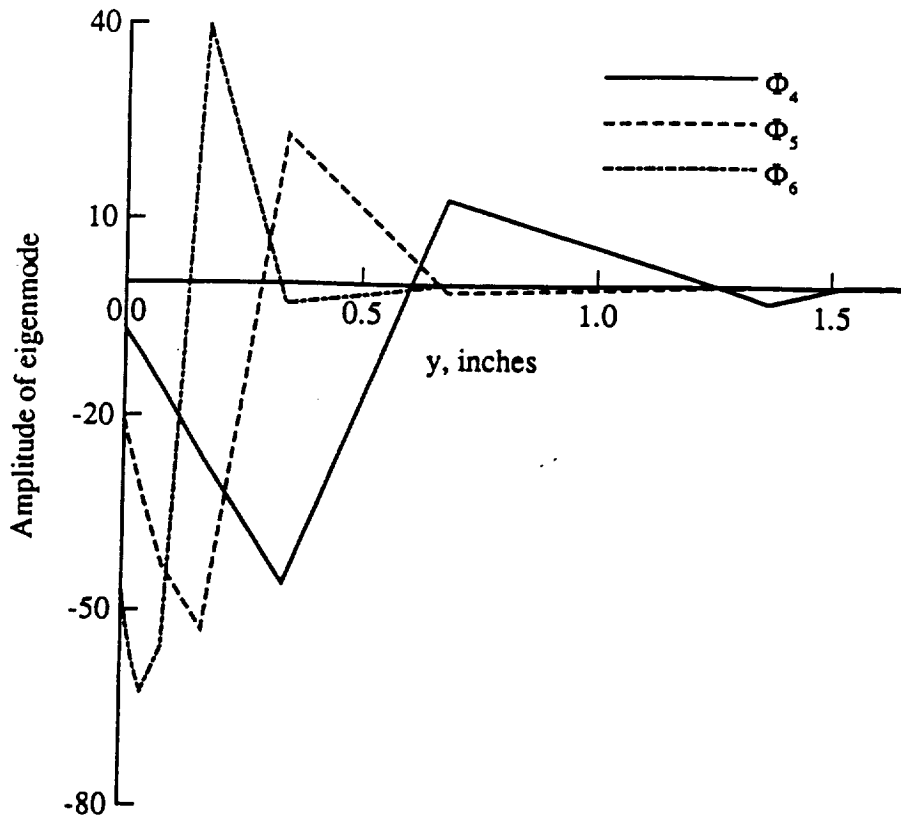


Fig. 6.23 Comparison of eigenvalues at time $t = 350$ sec of the different meshes for Shuttle one-dimensional thermal model.



a) Uniform mesh.

Fig. 6.24 Mode shapes at time $t = 350$ sec of the 16 DOF meshes for Shuttle one-dimensional thermal model.



b) Graded mesh.

Fig. 6.24 Concluded.

As in the previous examples, the MAM has achieved a remarkable improved reduction compared to the MDM for this one-dimensional model of the Shuttle example. For this example, although the heating history is transient, the FDM does not lead to any improvement over the MAM with any mesh. The number of modes required for convergence of the MDM and the MAM are based on the requirements for a stable as well as accurate solution over the entire time domain.

The corrections CMAM and CFDM discussed in Sec. 4.5, were computed for the 166 DOF mesh based on the initial eigensolution and the applied load at time $t = 50$ sec. As estimated from Fig. 6.25, the FDM and the MAM converge with four and eight modes respectively at time $t = 50$ sec and the corresponding distributions shown in Fig. 6.26 confirm the accuracy of these estimates. The convergence of CMAM and CFDM at different times shown for the 166 DOF and 16 DOF graded meshes in Figs. 6.27a and 6.27b were obtained using the corresponding full-system solutions at each time. As depicted qualitatively in these figures, the more-effective higher-order method and the modes required for convergence vary with time for this complex nonlinear problem with a transient load. That is, the correction offered by the FDM to the MAM becomes negligible rather early in time, whereas the correction offered by the MAM to the MDM remains significant even at a much later time $t = 950$ sec. This data was not used directly, however, to estimate the modes required for this problem.

Effect of Transient Load and Nonlinearity on the Performance of the Modal Methods

For this study a piecewise linear approach with $dt = 0.5$ sec was used. For the 166 DOF mesh, the response of the FDM with four modes becomes unstable after time $t = 200$ sec. Both the MAM and the FDM converge with the same number of modes after time $t = 250$ sec. Similarly for the 16 DOF mesh, the MAM and the FDM converge with five modes up to time $t = 300$ sec. Recalling the implementation described in Sec. 4.6, the full form of the generalized load vector was used for the MAM but only the

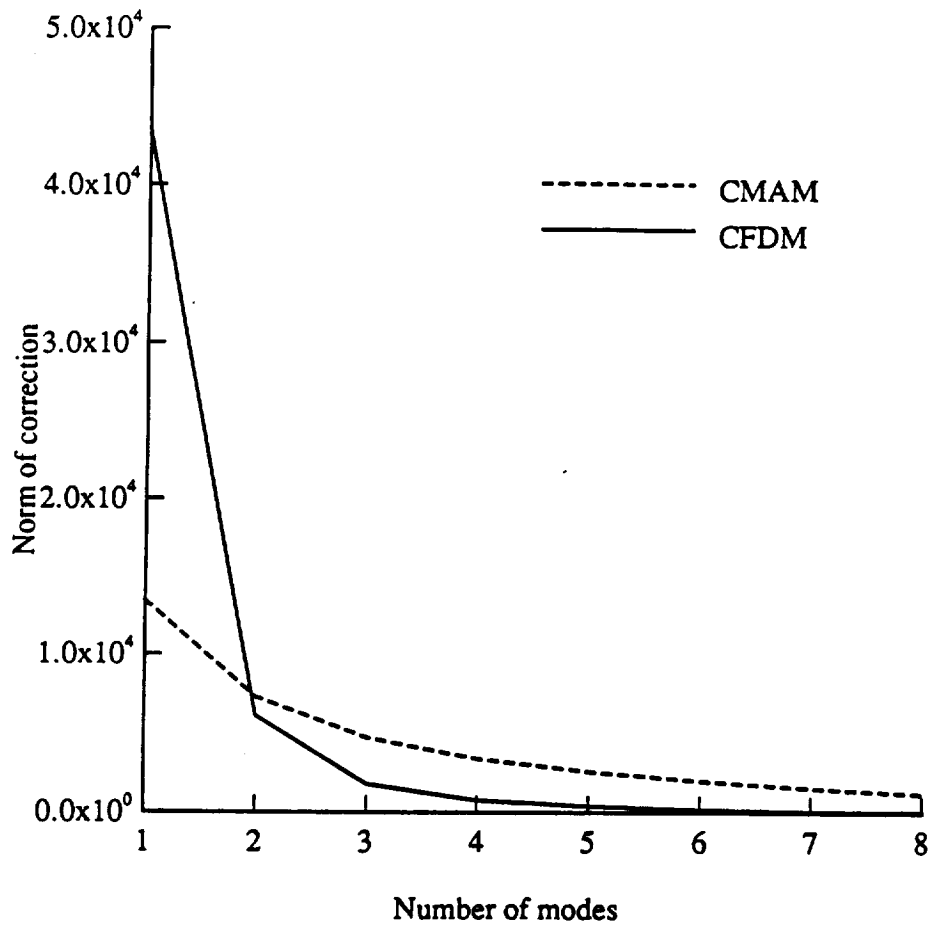


Fig. 6.25 Convergence of the corrections offered by the MAM and the FDM, CMAM and CFDM respectively, at time $t = 50$ sec using the Shuttle one-dimensional thermal model with 166 DOF.

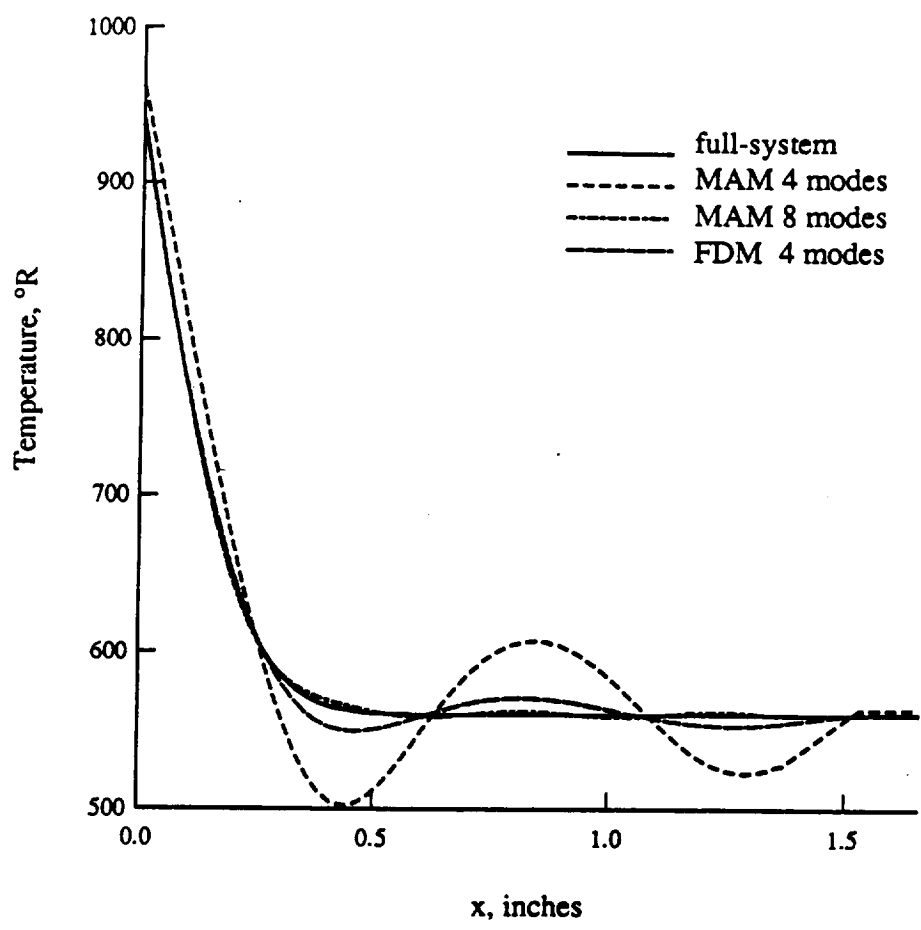
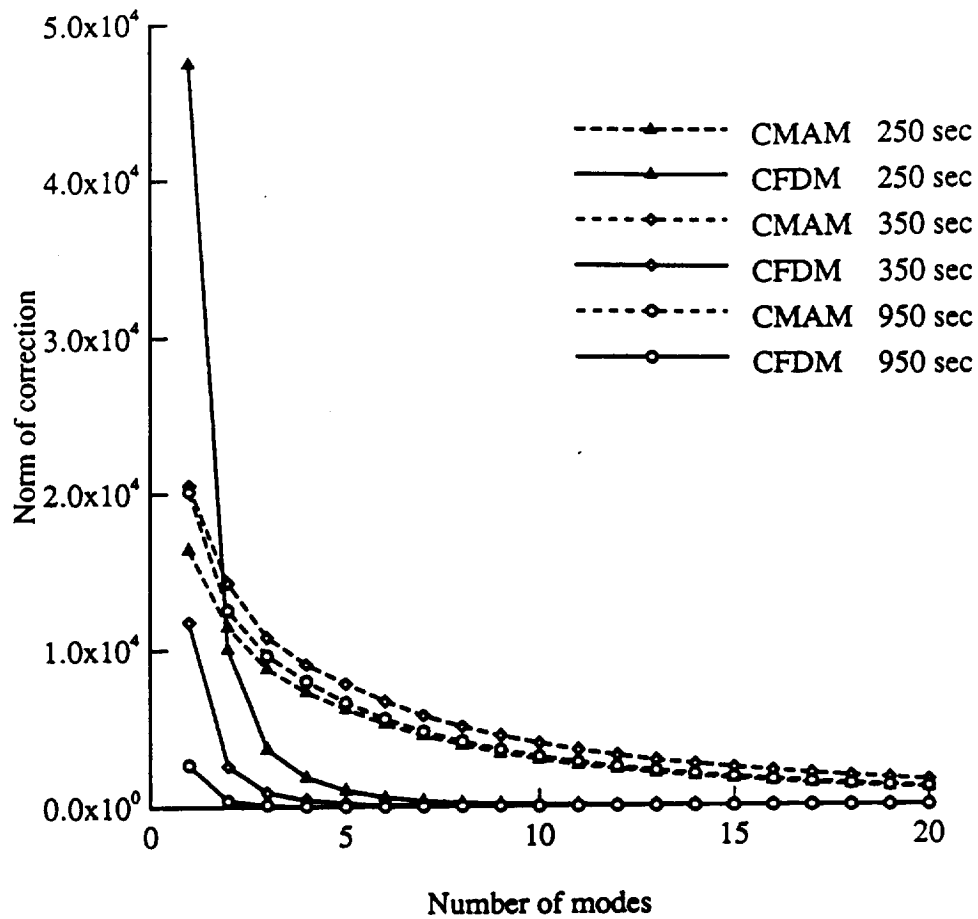


Fig. 6.26 Temperature distributions obtained by the MAM and the FDM at time $t = 50$ sec using the Shuttle one-dimensional thermal model with 166 DOF.



a) 166 DOF uniform mesh.

Fig. 6.27 Convergence of the corrections offered by the MAM and the FDM, CMAM and CFDM respectively, at different times for Shuttle one-dimensional thermal model.

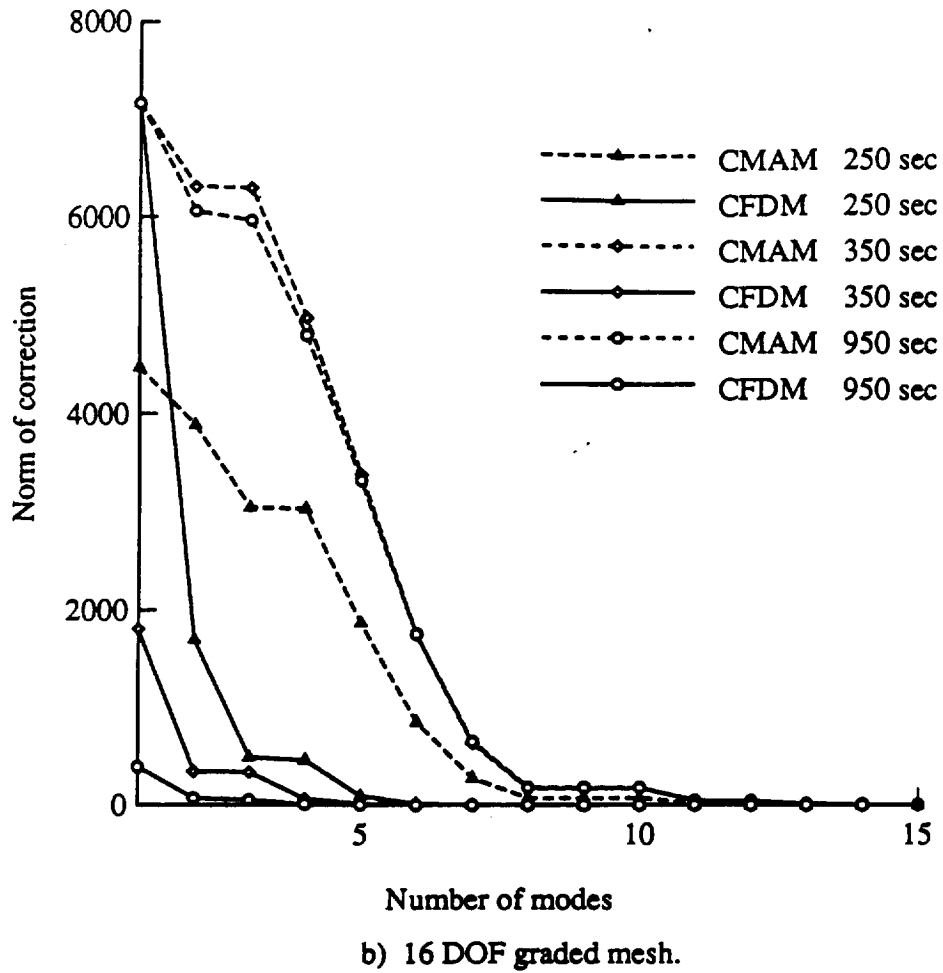


Fig. 6.27 Concluded.

approximate form of the derivative of the generalized load vector was used for the FDM. However, since the eigensolution was updated every time step in this study and no iterations were made, the nonlinear correction did not exist. Also for the 16 DOF graded mesh, the derivative of the nonlinear convection heat load vector (Fig. 6.28), computed based on the full-system solution, was included so that no approximation was actually made to the FDM.

In the early stages, CFDM is significant and increases with time (Figs. 6.27a, 6.27b) so that the FDM converges faster than the MAM. Later on, between times $t = 250$ sec and $t = 300$ sec, the trend reverses and CFDM decreases until the MAM becomes the most effective method. Figure 6.28 shows that the derivative of the applied heat load reaches a local peak at time $t = 250$ sec and then starts decreasing while the magnitude of the load itself is still increasing as seen in Fig. 6.29. The change in effectiveness of the FDM with time, which is experienced with both meshes, may be governed by the heating history for this problem.

Although the MAM gives a converged solution with five modes for the 16 DOF mesh up to time $t = 300$ sec, the eigenvalues (Fig. 6.30), and hence the response, exhibit unrealistic oscillations in time. The difficulty faced by the MAM in predicting a stable solution after time $t = 300$ sec can be qualitatively explained with the help of Fig. 6.31. The normalized participation factor gives a measure of the contribution of each mode in representing the total load vector at different times. The spatial distribution of the load does not change with time for this 1-D model; however, the mode shapes vary with time due to the temperature-dependence of the thermal properties. Although the magnitude of the load is increasing with time, Fig. 6.31 shows that the participation of the modes steadily decreases from the initial time and reaches a minimum between times $t = 300$ sec and $t = 400$ sec when the inclusion of sufficient modes becomes necessary for a stable solution after this time. This pattern was observed with the finer meshes too, which gave

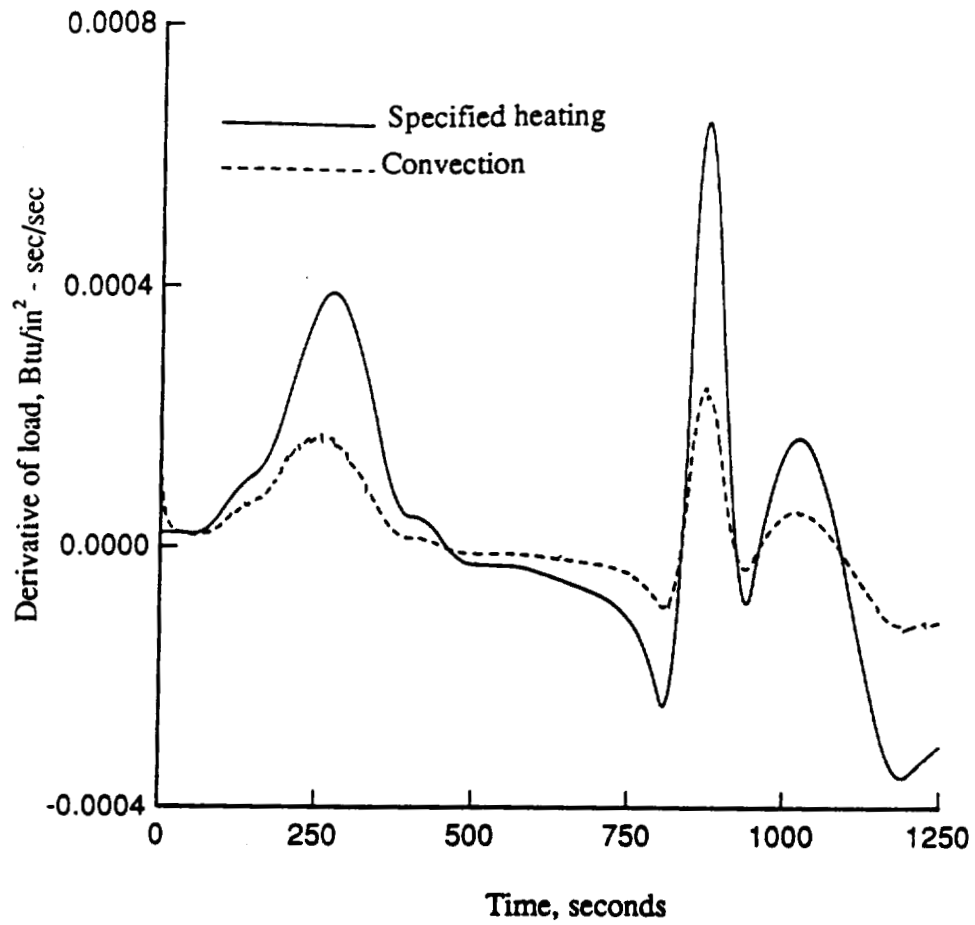


Fig. 6.28 Comparison of the histories of the first derivative of the specified and convective heat loads for the Shuttle one-dimensional thermal model.

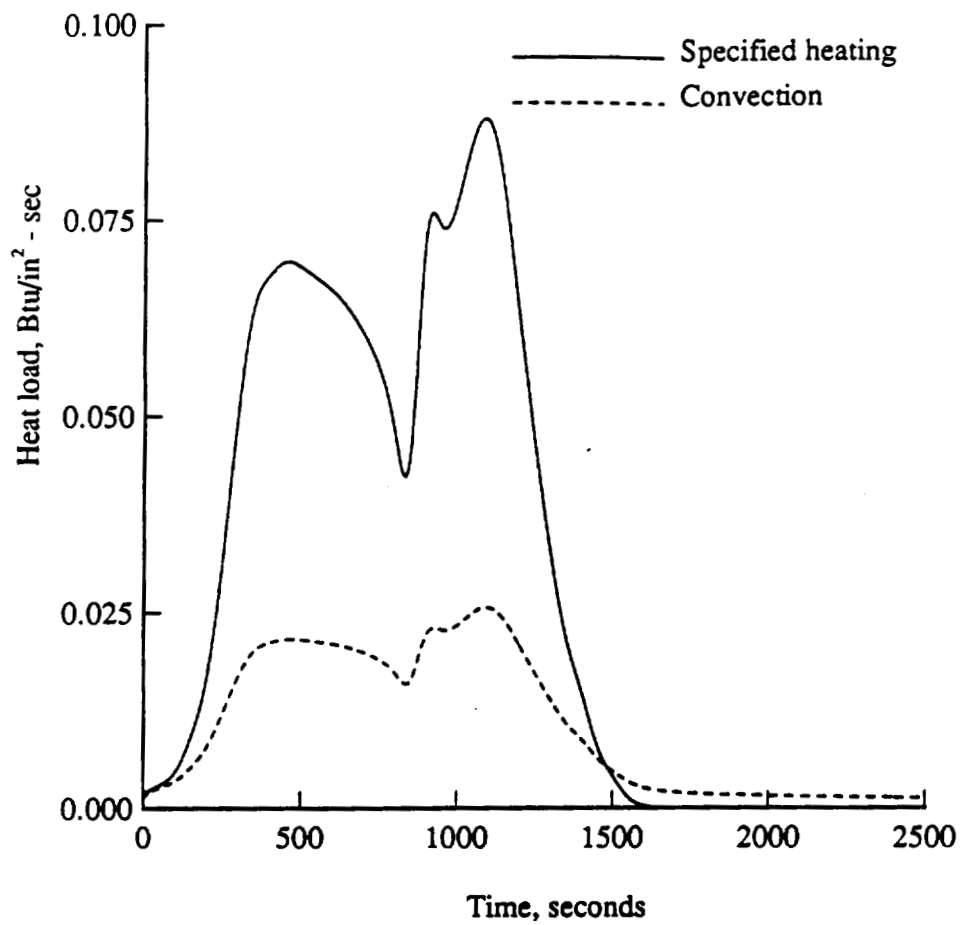


Fig. 6.29 Comparison of the histories of the specified and convective heat loads for the Shuttle one-dimensional thermal model.

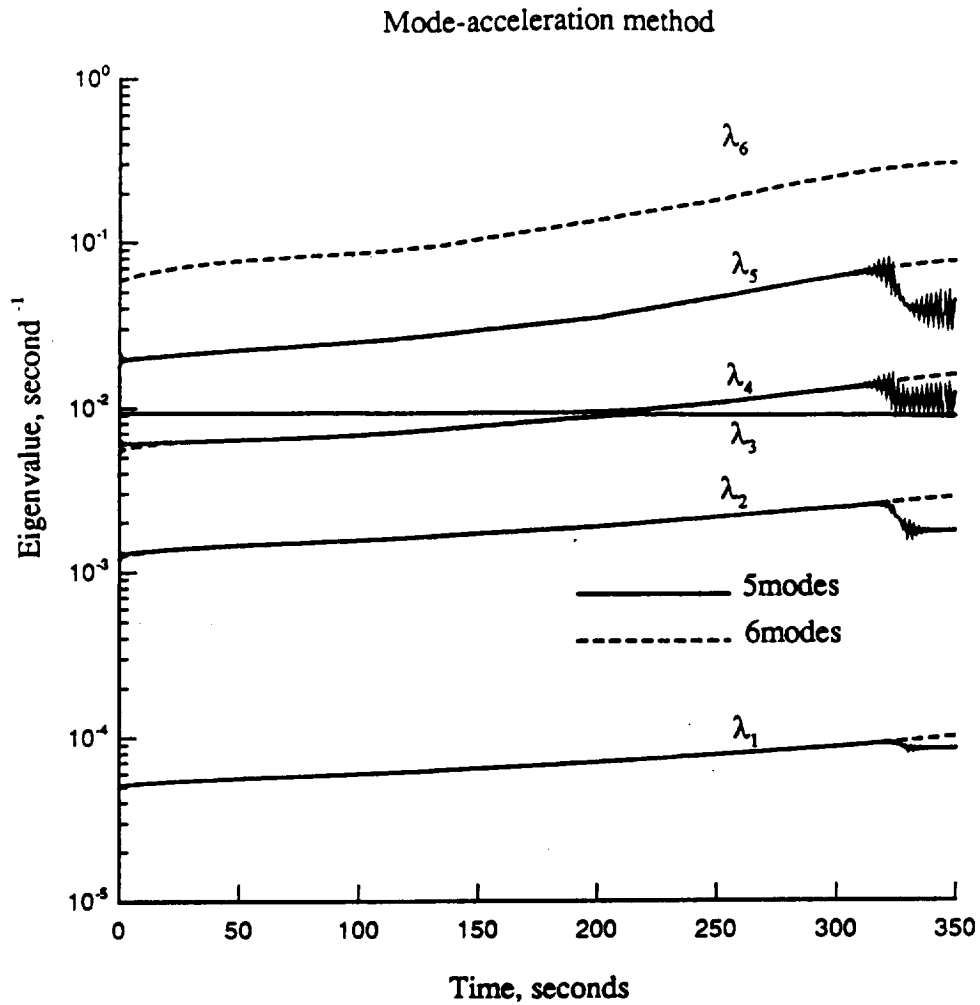


Fig. 6.30 Comparison of the histories of the eigenvalues of the 16 DOF graded mesh for Shuttle one-dimensional thermal model.

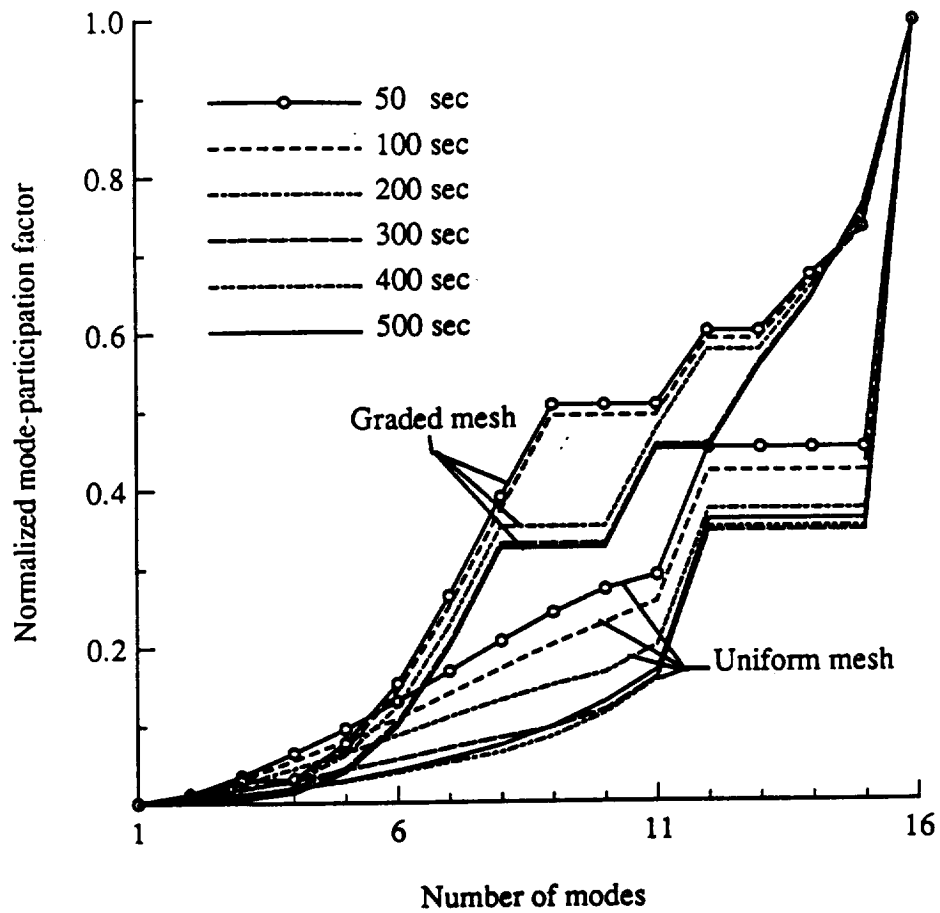


Fig. 6.31 Variation of the normalized mode-participation factors with time for different meshes of Shuttle one-dimensional thermal model.

a stable converged solution with 17 modes itself (instead of 20), provided the time step was decreased near time $t = 300$ sec. The MDM, however, is well-behaved even with much fewer modes than that required for convergence, although the solution is quite inaccurate as seen in Fig. 6.32.

6.2.2 Two-Dimensional Model

This example demonstrates the capability of the proposed higher-order modal method for solving complex situations with a much smaller set of equations than the MDM. Two-dimensional quadrilateral elements were used to model the HRSI, SIP and RTV while the aluminum structure, the heat load and the nonlinear surface convection were represented by line elements. Based on the experience with the 1-D model, the MAM was selected as the main focus in these analyses. For the 2-D model of the Shuttle problem (Fig. 6.15), the additional complexity involved is the spatial variation of the heat load. The magnitude of the load increases rapidly in a more or less spatially uniform manner from time $t = 200$ sec to time $t = 350$ sec (Fig. 6.17), and then the distribution becomes nonuniform. Also, around time $t = 700$ sec the pattern starts reversing, and by time $t = 850$ sec a step-like distribution pattern develops. Then the magnitude of the load increases at the maximum rate up to time $t = 900$ sec and after reaching the peak value at $t = 1000$ sec, the distribution becomes uniform again. A variation of the nonuniform load was also considered where the loads do not change abruptly as described earlier but in a much smoother manner as shown in Fig. 6.33.

It is therefore prudent to arrive at the optimum mesh which can accurately represent the gradients, which in this case occur not only across the HRSI thickness but along the wing surface as well. For both cases of the spatially-varying load, judging from the 1-D analysis results, the discretization of the 16 DOF graded mesh was chosen across the HRSI thickness, i.e., along the y-axis in Fig. 6.15, as it offers a higher increase in efficiency for a given number of DOF. In an attempt to improve the solution accuracy, it

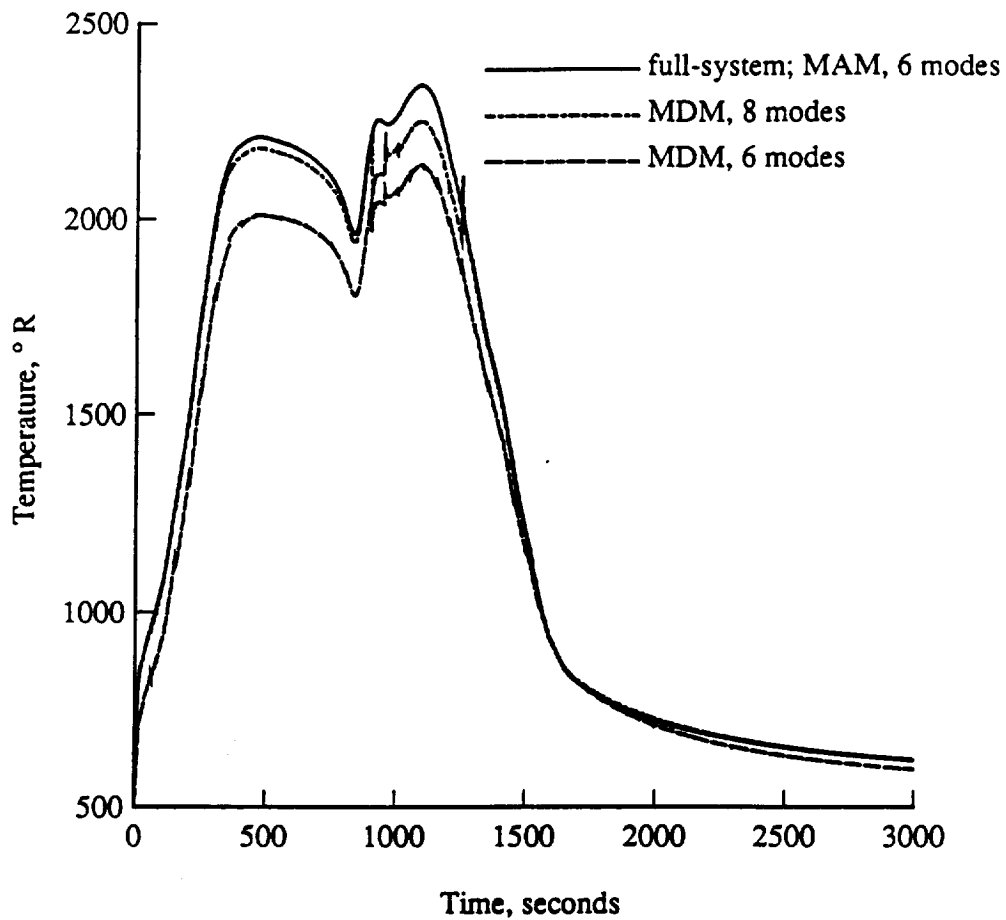


Fig. 6.32 Comparison of temperature histories of the different modal solutions for the 16 DOF graded mesh using a time step $dt = 2$ sec with the eigensolution updated every 50 sec for Shuttle one-dimensional thermal model.

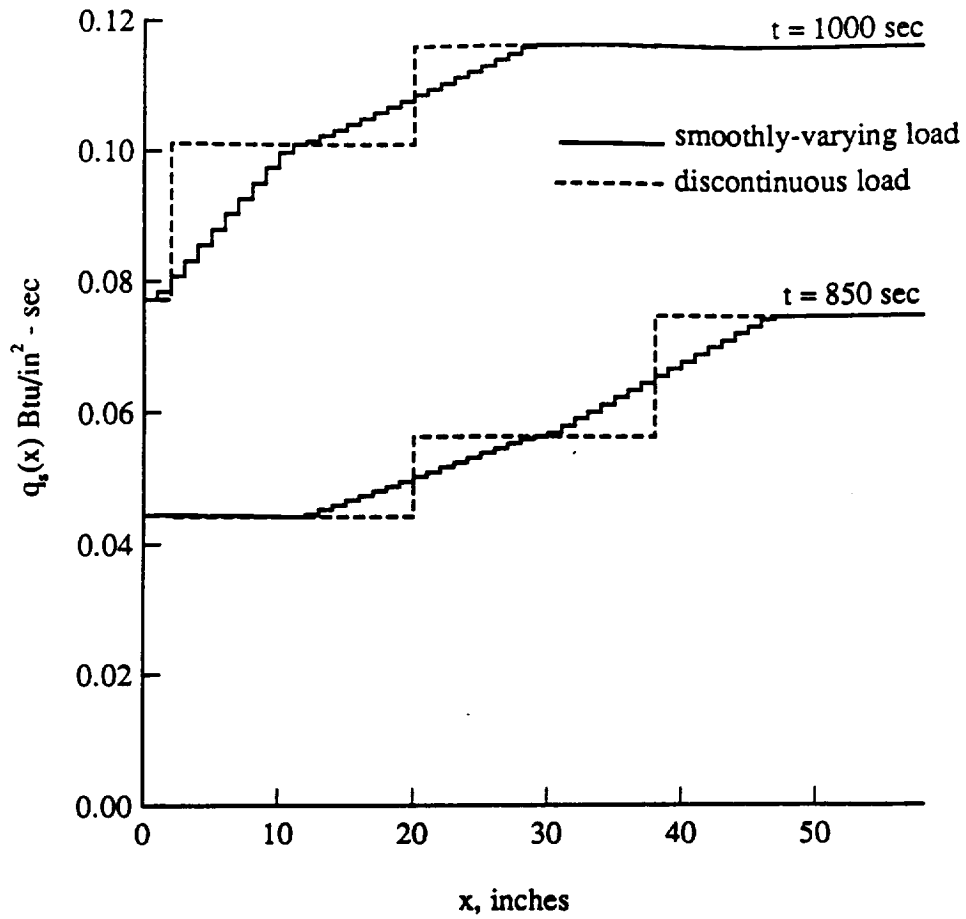


Fig. 6.33 Spatial distribution of heating on the lower surface of bay 3 at selected times (Smoothly-varying load).

was refined to include three more nodes at the mid-section where elements are rather large in the 1-D model. The discretization used along the x-axis is discussed separately for the two load cases.

Case 1: Nonuniform Load Distribution with Jump Discontinuities

The full-system solution at time $t = 1000$ sec obtained with a crude mesh of 187 DOF shows unrealistic spatial oscillations as in Fig. 6.34, due to the improper representation of the applied load. This mesh was obtained using only two elements each to represent each different load span (Fig. 6.15). For this load case shown in Fig. 6.17, the discretization along the wing surface, i.e., along the x-axis in Fig. 6.15, must be done bearing in mind that the calculation of the nodal load vectors involves the finite element approximation of lumping the element load equally at the two nodes. Consequently, a series of fine elements are necessary at the junction of the unequal input loads in order to accurately model the spatially-discontinuous load and thereby predict the temperature response reliably. The mesh thus generated after careful consideration consists of 578 nodes as shown in Fig. 6.35.

The temperature contours obtained from the full-system solution at time $t = 1000$ sec are shown in Fig. 6.36. It is evident that the temperature variation in the x-direction closely resembles the load distribution pattern causing a jump in the temperature of up to 150°R within a distance of 0.2 in. at locations where the load increases abruptly, and then the temperature remains constant (even if intermediate nodes are added) until the next jump location. To establish the suitability of the nodal locations along the x-axis for this problem, a mesh with 1683 nodes was employed along with a minor smoothing of the load changes over a thickness of about 1 in. The response was very similar to that of the 578 DOF mesh, that is, with similar jumps in temperature and temperature diffusion occurring only in the same width as the load smoothing in spite of the large array of very fine elements at the junctions. The adequacy of the discretization

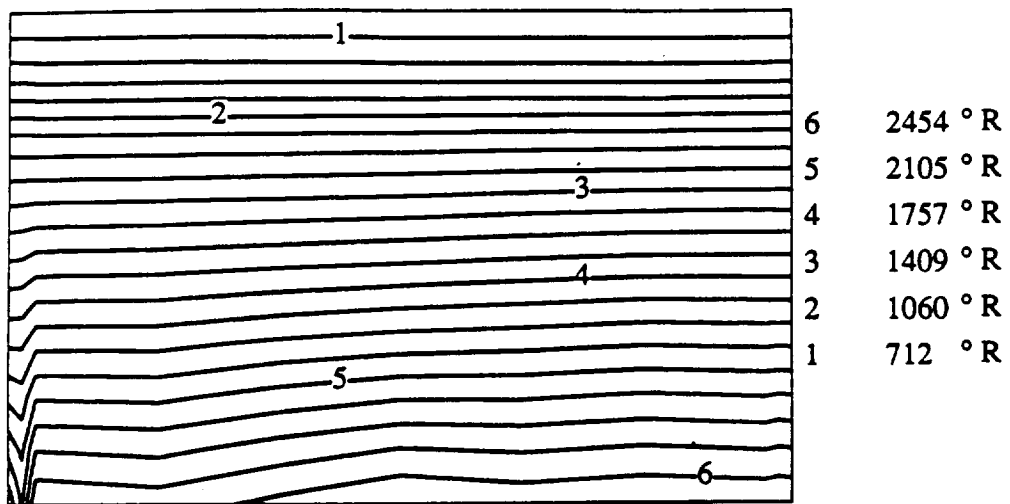


Fig. 6.34 Temperature contours at time $t = 1000$ sec of Shuttle two-dimensional thermal model with 187 DOF and discontinuous load.

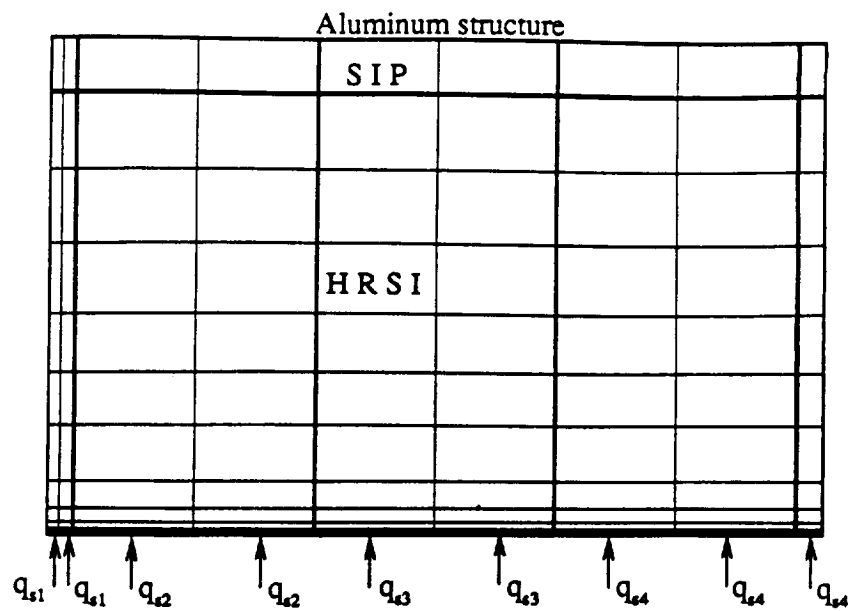


Fig. 6.35 Finite element mesh (578 DOF) for Shuttle two-dimensional thermal model with discontinuous load.

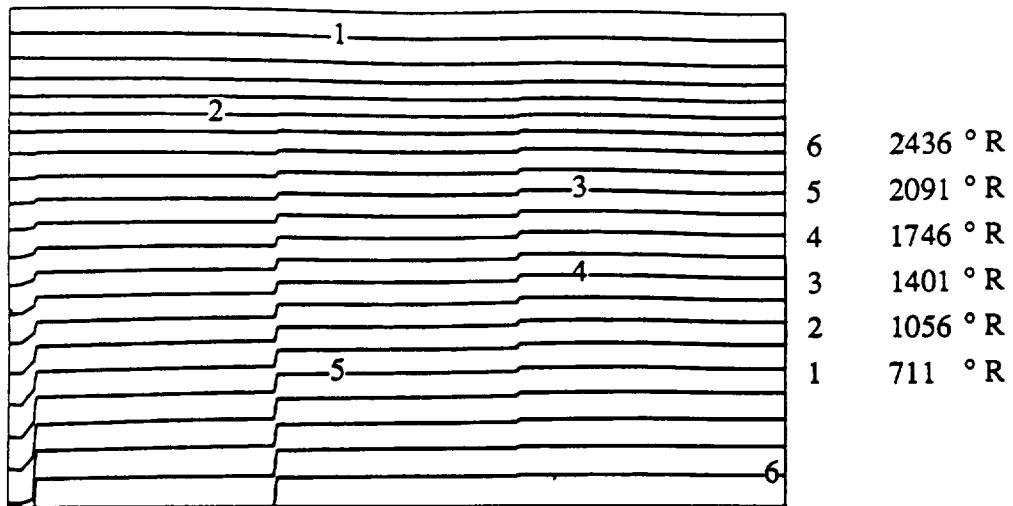


Fig. 6.36 Temperature contours at time $t = 1000$ sec of Shuttle two-dimensional thermal model with 578 DOF and discontinuous load.

in the y-direction was verified by comparing the distribution along the edge $x = 0.0$ with the full-system solution of the 1-D model using the 166 DOF mesh.

The convergence of the correction, CMAM, at time $t = 350$ sec (Fig. 6.37) is used to make a rough estimate of the number of modes required for convergence of the MAM. The reduced-system solution is considered to be converged when the error norm (based on the full solution) is acceptable throughout the solution time (Fig. 6.38). Based on this criterion, a subset of up to 400 modes (or 70%) are required by the MDM, whereas only 200 modes (or 35%) are required by the MAM as seen in Fig. 6.39; thus confirming the improved predictability of the MAM for problems with extreme temperature gradients, even an abrupt increase in temperature caused by a discontinuous load. Here again, the FDM shows no better convergence than the MAM as expected from Fig. 6.37 which shows that CFDM is insignificant compared to CMAM.

Case 2: Nonuniform Load Distribution with a Smooth Variation

The sudden jump in the thermal load at discrete points in Fig. 6.17 was smoothed by incrementing the load in small step sizes over the entire load span and the resulting distributions at times $t = 850$ sec and 1000 sec are shown in Fig. 6.32. Accordingly, a vast number of elements were used to model these loads producing the mesh comprised of 986 DOF shown in Fig. 6.40. As expected, a smooth temperature distribution occurs along the wing surface as seen in Fig. 6.41, to obtain which 850 modes (or 86%) are needed by the MDM (16% more than that required for Case 1). About the same increase in percentage of modes as that of the MDM is witnessed for the MAM which requires 550 modes (or 55%) for this case.

The two cases discussed above, which encompass a wide range of nonsymmetric load distribution, firmly establish the superior performance of the MAM over the MDM although the degree of the increase in efficiency could vary, depending on the nature of the load distribution and the finite element discretization.

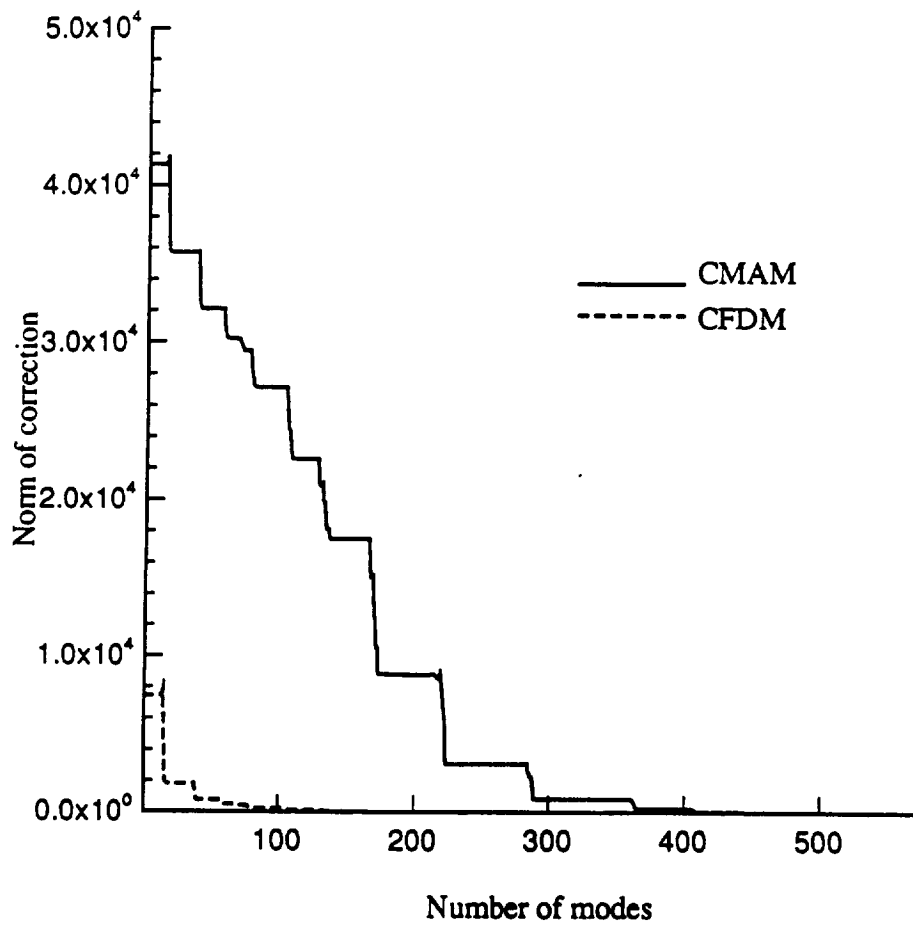


Fig. 6.37 Convergence of the correction offered by the MAM, CMAM, at time $t = 350$ sec using the Shuttle two-dimensional thermal model with 578 DOF and discontinuous load.

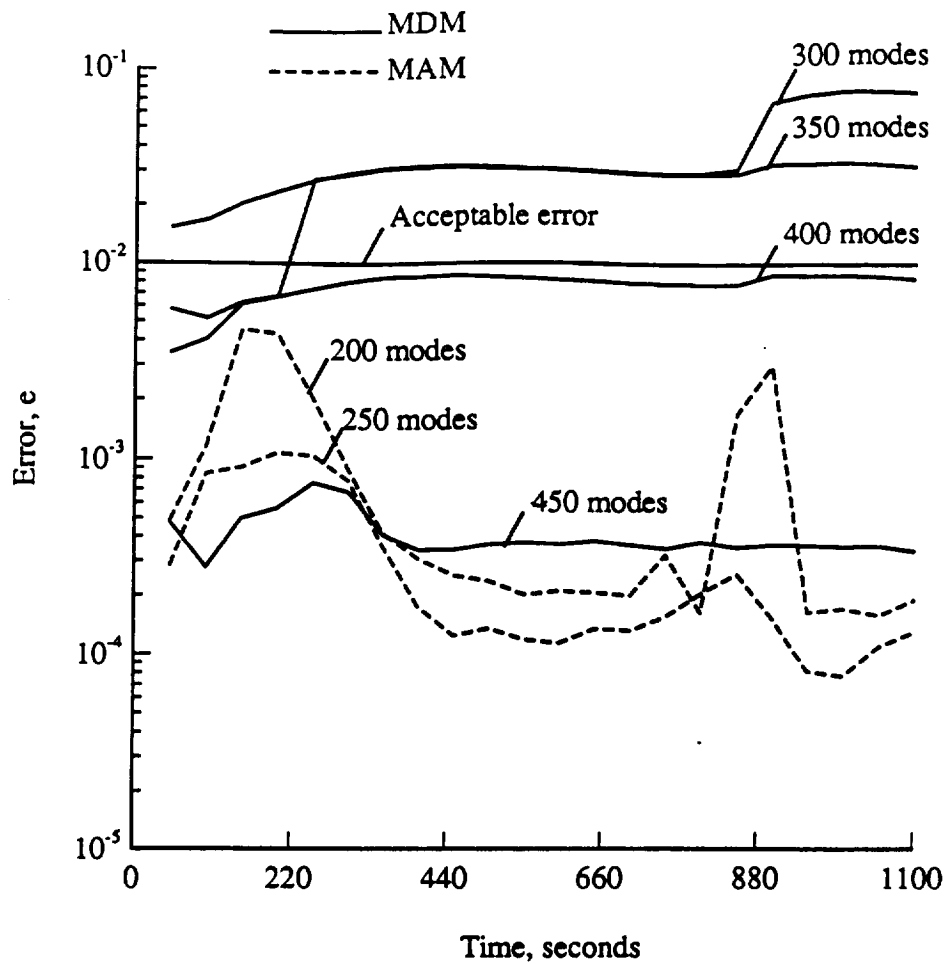


Fig. 6.38 Comparison of the error histories of the different modal solutions of the Shuttle two-dimensional thermal model with discontinuous load and 578 DOF.

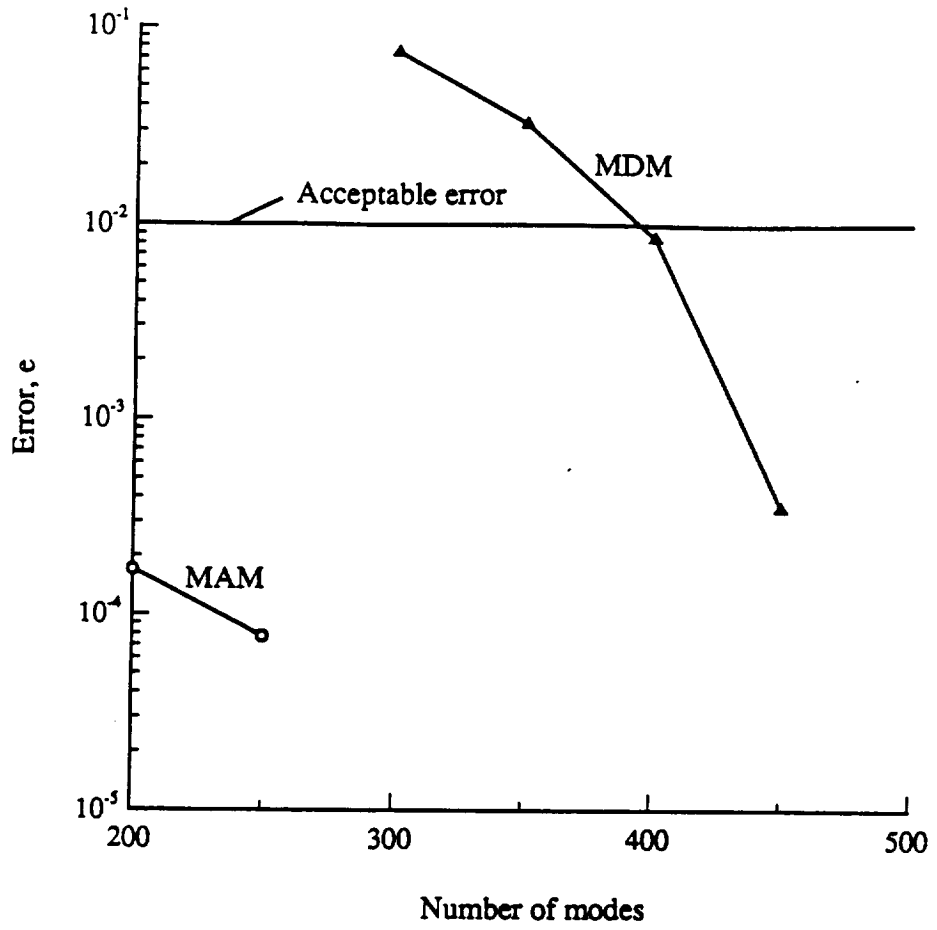


Fig. 6.39 Convergence of the MDM and the MAM at time $t = 1000$ sec using the Shuttle two-dimensional thermal model with 578 DOF and discontinuous load.

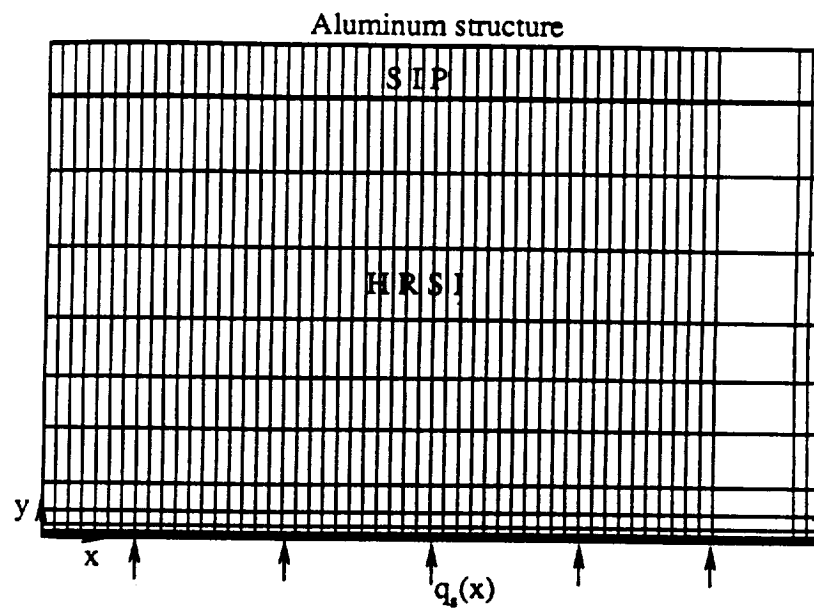


Fig. 6.40 Finite element mesh (986 DOF) for Shuttle two-dimensional thermal model with smoothly-varying load. (Also see Fig. 6.33).

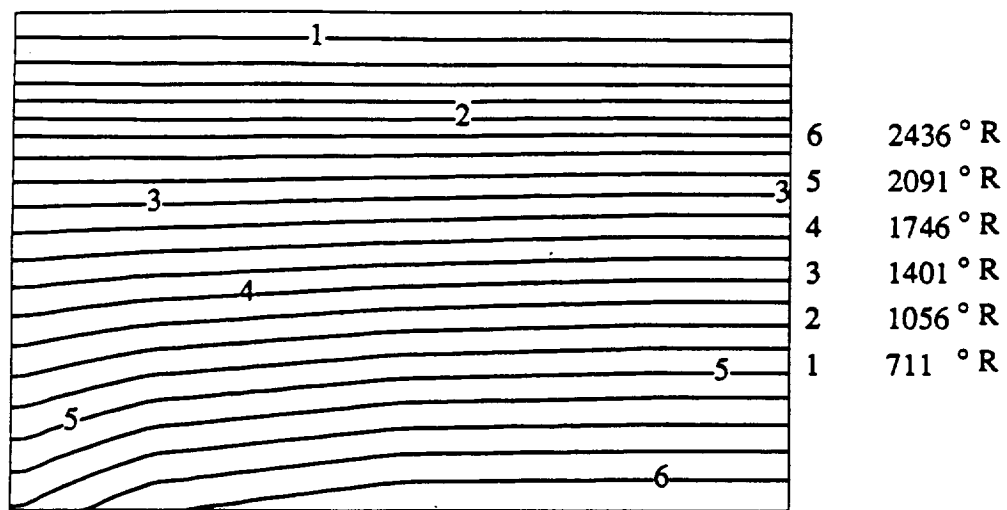


Fig. 6.41 Temperature contours at time $t = 1000$ sec of Shuttle two-dimensional thermal model with 986 DOF and smoothly-varying load.

Chapter 7

CONCLUSIONS AND RECOMMENDATIONS

The force-derivative method (FDM), which collectively represents a class of higher-order modal methods that improve the fundamental modal method, the MDM, with various-order correction terms, has been presented for nonlinear transient thermal analysis. The additional terms in the FDM include the forcing function and its derivatives with respect to time. A new algorithm incorporating the modal methods and a fixed-point iteration scheme has been implemented in an existing advanced finite element code, COMET, and validated with the aid of numerical examples. The solution is advanced in time with the nonlinear system matrices and load vectors being re-evaluated during the iterations at each time step, while the eigensolution is updated periodically to account for the change in the nonlinear basis vectors. For nonlinear problems, the first-order correction that the MAM offers to the MDM is fully realized by forming a generalized load vector, which in addition to the applied load vectors includes a corrective vector to account for the change in the nonlinear eigensolution between updates. The similar implementation of the second-order FDM in its entirety, requires the exact derivative of the generalized load vector which entails additional computational effort. Hence, in general, the highest-order FDM that may be employed, could be decided based on the order of the explicit time-dependence of the forcing function, as for linear problems.

In general, the results demonstrate the potential of the higher-order methods to effectively improve the reduction achieved for transient thermal problems. In this study,

the efficiency of the methods is measured only by the reduction achieved, in terms of the number of modes required, to obtain the response within the desired accuracy.

The first nonlinear example is a rod with a transient load and temperature-dependent thermal conductivity. The second nonlinear example involves a realistic structure, the lower surface of bay 3 of the Shuttle wing segment with nonlinear thermal properties. The complicated heat loads include specified surface heating which varies not only with time but in space as well, and nonlinear surface convection.

A number of factors that affect the performance of the modal methods have been identified. The need for a multi-step approach in time with periodic updates of the eigensolution has been established for nonlinear problems. Reduction of the time step size and eigensolution updates have either increased the solution accuracy or improved the convergence of the methods to some extent. The magnitude of the derivative of the transient load compared to that of the load itself, and the degree of temperature-dependence of the thermal conductivity are seen to affect the relative effectiveness of the FDM compared to the MAM.

The preliminary one-dimensional analysis of the Shuttle problem using different meshes clearly indicates that for a given number of degrees of freedom a suitably-graded mesh based on the expected response can upgrade the eigenmodes and thereby further enhance the faster convergence of the MAM over the MDM. For the two-dimensional problem with a discontinuous load distribution, the mesh is contrived in light of the above conclusion. Results confirm that the correction term of the MAM, which involves the load itself, is very effective in representing the neglected higher modes thus enabling the MAM to achieve a remarkable reduction of 65%, over twice that of the MDM, for this example with complex loading conditions.

The above examples have demonstrated that the FDM (the MAM in particular) is indeed a feasible, effective reduction method for nonlinear transient thermal problems.

To solve nonlinear problems more efficiently, future research must include easy but effective means to approximate the changing eigensolution. When coupled with a transient adaptive meshing scheme, the method shows potential to yield a reliable and efficient solution for problems with severe gradients.

In this study, it has been observed that the response of the MDM, though highly inaccurate, is well-behaved even with much fewer modes than that required for convergence. However, a minimum number of modes are required by the higher-order methods to yield a stable solution without unrealistic oscillations in time, regardless of how small the time step may be. This behavior of the MAM and the FDM exhibited in this study needs further investigation.

Error estimates based on the approximation of the pseudo steady-state response and its time-derivative by a subset of modes have been identified for linear transient analysis. Results of a linear problem with a spatially-uniform load but a linearly-varying transient load, although not conclusive, show how these error estimates can reliably predict the number of modes required by the MAM and the FDM throughout the time domain. The results also indicate the potential usefulness of the convergence of the correction terms of the MAM and the FDM in determining the effective method and the modes required, both of which may vary with time. Further study is required for a thorough interpretation of these correction terms, to decide how they may be obtained for nonlinear problems and for establishing convergence criteria to use them as a priori estimates.

The parallelization of the FDM is another subject identified for future study. The uncoupled nature of the modal equations and the numerous matrix-vector products involved in the modal solutions indicate that the computational efficiency can be improved by using parallel processing techniques.

REFERENCES

1. Wieting, A.R., and Guy, R.W., "Thermal-Structural Design/Analysis of an Airframe-Integrated Hydrogen-Cooled Scramjet," Journal of Aircraft, Vol. 13, March 1976, pp. 192-197.
2. "Martin Interactive Thermal Analyses System, Version 1.0," Martin-Marietta Corp., Denver, Colo., MDS-SPLPD-71-FD238 (REV3), March 1972.
3. Bhattacharya, M.C., "An Explicit Conditionally Stable Finite Difference Equation for Heat Conduction Problems," International Journal for Numerical Methods in Engineering, Vol. 21, February 1985, pp. 239-265.
4. Lick, W., "Improved Difference Approximations to the Heat Equation," International Journal for Numerical Methods in Engineering, Vol. 21, November 1985, pp. 1957-1969.
5. Rizzo, F.J., Shippy, D.J., "A Method of Solution for Certain Problems of Transient Heat Conduction," AIAA Journal, Vol. 11, 1970, pp. 2004-2009.
6. Rources, V. and Alarcon, E., "Transient Heat Conduction Problems Using B.I.E.M.," Journal of Computers and Structures, Vol. 16, 1983, pp. 717-730.
7. Zienkiewicz, O.C., and Cheung, Y.K., "Finite Elements in the Solution of Field Problems," The Engineer, Vol. 220, 1965, pp. 507-510.
8. Wilson, E.L., and Nickell, R.E., "Application of the Finite Element Method to Heat Conduction Analysis," Nuclear Engineering and Design, Vol. 4, 1966, pp. 276-286.
9. Becker, E.B., and Parr, C.H., "Application of the Finite Element Method to Heat Conduction in Solids," Technical Report S-117, Rohm and Haas, Redstone Research Laboratories, Huntsville, 1967.
10. Richardson, P.D., and Shum, Y.M., "Use of Finite Element Methods in Solution of Transient Heat Conduction Problems," ASME Paper No. 69-WA/HT-36.
11. Beckett, R.E., and Chu, S.C., "Finite Element Method Applied to Heat Conduction with Nonlinear Boundary Conditions," Journal of Heat Transfer, Vol. 95, 1973, pp. 126-129.
12. Aguirre-Ramirez, G. and Oden, J.T., "Finite Element Technique Applied to Heat Conduction in Solids with Temperature-Dependent Thermal Conductivity," International Journal for Numerical Methods in Engineering, Vol. 7, 1973, pp. 345-355.

13. Thornton, E.A., and Wieting, A.R., "A Finite Element Thermal Analysis Procedure for Several Temperature-Dependent Parameters," Journal of Heat Transfer, Vol. 100, August 1978, pp. 551-553.
14. Lyness, J.F., Owen, D.R.J., and Zienkiewicz, O.C., "The Finite Element Analysis of Engineering Systems Governed by a Nonlinear Quasi-Harmonic Equation," Journal of Computers and Structures, Vol. 5, 1975, pp. 65-79.
15. Thornton, E.A., and Wieting, A.R., "Finite Element Methodology for Transient Conduction/Forced-Convection Thermal Analysis," Heat Transfer, Thermal Control, and Heat Pipes, Vol. 70, 1979, pp.77-103.
16. Gurtin, N.E., "Variational Principles for Linear Initial Value Problems," Quarterly of Applied Mathematics, Vol. 22, 1964, pp. 252-256.
17. Wilson, E.L., Bathe, K.J., and Peterson, F.E., "Finite Element Analysis of Linear and Nonlinear Heat Transfer," Nuclear Engineering and Design, Vol. 29, 1974, pp. 110-124.
18. Huebner, K.H., and Thornton, E.A., The Finite Element Method for Engineers, Second Edition, John Wiley and Sons, 1982.
19. Hughes, T.J.R., "Unconditionally Stable Algorithm for Nonlinear Heat Conduction," Computer Methods in Applied Mechanics and Engineering, Vol. 10, 1977, pp. 135-139.
20. Myers, G.E., "The Critical Time Step for Finite Element Solutions to Two-Dimensional Heat Conduction Transients," Journal of Heat Transfer, Vol. 100, 1978, pp. 120-128.
21. Adelman, H.M., and Haftka, R., "On the Performance of Explicit and Implicit Transient Algorithms for Transient Thermal Analysis of Structures," NASA TM 81880, Langley Research Centre, Hampton, VA., September 1980.
22. Orivuori, S., "Efficient Method for Solution of Nonlinear Heat Conduction Problems," International Journal for Numerical Methods in Engineering, Vol. 14, 1979, pp. 1461-1476.
23. Hindmarsh, A.C., "A Collection of Software for Ordinary Differential Equations," Lawrence Livermore Laboratory Report No. UCRL-82091, January 1979.
24. Marlowe, M.B., Moore, R.A., and Whetstone, W.D., SPAR Thermal Analysis Processors Reference Manual, System Level 16. NASA CR-159162, 1979.
25. Thornton, E.A., and Dechaumphai, P., "A Taylor-Galerkin Finite Element Algorithm for Transient Nonlinear Thermal-Structural Analysis," Presented at the AIAA, ASME, AHS 27th Structures, Structural Dynamics and Materials Conference, San Antonio, Texas, May 19-21, 1986, AIAA No. 86-0911.
26. Dechaumphai, P., Thornton, E.A., and Wieting, A.R., "Flow-Thermal-Structural Study of Aerodynamically Heated Leading Edges," AIAA Paper no. 88-2245-CP, April 1988.

27. Pandey, A.K., Dechaumphai, P., and Wieting, A.R., "Thermal-Structural Finite Element Analysis Using Linear Flux Formulation," AIAA Paper No. 89-1224-CP, April 1989.
28. Tamma, K.K., and Namburu, R.R., "Explicit Second-Order Accurate Taylor-Galerkin Based Finite Element Formulations for Heat Transfer," Presented at the AIAA 22nd Thermophysics Conference, Honolulu, Hawaii, June 1987, AIAA No. 87-1549.
29. Thornton, E.A., and Balakrishnan, N., "A Finite Element Solution Algorithm for Nonlinear Thermal Problems with Severe Gradients," Presented at the 27th Aerospace Sciences Meeting, Reno, Nevada, January 1989, AIAA No. 89-0520.
30. Chen, H.T., and Chen, C.K., "Hybrid Laplace Transform/ Finite Difference Method for Transient Heat Conduction Problems," International Journal for Numerical Methods in Engineering, Vol. 26, 1988, pp. 1433-1447.
31. Chen, H.T., and Chen, C.K., "Hybrid Laplace Transform/ Finite Element Method for Two-Dimensional Transient Heat Conduction Problems," Journal of Thermophysics and Heat Transfer, Vol. 2, No. 1, January 1988, pp. 31-36.
32. Tamma, K.K., and Railkar, S.B., "A Hybrid Transfinite Element Approach for Nonlinear Transient Thermal Analysis," Presented at the AIAA 25th Aerospace Sciences Meeting, January 1987, Reno, Nevada, AIAA Paper No. 87-0149.
33. Tamma, K.K., and Railkar, S.B., "Transfinite Element Methodology for Nonlinear/Linear Transient Thermal Modeling/Analysis," Progress and Recent Advances, International Journal for Numerical Methods in Engineering, Vol. 25, 1988, pp. 475-494.
34. Cerro, J.A., and Scotti, S.J., "Evaluation of a Transfinite Element Numerical Solution Method for Nonlinear Heat Transfer Problems," Numerical Methods in Thermal Problems, Vol. VII, Part 2, July 1991.
35. Thornton, E.A., and Dechaumphai, P., "A Hierarchical Finite Element Approach for Integrated Thermal-Structural Analysis," Presented at the 25th Structures, Structural Dynamics and Materials Conference, May 1984, Palm Springs, California, AIAA Paper No. 84-0939-CP.
36. Dechaumphai, P., "Evaluation of an Adaptive Unstructured Remeshing Technique for Integrated Fluid-Thermal-Structural Analysis," Journal of Thermophysics and Heat Transfer, April 1991.
37. Thornton, E.A., and Vemaganti, G.R., "An Adaptive Remeshing Method for Finite Element Thermal Analysis," Presented at the AIAA Thermophysics, Plasmadynamics and Lasers Conference, June 1988, San Antonio, Texas, AIAA Paper no. 88-2662.
38. Biot, M.A., and Bisplinghoff, R.L., "Dynamic Loads on Airplane Structures During Landing," NACA Wartime Report W-92, October 1944.
39. Bathe, K.J., and Gracewski, S., "On Nonlinear Dynamic Analysis Using Substructuring and Mode Superposition," Journal of Computers and Structures, Vol. 13, 1981, pp. 699-707.

40. Noor, A.K., "Recent Advances in Reduction Methods for Nonlinear Problems," Journal of Computers and Structures, Vol. 13, 1981, pp. 13-44.
41. Idelsohn, S., and Cardona, A., "Recent Advances in Reduction Methods in Nonlinear Structural Dynamics," Proc. 2nd Intl. Conf. on Recent Advances in Structural Dynamics, Southampton, April 1984.
42. Idelsohn, S., and Cardona, A., "A Load-Dependent Basis for Reduced Nonlinear Structural Dynamics," Journal of Computers and Structures, Vol. 20, No. 1-3, 1985, pp. 203-210.
43. Kline, K.A., "Dynamic Analysis Using a Reduced Basis of Exact Modes and Ritz Vectors," AIAA Journal, Vol. 24, No. 12, December 1986, pp. 2022-2029.
44. Ramberg, W., "Transient Vibration in an Airplane Wing Obtained by Several Methods," Journal of Research of the National Bureau of Standards, Research Paper RP 1984, Vol. 42, May 1949.
45. Leung, Y.T., "Fast Response Method for Undamped Structures," Engineering Structures, Vol. 5, April 1983, pp. 141-149.
46. Likhoded, A.I., "Convergence of the Method of Expansion in Natural Vibration Modes in Programs of Dynamic Loading," Izv. AN SSSR. Mekhanika Tverdogo Tela, Vol. 21, No. 1, 1986, pp. 180-188.
47. Borino, G. and Muscolino, G., "Mode-Superposition Methods in Dynamic Analysis of Classically and Non-Classically Damped Linear Systems," Earthquake Engineering and Structural Dynamics, Vol. 14, 1986, pp. 705-717.
48. Camarda, C.J., Haftka, R.T., and Riley, M.F., "An Evaluation of Higher-Order Modal methods for Calculating Transient Structural Response," Journal of Computers and Structures, Vol. 27, No. 1, 1987, pp. 89-101.
49. Camarda, C.J., and Haftka, R.T., "Development of Higher-Order Modal Methods for Transient Thermal and Structural Analysis," NASA TM 101548, February 1989.
50. Camarda, C.J., "Development of Advanced Modal Methods for Calculating Transient Thermal and Structural Response," NASA TM 104102, December 1991.
51. McGowan, D.M., and Bostic, S.W., "Comparison of Advanced Reduced-Basis Methods for Transient Structural Analysis," Presented at the AIAA/ASME/ASCE/AHS/ACE 32nd Structures, Structural Dynamics and Materials Conference, Baltimore, Maryland, April 1991, AIAA Paper No. 91-1059.
52. McGowan, D.M., and Bostic, S.W., and Camarda, C.J., "Development and Comparison of Advanced Reduced-Basis Methods for the Transient Structural Analysis of Unconstrained Structures," NASA TM 109015, November 1993.
53. Bushard, L.B., "On the Value of Guyan Reduction in Dynamic Thermal Problems," Journal of Computers and Structures, Vol. 13, 1981, pp. 525-531.
54. Biot, M.A., "New Methods in Heat Flow Analysis with Application to Flight Structures," Journal of the Aeronautical Sciences, Vol. 24, No. 12, December 1957, pp. 857-873.

55. Nour-Omid, B., Parlett, B.N., and Taylor, R.L., "Lanczos Versus Subspace Iteration for Solution of Eigenvalue Problems," International Journal for Numerical Methods in Engineering, Vol. 19, 1983, pp. 859-871.
56. Nour-Omid, B., "Lanczos Method for Heat Conduction Analysis," International Journal for Numerical Methods in Engineering, Vol. 24, 1987, pp. 251-262.
57. Coutinho, A.L.G., Landau, L., Wrobel, L.C., and Ebecken, N.F.F., "Modal Solution of Transient Heat Conduction Utilizing Lanczos Algorithm," International Journal for Numerical Methods in Engineering, Vol. 28, 1989, pp. 13-25.
58. Cardona, A., and Idelsohn, S., "Solution of Nonlinear Thermal Transient Problems by a Reduction Method," International Journal for Numerical Methods in Engineering, Vol. 23, 1986, pp. 1023-1042.
59. Noor, A.K., Balch, C.D., and Shibut, M.A., "Reduction Methods for Nonlinear Steady-State Thermal Analysis," NASA TP-2098, March 1983.
60. Shore, C.P., "Status Report on Development of a Reduced Basis Technique for Transient Thermal Analysis," NASA CP 2216, 1982, pp. 133-146.
61. Shore, C.P., "Application of the Reduced Basis Method to Nonlinear Transient Thermal Analysis," Research in Structural and Solid Mechanics-1982, NASA CP-2245, 1982, pp. 49-65.
62. Shore, C.P., "Reduction Method for Thermal Analysis of Complex Aerospace Structures," NASA TP-2373, January 1985.
63. Stewart, C.B., "The Computational Structural Mechanics Testbed User's Manual," NASA TM 10064 (1989).
64. Thornton, E.A., "Thermal Structures: Four Decades of Progress," Presented at the AIAA/ASME/ASCE/AHS/ACE 31st Structures, Structural Dynamics and Materials Conference, Long Beach, California, April 1990, AIAA Paper No. 90-0971.
65. E.L. Wilson, M. Iwan, and J.M. Dickens, "Dynamic Analysis by Direct Super-position of Ritz Vectors", Earthquake Engineering and Structural Dynamics, Vol. 10, pp. 813-821 (1982).
66. Burden, R.L., Faires, J.D., and Reynolds, A.C., Numerical Analysis, Second Edition, Prindle, Weber & Schmidt, 1981.
67. Balakrishnan, N., "Implementation of the Force-Derivative Method for Nonlinear Transient Thermal Problems in the Computational Structural Mechanics Testbed," Research Skill Report, Old Dominion University, Norfolk, VA, April 1995.

Appendix

COMPUTATIONAL PROCEDURES USED IN THE IMPLEMENTATION OF THE MDM, MAM AND THE FDM

The sequence of the steps to be followed in the solution of transient thermal problems using the modal methods is presented below.

1. Input the number of modes to be included in the solution.
Input the number of time steps before every EVP update, m .
At initial time $t = 0$:
Evaluate the nonlinear system matrices, K_0 and C_0 .
Evaluate the linear and nonlinear applied load vectors, R_{L0} and R_{NL0} , and their time derivatives, \dot{R}_{L0} and \dot{R}_{NL0} .
2. Apply the boundary conditions.
3. Solve the initial EVP, Eq. (4.25), to get $\hat{\Phi}_0$ and $\hat{\Lambda}_0$.
Factor K_0 .
Set the indicator for EVP update, k , to zero. See Eq. (4.40).
4. For $n = 1, 2, \dots$ total number of timesteps; loop through step 27.
Increment k ; $k = k+1$.
5. Evaluate the linear applied load and its time derivative at current time, R_{Ln} and \dot{R}_{Ln} .

6. Initialize the modal coordinates, z_{n-1} , Eq. (4.45).
7. Compute the linear part of the modal coordinates; sum of the first two terms on the right-hand side of Eq. (4.53).
8. For $i = 1, 2 \dots$ until the iterations converge, loop through step 24.
9. Compute the nonlinear corrective load vector, $Q_{NL_n}^{i-1}$, Eq. (4.41), and add to the nonlinear applied load vector, $R_{NL_n}^{i-1}$ to form the nonlinear part of the generalized load vector.
10. Obtain the modal coordinates, z_n , by adding the nonlinear part (third term on the right-hand side of Eq. (4.53)) to the linear part computed in step 7.
11. Get the approximate response, T_n^i , by the MDM, Eq. (4.48). If the MDM is the chosen method, go to step 21.
12. Otherwise, assemble the generalized load vector Q_n^{i-1} , Eq. (4.42), by adding the linear component from step 5 to the nonlinear component from step 9.
13. Solve the set of linear equations $K_{n-k} r = Q_n^{i-1}$ to obtain $K_{n-k}^{-1} Q_n^{i-1}$.
14. Compute $\hat{\Phi} \frac{1}{\Lambda} \hat{\Phi} Q_n^{i-1}$.
15. Get the response of the MAM, Eq. (4.49). If the MAM is the desired method, go to step 21.

16. Otherwise, using the approximate form of \dot{Q}_n^{i-1} , Eq. (4.52), solve $K_{n-k} r = \dot{Q}_n^{i-1}$ to yield $K_{n-k}^{-1} \dot{Q}_n^{i-1}$.
17. Compute $C_{n-k} K_{n-k}^{-1} \dot{Q}_n^{i-1}$.
18. Solve $K_{n-k} r = C_{n-k} K_{n-k}^{-1} \dot{Q}_n^{i-1}$ to yield $K_{n-k}^{-1} C_{n-k} K_{n-k}^{-1} \dot{Q}_n^{i-1}$.
19. Compute $\hat{\Phi} \frac{1}{\hat{\Lambda}^2} \hat{\Phi}^T \dot{Q}_n^{i-1}$.
20. Get the response of the second-order FDM, Eq. (4.50).
21. Use the new temperature vector to update the nonlinear system matrices and load vector for the next iteration or time step.
22. Apply the boundary conditions.
23. If the iterations have converged, Eq. (4.54), go to step 25.
24. Otherwise, go to the next iteration, step 8.
25. If this is the last time step, STOP.
26. Otherwise, check if it is time to update the EVP; if it is not, i.e., $k \neq m$, go to the next time, step 4. If it is, then obtain the new set of eigenmodes, $\hat{\Phi}_n$ and $\hat{\Lambda}_n$.
Factor K_n .
Reset $k = 0$.
Go to step 4.

BIOGRAPHY

Narayani Balakrishnan was born in [REDACTED] on [REDACTED]. She received her Bachelor's degree in Civil Engineering from the College of Engineering, Madras, India in 1982, and her Master's degree in Structural Engineering from the Indian Institute of Technology, Madras, India in 1984. In January 1986, she enrolled in the Doctoral program in Engineering Mechanics at Old Dominion University, Norfolk, Virginia. During her graduate studies, the author worked as a research assistant at the Aerothermal Loads Branch and the Thermal Structures Branch of NASA Langley Research Center, Hampton, Virginia.